Copyright Warning & Restrictions

The copyright law of the United States (Title 17, United States Code) governs the making of photocopies or other reproductions of copyrighted material.

Under certain conditions specified in the law, libraries and archives are authorized to furnish a photocopy or other reproduction. One of these specified conditions is that the photocopy or reproduction is not to be "used for any purpose other than private study, scholarship, or research." If a, user makes a request for, or later uses, a photocopy or reproduction for purposes in excess of "fair use" that user may be liable for copyright infringement,

This institution reserves the right to refuse to accept a copying order if, in its judgment, fulfillment of the order would involve violation of copyright law.

Please Note: The author retains the copyright while the New Jersey Institute of Technology reserves the right to distribute this thesis or dissertation

Printing note: If you do not wish to print this page, then select "Pages from: first page # to: last page #" on the print dialog screen

ABSTRACT

INVESTIGATIONS INTO B-O DEFECT FORMATION-DISSOCIATION IN CZ-SILICON AND THEIR EFFECT ON SOLAR CELL PERFORMANCE

by
Prakash M. Basnyat

About 30% of the total market share of industrial manufacture of silicon solar cells is taken by single crystalline Czochralski (CZ) grown wafers. The efficiency of solar cells fabricated on boron-doped Czochralski silicon degrades due to the formation of metastable defects when excess electrons are created by illumination or minority carrier injection during forward bias. The recombination path can be removed by annealing the cell at about 200° C but recombination returns on exposure to light.

Several mono-crystalline and multi-crystalline solar cells have been characterized by methods such as laser beam induced current (LBIC), Four-Probe electrical resistivity etc. to better understand the light induced degradation (LID) effect in silicon solar cells. All the measurements are performed as a function of light soaking time. Annealed states are produced by exposing the cells/wafer to temperature above 200° C for 30 minutes and light soaked state was produced by exposure to 1000 W/m^2 light using AM1.5 solar simulator for 72 hours. Dark I-V data are analyzed by a software developed at NREL.

This study shows that LID, typically, has two components- a bulk component that arises from boron-oxygen defects and a surface component that appears to be due to the SiN_x:H-Si interface. With the analysis of dark saturation current (J_{02}), it is seen that the surface LID increases with an increase in the q/2kT component. Results show that cell performance due to bulk effect is fully recovered upon annealing where as surface LID does not recover fully. This statement is also verified by the study of mc- silicon solar

cells. Multi-crystalline silicon solar cell has very low oxygen content and, therefore, recombination sites will not be able to form. This shows that there is no bulk degradation in mc- Si solar cells but they exhibit surface degradation. The results suggest that a typical Cz-silicon solar cell with an initial efficiency of ~ 18% could suffer a reduction in efficiency to ~ 17.5% after the formation of a metastable defect, out of which ~ 0.4% comes from a bulk effect and ~0.1% is linked to a surface effect.

INVESTIGATIONS INTO B-O DEFECT FORMATION-DISSOCIATION IN CZ-SILICON AND THEIR EFFECT ON SOLAR CELL PERFORMANCE

by
Prakash M. Basnyat

A Dissertation
Submitted to the Faculty of
New Jersey Institute of Technology
and Rutgers, The State University of New Jersey – Newark
in Partial Fulfillment of the Requirements for the Degree of
Doctor of Philosophy in Applied Physics

Federated Department of Physics

May 2013

.

APPROVAL PAGE

INVESTIGATIONS INTO B-O DEFECT FORMATION-DISSOCIATION IN CZ-SILICON AND THEIR EFFECT ON SOLAR CELL PERFORMANCE

Prakash M. Basnyat

Dr. N.M. Ravindra, Dissertation Co-Advisor — Date
Professor, Department of Physics, NJIT

Dr. Bhushan Sopori, Dissertation Co-Advisor — Date
Principal Engineer, National Renewable Energy Laboratory, Golden, CO

Dr. Anthony Fiory, Committee Member — Date
Research Professor, Department of Physics, NJIT

Dr. Tao Zhou, Committee Member — Date
Associate Professor, Department of Physics, NJIT

Dr. Ken H. Ahn, Committee Member — Date
Assistant Professor, Department of Physics, NJIT

BIOGRAPHICAL SKETCH

Author: Prakash M. Basnyat

Degree: Doctor of Philosophy

Date: May 2013

Undergraduate and Graduate Education:

- Doctor of Philosophy in Applied Physics,
  New Jersey Institute of Technology, Newark, NJ, 2013
- Master of Science in Physics,
  Southern Illinois University Carbondale, IL, 2006
- Master of Science in Physics,
  Tribhuvan University, Kathmandu, Nepal, 1995
- Bachelor of Science,
  Tribhuvan University, Kathmandu, Nepal, 1992

Major: Applied Physics

Presentations and Publications:

P. Basnyat, S. Devayajanam, N.M. Ravindra, J. Binns, J. Appel, B. Sopori, "Experimental study of surface contribution on light induced degradation of crystalline silicon solar cells", Under publication.

B. Sopori, S. Devayajanam, P. Basnyat, S. Shet, D. Guhabiswas, S. Sahoo, V. Mehta, and R. Rivero, "Crystalline and multicrystalline silicon: Recent advances in the material growth and solar cell processing", *Proc. 6th International Symposium on advanced science and technology of silicon materials,* Honolulu, Hawaii, 2012,

B. Sopori, P. Basnyat, S. Shet, V.Mehta, S. Devayajanam, J. Binns, and J. Appel, "Experimental study of light induced degradation in c-Si solar cells: Separating the bulk and the surface contributions", *Proc. 22nd Workshop on crystalline silicon solar cells and modules: materials and processes,* Vail, CO, pp. 135 (2012).

B. Sopori, P. Basnyat, S. Shet, V. Mehta, S. Devayajanam, J.Binns, and J. Appel, "Understanding light induced degradation of c-Si solar cells", *Proc. 38th IEEE Photovolaic Specialists Conference*, Austin, TX, pp. 001115 (2012).

B. Sopori, P. Rupnowski, P. Basnyat, V.Mehta, "Screening wafers to improve yield in silicon solar cell production", *Poster session presented at Second MRS workshop on photovoltaic materials and manufacturing issues,* Denver, CO (October 4-7, 2011).

B. Sopori, P. Rupnowski, P. Basnyat, V. Mehta,"A noncontact system for screening silicon wafers prior to solar cell production", *Proc. 21st Workshop on crystalline silicon solar cells and modules: materials and processes,* Breckenridge, CO, pp. 202 (2011).

B. Sopori, P. Rupnowski, P. Basnyat, V. Mehta, "A high throughput, noncontact system for screening silicon wafers predisposed to breakage during solar cell production", *Proc. 37th IEEE Photovoltaic Specialists Conference*, Seattle, Washington, pp. 001134 (2011).

A.K. Pathak, I. Dubenko, C. Pueblo, P. Basnyat, S. Stadler, and N. Ali, "The effect of partial substitution of Ni by Co on the magnetic and electrical properties of $Ni_{50}Mn_{35}In_{15}$ Heusler Alloy", *IEEE Trans. Magn.,* vol. 46, no. 6, pp. 1444 (2010).

A.K. Pathak, P. Basnyat, I. Dubenko, S. Stadler, N. Ali, "Influence of the small substitution of Z = Ni, Cu, Cr, V for Fe on the magnetic, magnetocaloric, and magnetoelastic properties of $LaFe_{11.4}Si_{1.6}$", *J. Magn. Magn. Mater.*, vol. 322, pp. 692 (2010).

A.K. Pathak, P. Basnyat, I. Dubenko, S. Stadler, N. Ali, "Magnetic, magnetocaloric and magnetoelastic properties of $LaFe_{11.57}Si_{1.43}B_x$ compounds", *J. Appl. Phys.,*vol. 106, no. 6, pp. 063917 (2009).

P. Basnyat, B. Luster, C. Muratore, A. Voevodin, R. Haasch, R. Zakeri, P. Kohli, S.M. Aouadi; "Surface texturing for adaptive solid lubrication", *Surf. Coat. Technol.*, vol. 203, pp. 73 (2008).

P. Basnyat, S. M. Aouadi, B. Luster, C. Muratore, A.A. Voevodin, P. Kohli; "Surface texturing for adaptive solid lubrication", *STLE Annual Meeting*, Cleveland, OH (May 18-22, 2008).

Y. Paudel, P. Basnyat, S. Stadler, J. Xu, S.R. Mishra, S.M. Aouadi, " A comparative study of the tribological properties of Mo_2N-based self-lubricating films", *Poster session presented at STLE Annual Meeting*, Cleveland,OH (May 18-22, 2008).

P. Basnyat, B. Luster, S.M. Aouadi, C. Muratore, A.A. Voevodin, P. Kohli, "Surface texturing by using reactive ion etching for adaptive solid lubrication", *Poster session presented at International Conference on Metallurgical Coating and Thin Films,* San Diego, CA (April 28-May 2, 2008).

P. Basnyat, B. Luster, Z. Kertzman, S. Stadler, P. Kohli, S.M. Aouadi, J. Xu, S.R. Mishra, O. Eryilmaz, A. Erdemir, "Mechanical and tribological properties of CrAlN-Ag self-lubricating nanocomposite films", *Surf. Coat. Technol., vol.* 202, pp. 1011 (2007).

P. Basnyat, B. Luster, Z. Kertzman, S. Stadler, J. Xu, S.R. Mishra, S.M. Aouadi, "Mechanical and tribological properties of CrAlN-Ag nano-composite films'', *International Conference on Metallurgical Coatings and Thin Films*, San Diego, CA (April 23-27, 2007).

S.M. Aouadi, C. Bradley, B. Luster, P. Basnyat, R. Zakery, P. Kohli, "Development of nano textured self-lubricating adaptive coatings", *International Conference on Metallurgical Coatings and Thin Films*, San Diego, CA (April 23-27, 2007).

P. Basnyat, A. Aul, S.M. Aouadi, P. Kohli, J. Xu, S.R. Mishra, O. Eryilmaz, J.A. Jhonson, A. Erdemir, "Mechanical, tribological, and heamocompatibility properties of ZrN-Ag, ZrN-Au, and ZrN-Pd nanocomposite films", *International Conference on Metallurgical Coatings and Thin Films*, San Diego, CA (May 1-5, 2006).

S.M. Aouadi, P. Basnyat, Y. Zhang, Q. Ge, P. Filip, " Grain boundary sliding mechanism in metallurgical coatings and thin films", *International Conference on Metallurgical Coatings and Thin Films*, San Diego, CA (May 1-5, 2006).

S.M. Aouadi, P. Basnyat, Y. Zhang, S. Stadler, "Physical and chemical properties of sputter deposited Ta-C-N films", *J. Phys. Condens. Matter,* vol. 18, pp. 1977 (2006).

S.M. Aouadi, P. Basnyat, Y. Zhang, Q. Ge, P. Filip, "Grain boundary sliding mechanism in ZrN-Ag, ZrN-Au, and ZrN-Pd nano composite films", *Appl. Phys. Lett.,* vol. 88, no. 2, pp. 021902 (2006)

Dedicated to my father Karna Bahadur Basnyat
To my mother Sabitri Basnyat,
For inspiring me
To learn, explore, and do well all the time.
To my wife Laxmi Basnyat,
For standing next to me unconditionally.

ACKNOWLEDGEMENTS

I would like to acknowledge and express my deepest gratitude to my co-advisor, Professor N.M. Ravindra for his valuable guidance, moral support and encouragement to work in the exciting field of silicon solar cells. I am most grateful to my co-advisor Dr. Bhushan Sopori, Principal Engineer, NREL, for giving me opportunity to carry out my research and for his outstanding mentorship in a truly exceptional research environment.

I am very thankful to Dr. Anthony Fiory, Dr. Tao Zhou, and Dr. Ken Ahn for serving on my doctoral committee and sparing their valuable time for me, by giving constructive suggestions at all stages of this work. I am greatly indebted to Dr. Keith Emery, Dr. John Pern, and Charles Mack, from NREL for their assistance and valuable suggestions in time of need.

It is my great pleasure to thank all my colleagues who have helped me during this research work. I would like to extend my appreciation to Dr. Sudhakar Shet, Dr. Vishal Mehta, and Dr. Vinay Budhraja for their assistance with sample preparation and measurements. I would like to thank especially Mr. Srinivas Devayajanam for his friendship and working with me in various projects related to this research. I owe a special debt of thank to my longtime friends Ramjee Pahadee, Sajal Dhungana, and S. Ulak for invaluable help, unwavering friendship, and continuous encouragement.

I would like to express my sincere gratitude to my mother, brothers, and sisters for all the unconditional love and support they have provided me in every walk of my life. Most of all, I want to thank Laxmi Basnyat, my dear wife and soul mate, for her inspiration, counsel, friendship and love all the time. This work is dedicated to her.

TABLE OF CONTENTS

TABLE OF CONTENTS
(Continued)

Chapter **Page**

TABLE OF CONTENTS
(Continued)

LIST OF TABLES

LIST OF FIGURES

LIST OF FIGURES
(Continued)

Figure **Page**

CHAPTER 1

INTRODUCTION

Even though solar cells hold great promise for use as an environmentally friendly renewable energy source, they are not free from their own problems. The problems remain as unresolved technical issues some of which are quite significant and need to be resolved. One of the issues is degradation in efficiency. Efficiencies of silicon solar cells decrease over time because of several factors which can affect the reliability and performance of the cells. Some of the factors which might cause them to perform poorly are due to thermally produced stresses because of diurnal and seasonal temperature variations, oxidation or corrosion produced by humid air etc. These causes are taken into consideration during encapsulation of the cells [1, 2]. It is widely known that the light induced degradation of solar cell is a serious problem. Crystalline silicon solar cells exhibit changes in cell performance upon exposure to light.

Single crystalline Si-solar cells made from Czochralski (CZ) wafers show degradation in the presence of light, but the silicon solar cells made from Float-zone (FZ) wafers do not show such effect. The main difference between CZ and FZ single crystalline silicon is the amount of oxygen they contain. In CZ wafers, presence of oxygen is more than $1x10^{18}$ atoms/cm^3 and that in FZ wafer is less than $1x10^{16}$ atoms/cm^3. This indicates that the light induced degradation in CZ grown silicon solar cell is linked with oxygen. Also, silicon solar cells developed using CZ wafers, doped by acceptors such as gallium, do not show degradation in their electrical characteristics. Only boron doped CZ wafers show the LID effect. This confirms that the LID effect in

single crystalline Si solar cells made from CZ wafers are related to boron and oxygen complexes. Active p-type material of the cell degrades by the interaction of boron-oxygen complexes formed due to charge carries generated by the effect of light [3].

Light induced degradation of crystalline silicon solar cell is characterized in n+/p cells by a time dependent reduction in cell parameters. The reduction is observed either when the cells are operated at open circuit under illumination or operated in the dark under forward bias conditions [4, 5]. In both the cases, the formation of metastable recombination centers takes place which is related to the boron and oxygen content in the base material of crystalline silicon solar cells. The energy level of the light induced recombination center is relatively close to the middle of the silicon band gap [6, 7]. Because of boron-oxygen related defects, bulk carrier lifetime decreases until a stable level is reached.

Light induced degradation of crystalline silicon solar cells, fabricated on low iron substrates, can be recovered by annealing them at a temperature of 200 °C for about half an hour. The recombination path can be removed upon annealing, which causes dissociation of the B-O complex. The degradation of lifetime of the wafer is thought to be fully recoverable after annealing and it should bring all the solar parameters back to their initial states. The degradation, produced both by illumination and by using forward voltage, suggests that the time constant of the degradation and reactivation of the responsible recombination center, is not dependent on illumination but excess charge carriers. All these effects have important practical disadvantages in commercial terms and a more satisfactory solution would be to understand the formation mechanism of the

defects that are responsible for the degradation and eliminate them in conventional CZ and cast material.

1.1 Motivation

The effect of light induced degradation (LID) in Czochralski silicon solar cells has been reported in the literature as early as 1973 [8]. In the following years, several attempts were made to develop a defect model to explain observed lifetime instabilities in boron doped CZ- silicon solar cells. Experiments show that, if both boron and oxygen are present in more than limited amount in silicon wafer, only then prolonged illumination reduces the minority carrier lifetime. The light induced degradation is attributed to a reduction of the minority carrier lifetime as a result of the formation of highly recombination-active boron oxygen complexes under carrier injection. Various defect models have been proposed in the literature. The first defect reaction model proposed which did not involve any metallic impurities was B_iO_i model [9]. The important feature of this model was the formation of a defect pair composed of one interstitial boron and one interstitial oxygen atom (B_iO_i) during illumination of CZ silicon. Since energy determined by deep level transient spectroscopy for B_iO_i did not match with energy level of light induced boron-oxygen center, Schmidt and Cuevas proposed a new core structure consisting of one substitutional boron atom and several interstitial oxygen atoms [10].

Bourgoin et al. proposed a possible atomic configuration of the boron-oxygen complex in which the B_s atom is surrounded by three O_i atoms [11]. Based on the measured normalized defect concentration as function of boron concentration [B_s] and oxygen concentration [O_i], Schmidt and Bothe proposed a defect model involving interstitial oxygen dimers (O_{2i}) [12]. In this model, fast diffusing oxygen dimers are

captured by substitutional boron to form a B_s-O_{2i} complex, which acts as a highly effective recombination center [13].

Even for one substitutional boron and interstitial oxygen dimers defect model, researchers have proposed several types of oxygen dimers in trying to relate the clustering of oxygen to the formation kinetics. Some of them are: staggered oxygen dimers, skewed dimers and double Y-lid dimers [14, 15]. Almost all models assume an oxygen containing fast diffusing species with a low activation energy for migration. Diffusion of oxygen dimers through silicon depends on the orientation of both dimers as well as silicon crystal [16].

It is shown that the substitutional boron atom which has trapped an oxygen dimer, B_s-$O_{2i,}$ exhibits a charge driven bistability. The two most stable structures are square form of B_s-O_{2i} (B_sO_{2i} sq) and staggered form of B_s-O_{2i} (B_sO_{2i}st) [17]. Calculations later showed that, under light, transition from squared dimer to staggered and vice-versa (sq ↔st) takes place in an efficient way [18]. Recently, it is found experimentally that the saturated concentration of B-O complexes is proportional to the staggered O_{2i} concentration in CZ silicon samples [19]. In spite of many models, some of the fundamental questions are left still unanswered: (i) How do electrons and holes recombine through the B_sO_{2i} complex? (ii) Why is the B_sO_{2i} complex a more effective recombination center than the uncomplexed O_2 dimer? (iii) What explains the observed light induced B_sO_{2i} formation kinetics? A comprehensive understanding of the physical mechanism of light induced degradation of B-doped Cz silicon solar cell is still to be found.

Light induced degradation is a current topic in silicon solar cell research and is studied by a rather small number of research groups, using relatively small sets of samples [20-22]. Consequently, there is a large diversity in the results reported in the literature, and the details of cell degradation and recovery mechanisms are sketchy. For example: (i) Reported degradation in the efficiency of the cells fabricated on the wafers of about same resistivity ranges between 0.5 and 1.5% absolute (up to 10% relative) [13, 23, 24]. (ii) It is believed that LID can be fully recovered upon annealing [8, 22]. (iii) There is a vast difference in temperature-time performance for recovery by thermal annealing, for example, 350 °C for 10 minutes [9], 200 °C for 30 minutes [17, 25], 200 °C for 10 minutes [26], or 820 °C for 8 seconds [27].

Researchers who worked on LID effect of silicon solar cells are claiming that LID is either by boron-oxygen complexes or by iron-boron complexes [28, 29]. Main objective of this research is to see if there is another component in LID other than B-O complex in CZ silicon solar cell containing low iron. One issue that has not been addressed to date is that a finished solar cell has a multilayer structure, and that is also possible to have some degradation at the interfaces upon illumination. In particular, it is known that the SiN:H/Si interface has defects and a strong positive charge accumulation that can be affected by light [30, 31]. Hence, LID is expected to have an interface/surface component, if ionization of this charge occurs or if there is an increase in the density of interface states, D_{it}.

Recently, much effort has been put into mitigating light induced degradation, since LID causes severe efficiency loss even during one day of solar illumination. Up to now, electrical and structural characteristics of the B-O trap are not fully understood.

Thus trap formation and annihilation mechanism need to be further investigated to find the conclusive explanation of the effect.

1.2 Statement of the Problem

Because of the growing population of the world and change in lifestyle, worldwide demand for electrical energy is increasing day by day. But the conventional sources of energy such as coal, natural gas, oil etc. have limited reserve. Burning of the fossil fuels is resulting in significant increase in carbon dioxide (CO_2) and other greenhouse gases in the environment. The earth is being pushed to the state of high CO_2 concentration leading to high pollution and potential global warming. If the fossil fuel is used at the same rate as being used now, warming of the earth over the next 40-50 years could have devastating effect on sea levels, climate, agriculture and economic developments.

One method of weaning away from the fossil fuel is to use alternative renewable energy to produce fuels and electricity. Among the various alternatives, photovoltaic (PV) or solar electricity offers a unique opportunity to solve the energy and pollution problem at the same time. Photovoltaics represents one of the evolving sources of energy in which sunlight is directly converted into electrical energy by using semiconductors that exhibit the photovoltaic effect. Solar energy is free, unlimited, and not localized in specific part of the earth. Solar cells have numerous advantages such as reliability, long lifetime, silence, flexibility, relatively low maintenance cost, pollution free operation are few to name.

Photovoltaic power generation employs solar panels composed of a number of solar cells made from photovoltaic materials. Materials currently used for photovoltaics includes crystalline silicon (mono and multi), amorphous silicon, cadmium telluride

(CdTe), copper indium gallium selenide/sulphide (CIGS), organic/polymer thin films, single junction III-V cells and multi-junction cells. Crystalline silicon (c-Si) based photovoltaic technologies are the major part of the energy market today and will occupy an increasingly prominent role in the future. They are the most mature of all PV technologies and compare successfully against other competitors. This is shown in Figure 1.1, with c-Si solar cells contributing 81% of the world's market, while other PV technologies are in single digits [32]. However, contribution of solar cells to the total energy supply of the world is a small fraction [33]. This is because of the cost of generating electricity from solar cells. Solar electricity is still more expensive than most of the other forms of small-scale alternative energy production from conventional fossil fuels [34].

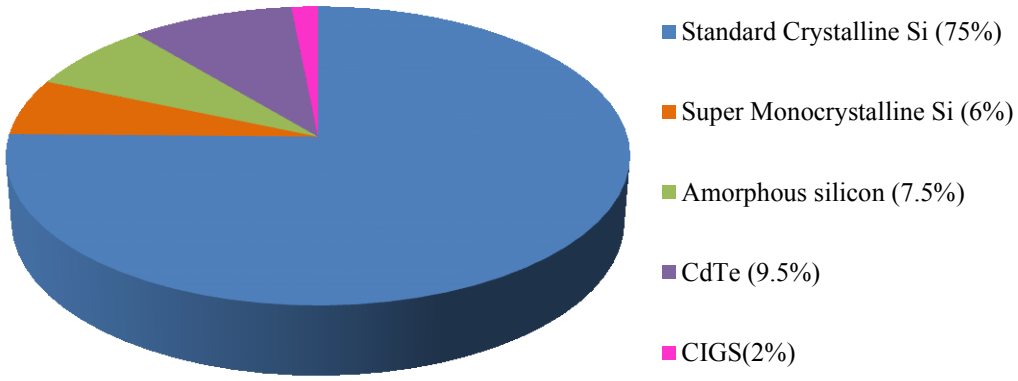

Figure 1.1 PV cells production in 2011, from [32].

In CZ Si photovoltaic technology, approximately 30% of the costs are in the crystal ingot, with 20% in wafering, 20% in cell fabrication, and 30% in module

preparation. So the best way of reducing cost of silicon based PV modules is to minimize the use of the silicon by reducing thickness of the solar cell and reduce the cost of wafer production techniques involved. It should be kept in mind that cost reducing methods should not decrease the efficiency of the solar cells.

The theoretical limit of energy conversion efficiency of single junction crystalline silicon solar cells under one sun illumination is about 31% [35]. Later it was improved in calculation and found to be 34% [36]. But highest efficiency achieved for silicon solar cell (FZ) in laboratory is 25% [37]. On the other hand, current industrial cell efficiencies are only in the range of 15-22% [38]. There is a need for a low cost solution to increase efficiencies of the commercial cells. Improvements in light trapping in silicon solar cell, contact formation, surface passivation etc. definitely result in increase in efficiency.

Czochralski silicon has been a dominant source for PV substrates. Almost 30 % of the PV modules produced currently is based on CZ silicon. But light induced degradation in boron doped CZ silicon solar cells has been recognized as a significant cause for minority carrier lifetime degradation during cell operation. The decrease in minority carrier lifetime due to metastable defect formation during carrier injection reduces efficiency of the CZ silicon solar cells.

The objective of the research in this thesis is to study B-O defect formation and dissociation in CZ Si experimentally and their effects on solar cell performance. Up to now, electrical and structural characteristics of the B-O trap are not fully understood. Thus trap formation and annihilation mechanism need to be further investigated to find the conclusive explanation of the effect. This is done by addressing the major efficiency

limiting mechanism in each cell. These studies have been performed using facilities that are available at the National Renewable Energy Laboratory, Golden, Colorado.

This project proposes to expand upon previous works in the area of B-O defect formation and dissociation in boron doped Cz silicon solar cells. The influence of light illumination on open circuit for minority carrier degradation and recovery process in silicon wafer as well as in silicon solar cells will be studied. The dark I-V characteristics will be used to calculate series and shunt resistance present in the cells. These two resistances for different light soaking time will be calculated and their effect on LID will be explained. Dark I-V characteristics will be used to deduce the saturation current densities J_{01} and J_{02} using the two diode model of the solar cell. Increase or decrease in the values of saturation current densities as a function of light soaking time or annealing will be explained on the basis of loss or recovery of bulk life time. Contribution of bulk and surface effect on LID will be separated. For this purpose, degradation produced in the CZ - silicon solar cell will be compared with their sister wafers. Surface related degradation is mostly because of the SiN:H-Si interface. This interface is known to have interface defects and a strong positive charge accumulation that can be affected by light.

Good solar cells must absorb the incident light strongly. By using the spectral response technique, whether the degradation of silicon solar cell is dependent on infrared or ultraviolet light or it is independent of the illumination spectra is studied. Ultraviolet rays are absorbed at the surface of the cell, which will be advantageous to differentiate between surface and bulk effects. Four-point probe technique will be used to measure the resistivity of the silicon wafer as a function of light soaking time.

Cast multi-crystalline silicon is also used for silicon PV. Mc-Si used for industrial photovoltaic production also contains boron and oxygen. The extent of the effect of LID on low cost mc-Si is still unknown. Limited information exists on cast multi-crystalline silicon. LID has been observed on some cast mc-Si with minority carrier lifetime greater than 5-10 μs [39, 40]. In mc-Si material, lifetime is generally too low to detect any LID. But there are recent reports on small LID (about 1% relative) in multi-crystalline Si solar cells [41]. Special attention is given to show whether this small LID effect in mc-Si is associated with the surface effect or something else.

1.3 Thesis Structure

The main aim of the work presented in this thesis is to investigate the formation and dissociation of the boron and oxygen related metastable defect in single crystalline CZ solar cells generated due to excess charge carrier by the effect of illumination or forward bias in dark. This will help to understand the light induced degradation of silicon solar cells and the associated major contributors for the loss of energy conversion efficiency.

This thesis has been arranged in the following manner.

Chapter 2 deals with the review of the solar cell fundamentals. Basic equations for various critical parameters of silicon wafer and solar cells are presented. The physics of the working of silicon solar cell, related loss of the energy due to reflection from the surface etc. are also explained in this chapter.

The experimental procedure and techniques used in the course of this work, together with the description of the instrumentation, are described in Chapter 3. This includes details of the working principles of XT-10 DC testing system, Concentrator cell

flash tester, Quantum Efficiency, Lifetime measurement system, PVSCAN for LBIC measurement, and four-point probes.

In Chapter 4, a review of light induced degradation in silicon solar cell is presented to provide the most recent understanding in the field of boron-oxygen related metastable defects formation. Experimental details of sample preparation along with important processes occurring during data collection are discussed in Chapter 5.

In Chapter 6, results and discussions are presented. Variation in electrical properties of the mono-crystalline silicon solar cell as a function of illumination time is investigated. Formation of defect density and its effect on carrier lifetime of silicon wafer due to excess charge carriers is given. Based on the observed changes in cell parameters, a new component of light induced degradation is proposed. This is the first time wherein the interface effect is considered as one contributor to the LID of silicon solar cells. In order to verify this claim, light induced degradation of multi-crystalline silicon solar cell was also investigated toward the end of this chapter.

CHAPTER 2

SOLAR CELL FUNDAMENTALS

2.1 Silicon Materials

Crystalline silicon solar cells are made from silicon semiconductor material, which is made from SiO_2, or sand. It is actually a special kind of sand with a minimum amount of impurities. Measured by mass, silicon is the second most abundant (27.7% in the earth's crust) raw material in the earth [42]. The mining and transport of silicon do not require high-tech equipment but still use large amount of energy in the form of labor and needs expensive purification processes.

Silicon is an environmentally friendly material and its waste does not pose any special problems. It can be easily melted, shaped and formed into mono-crystalline or multi-crystalline ingots and wafers. High purity silica sand found in several areas around the earth is loaded into huge electrode-arc type furnaces and it is melted at a temperature of about 1500-2000 °C. During melting, carbon is mixed with silica; this results in oxygen being removed from the silica in the form of carbon dioxide or carbon mono-oxide. In this way, molten metallurgical grade (MG) silicon is obtained which is further treated for the removal of other impurities. MG silicon is reacted with hydrochloric acid (HCl) to make silicon containing gases ($SiCl_4$ or $SiHCl_3$). These silicon compound gases undergo some distillation and purification process to isolate the main silicon containing gas trichlorosilane (TCS), $SiHCl_3$. Trichlorosilane gas is processed in a plasma reactor and solidified in the form of solar grade (SG) multi-crystalline ingots.

The solar grade ingots, obtained in this way, are still not good enough for making solar cells. They are again melted and doped with suitable impurity to obtain high purity doped ingots from which solar grade wafers are sliced and developed as solar cells**.**

2.1.1 Single Crystalline Silicon

Single-crystal silicon used in solar cell does not contain grain or grain boundaries. The material is one crystal. Crystalline silicon has an ordered crystal structure, with each atom ideally lying in a pre-ordained position. It therefore allows ready application of the theories and techniques developed for the crystalline material and exhibits predictable and uniform behavior. It is, however, the most expensive type of silicon, because of the careful and slow manufacturing processes required. The cheaper multicrystalline or polycrystalline silicon, and amorphous silicon are, therefore, increasingly being used for solar cells, despite their less ideal qualities.

Float Zone (FZ) and Czochralski (CZ) grown methods are relatively well known for single crystalline silicon growth. Because of the large difference in cost premium (100% or more), at the present time, FZ Si is used for premium high efficiency cell application and CZ silicon is used for higher volume, lower cost applications.

In the Czochralski method of single crystalline silicon growth, ingots are produced by melting purified multi-crystalline SG silicon in a special quartz furnace, in which a long, cylindrical silicon ingot is pulled up from the melt as single crystal silicon. Usually 30-40 kWh/kg energy is used during single crystalline silicon growth by this method. For solar cell applications, a calculated amount of boron salt, a p-type dopant is added in this stage. The ingots, 10-15 cm in diameter and 1 to 2 m in length are grown by this method. The most cost conscious PV industry has achieved electrical power

reduction by 40%, argon usage by 50% and productivity increase by 15% by using improved Czochralski method [43].

2.1.2 Multi-Crystalline Silicon

Multicrystalline silicon refers to the silicon with crystals or equivalent grains separated by disordered regions called grain boundaries. They are composed of many single-crystal regions. These single crystal regions (grain) exhibit long-range order. The various grains comprising a poly-crystalline solid may or may not have their lattices randomly oriented with respect to one another. The grains can be thought as separate pieces of single crystal silicon separated by boundaries. There are numerous defects (grain boundaries and dislocations) which prevent electrons and holes from freely moving across, and contribute to the recombination process, minimizing the photoelectric effect. If there is correlation in the orientations of the grains, the material is referred to as being an oriented polycrystalline solid. Grain boundaries can have a significant influence on physical properties. For example, they can getter dopants or other impurities, store charge in localized states arising from bonding defects, and, through the stored charge, give rise to electrostatic potential energy barriers that impede transport [44].

The techniques for the production of multicrystalline or polycrystalline silicon are less critical and hence cheaper, than those required for single crystalline silicon. The grain boundaries reduce the cell performance by blocking carrier flows, allowing extra energy levels in the forbidden gap, thereby providing effective recombination sites, and providing shunting paths for the current flow across the p-n junction.

To avoid significant recombination losses at grain boundaries, grain sizes in the order of a few millimeters are required. This also allows single grains to extend from the

front to the back of the cell, providing less resistance to carrier flow and generally decreasing the length of the grain boundaries per unit cell. Such multicrystalline material is widely used for commercial solar cell production. Multi-crystalline silicon material is produced by melting SG silicon in a large cube like crucible by directional solidification or electromagnetic semicontinuous casting techniques [45]. Large (mm to cm in width), randomly oriented grains (columns), crisscross the bulk.

2.1.3 Silicon Wafer Manufacturing Process

After an ingot is grown, its surfaces must be trimmed off to make it a square ingot by using ingot saw. The smooth squared block of silicon is then sectioned into square bars of desired dimensions and variable lengths. High speed wire saws are used to slice the wafers from the bars. Wafer production is dominated by the use of multiple wire slurry sawing which uses brass-plated steel wire and silicon carbide abrasive. The wire used for wafer sawing must be of exceptional quality, with no defects that could cause breakage during a cut. Wafers are sliced to the desired thickness and removed from the wire saw with the holders. The wafers are separated and cleaned to remove cutting oils and abrasive residues left on the wafer surfaces from the slicing process. Additional inspection and testing procedures are carried out as needed to ensure the quality of the wafers prior to processing into solar cells [46].

2.2 The p-n Junction

The p-n junction is the integral part of the solar cell operation, since it is where photoelectric process starts and electric current is generated. A p-n junction is established when a layer of p-type semiconductor and a layer of n-type material meet together

metallurgically. The n-region and the resulting p-n junction are created during the diffusion process by doping the top of the p-type wafer with phosphorous [47].

Positive charge carriers can move in p-silicon and negative ones in n-silicon. If two electrically neutral p-and n materials are brought together, there is no electrical impulse (electric field) which could lead to a spontaneous union of the positive and negative charge carriers. As a result of natural mobility (thermal agitation), however, holes from the p-side diffuse in the boundary layer into the n-silicon and recombine there with the electrons. Conversely, there is also a diffusion of electrons from the n-layer into the p-layer. This process is not kept up long enough for all the free electrons to be combined with holes or vice versa. As long as the diffusion succeeds, there is an electric field between the positive donors and the negative acceptors which are no longer neutralized by increasing diffusion. Figure 2.1 shows the p-n junction.

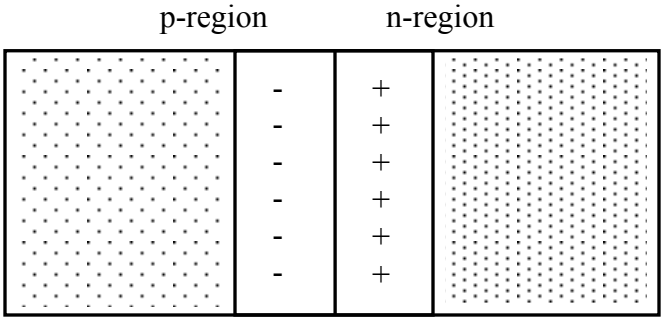

Figure 2.1 Formation of p-n junction showing depletion region.

The resulting charge field is now so directed that it counteracts the combination, that is, the straying of the electrons towards the p-silicon and the movement of the holes toward the n-silicon. Therefore all the holes cannot combine with the electrons. Equilibrium is produced between the effect of diffusion and the reversing energy of the

space charge field, i.e., the space charge density is at its greatest. The space charge sets up an electrostatic field which opposes further diffusion across the junction. At this point, the Fermi levels of the p and n type layers are equal. The magnitude of the potential step is equal to the difference between the Fermi level locations on the two sides of the junction. In other words, the difference in the work function is taken by a step in the conduction and valence band edges, called the built-in bias (barrier potential) V_b. The expression for potential threshold results from the fact that the electrons or holes remaining behind cannot jump this potential threshold unless energy is supplied in the form of heat. Figure 2.2 shows the band bending of a p-n junction in equilibrium.

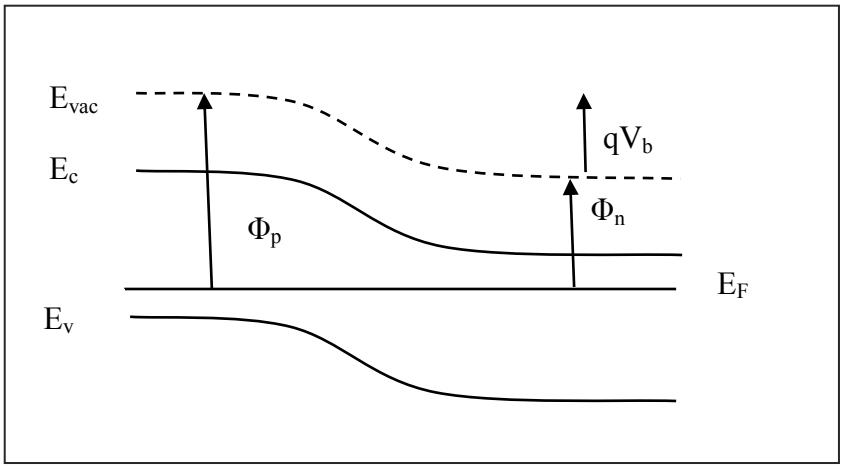

Figure 2.2 Energy band diagram of a p-n junction solar cell in equilibrium.

The energy difference between the top of the valence band (electron at rest) and the bottom of the conduction band (electron with extra energy) is known as the band gap. Different materials have different band gap energy and, that, for silicon is 1.1 eV; this corresponds to the threshold wavelength of 1100 nm.

2.2.1 p-n Junction Under Illumination

When photons from sunlight with proper energy impinge on a p-n junction, they penetrate into the cell material and impact onto the electrons thus transferring energy to them and breaking the electron hole pairs. This creates free electrons which start moving around, while the holes from the corresponding electron hole pairs are left in their original place. Thus n and p regions are then enhanced above their equilibrium values, and the electron and hole quasi Fermi levels are split. If electron hole pairs are generated within the depletion region of the p-n junction, the electric field at the depletion region effectively separates the holes from the electrons which are forced towards the n-type region and are finally extracted from the cell as electric current. Figure 2.3 shows the energy band diagram for a p-n junction solar cell, including the generation of the charge carriers.

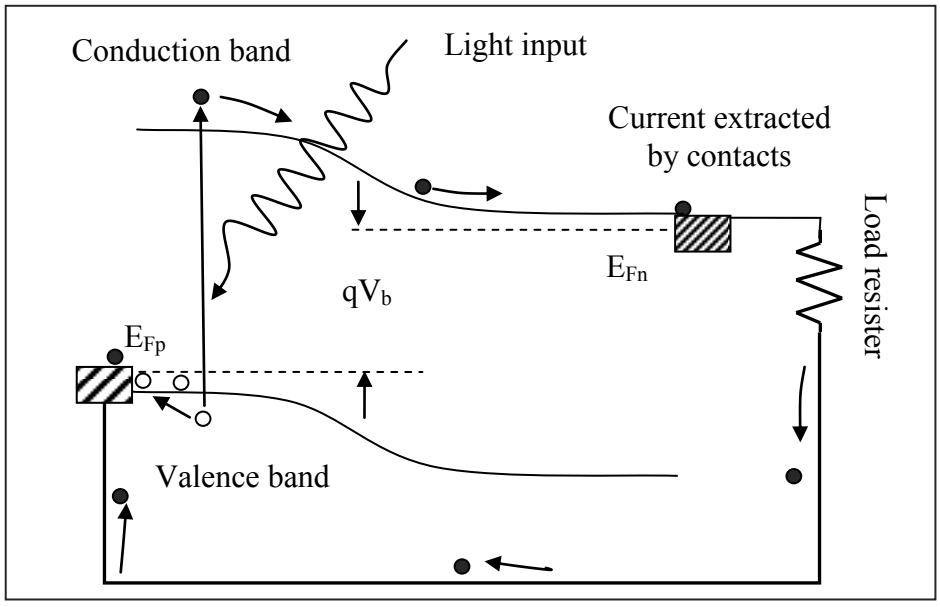

Figure 2.3 Energy band diagram for a p-n junction solar cell showing the generation and transport of charge carriers.

Electrons and holes created by the action of light are first elevated to higher energies. Instead of being collected by external junction and external electrical contacts, these charge carriers can come back together and recombine in three different ways: (i) radiatively, giving up the excitation energy in the form of an emitted photon; (ii) nonradiatively through traps, recombination centers; (iii) through excitation of conduction band electrons to higher levels producing a phonon or lattice vibration. They are described in detail in Section 2.2.4.

2.2.2 Power Generation

Solar cells are characterized by the power they generate, which is at a maximum when the current and voltage are at their maximum levels. If the electron in the conduction band survives the aforementioned recombination processes, it may be collected by the external circuit to produce a voltage, as it recombines with a hole in the ground state or valence band. This voltage, generated by the solar cell, is the difference between the chemical potentials of the electron and the hole in conduction band and valence band respectively. These are the Fermi levels of holes in p-side, E_{Fp}, and electrons in n-side, E_{Fn}, shown by dotted lines in Figure 2.3.

A combination of maximum current and maximum voltage maximizes the generated power and is called the maximum power point (MPP) of the cell.

$$MPP = I_{max} * V_{max} \tag{2.1}$$

2.2.3 Light Absorption

The number of photons that can be absorbed by a solar cell is determined by the optical property of the material. There are several fundamental parameters that need to be considered when characterizing a solar cell material. They are the complex index of

refraction, the extinction coefficient, the absorption coefficient and absorptivity. Optical constant of a material is expressed as a complex dielectric function $\varepsilon = \varepsilon_1+i\varepsilon_2$ or as a complex refractive index [48]:

$$n(\lambda) = n_1(\lambda)+iK(\lambda) \tag{2.2}$$

The real part of the refractive index, n_1, represents the speed of light in vacuum compared to the speed of light in the medium, and imaginary part, K, corresponds to the amount of light absorbed as it passes through the material (extinction coefficient of material) and is responsible for damping of the wave. The extinction coefficient is related to the absorption coefficient by the relationship:

$$\alpha(\lambda) = \frac{4\pi K(\lambda)}{\lambda} \tag{2.3}$$

The absorption coefficient, $\alpha(\lambda)$, is critical to solar cell performance, which describes the decrease in light intensity as the beam of light passes through the material. If reflection and interference effects are not important in a solar cell structure, then monochromatic light entering the cell's absorber at x=0 with intensity $I_0(\lambda)$ (photons per unit area per unit time per unit bandwidth) is expected to have the intensity $I(\lambda,x)$ at some point x in the material and is given by:

$$I(\lambda,x) = I_0(\lambda)\exp\{-\alpha(\lambda)x\} \tag{2.4}$$

Equation (2.4) is known as the Beer-Lambert law [49]. When Beer-Lambert law is valid, absorption coefficient, $\alpha(\lambda)$, has a very simple interpretation that $1/\alpha(\lambda)$ is the absorption length for light of wavelength λ in a material with $\alpha(\lambda)$. It should be pointed out that the absorption coefficient of a material, although a function of wavelength, is not affected by the thickness of the wafer, but the optical absorption is a strong function of the thickness and geometry of the solar cell.

The quantum absorptivity is the fraction of the incoming light at a given photon energy, that is absorbed by the material to produce an excited state such as an electron-hole pair. Not all the absorption in a solar cell material creates electron-hole pairs. (i) Photons with energy less than the band gap energy will interact weakly with semiconductor material, passing through it as if it were transparent. (ii) Photons with just enough energy to create electron-hole pairs and which are efficiently absorbed to generate free electrons can produce power as a result. (iii) Photons with energy much greater than the band gap that are strongly absorbed will not contribute to liberating electrons because such electrons quickly thermalize down to the band edges.

2.2.4 Carrier Lifetime and Recombination in Silicon

In extrinsic semiconductors, there are thermally generated minority and majority carriers. They are continuously created and destroyed. The time between the generation and recombination of an electron is called the lifetime. It varies from a few nanoseconds to several microseconds depending on the perfection of the crystal and other factors.

Extra electrons and holes can be created by photo excitation. When an external stimulus is applied to a semiconductor such as light, heat, or voltage, carriers are injected in excess of equilibrium values. When the light is switched off, the system must return to a state of equilibrium and the electron-hole pairs generated by the light must disappear. With no external source of energy, the electrons and holes wander around until they meet up and recombine. The average time required for these excess carriers to recombine with each other is referred as the minority carrier recombination lifetime. For silicon, this is typically 1 μs. Similarly, the carrier diffusion length is the average distance a carrier can move from the point of generation until it recombines. For silicon, this is typically 100-

300 μm. These two parameters give an indication of material quality and suitability for solar cell use. This merging of free electron and a hole is called recombination. Any defects or impurities within or at the surface of the semiconductor promote recombination. Recombination can occur either at the surface of the semiconductor or within the bulk of the device. A typical silicon solar cell wafer is 300 μm thick. A large number of the excited carriers can be affected by bulk and surface recombination [50].

2.2.4.1 Bulk. Bulk recombination is characterized by three recombination mechanism that vary in importance, depending on the following: (i) the level of external stimulus applied, (ii) the semiconductor band gap type (direct or indirect), and (iii) the amount and type of impurities present. These mechanisms are Shockley-Read-Hall recombination, Auger recombination, and radiative band to band recombination. These mechanisms can occur in parallel; in such case, the recombination rate is just the sum of those for individual processes. These mechanisms are well documented in the literature [1, 47, 51]. Recombination of excess carriers occurs after an external stimulus (voltage or light) is applied. Under steady state conditions, the recombination rate is equal and opposite to the generation rate. When the stimulus is removed, the injected carriers, Δn, recombine and the sample reverts to the equilibrium state. Bulk lifetime is defined as:

$$\tau = \frac{\Delta n}{R} \tag{2.5}$$

where, R is the recombination rate, τ is the minority carrier lifetime, and Δn is the excess minority carrier concentration.

2.2.4.2 Shockley-Read-Hall Recombination. The most common type of recombination in the bulk or base of the solar cell takes place via energy levels within the forbidden energy gap of the semiconductor. It is plausible that the inclusion of atoms that do not have electron structure of pentavalent or trivalent dopant will give rise to defect levels with energy levels that need not lie near the edge of the band. They may lie deeper in the forbidden gap, and are thus called deep defects. These impurity levels trap the charge carriers, so they are also called trap levels.

Crystalline silicon is an indirect bandgap semiconductor and hence recombination losses in this material occur largely via defect levels within the band gap. These defects are located within the volume and at the surfaces of the sample. An electron from conduction band recombines with a hole in valence band via a defect level within the band gap. The theory of this mechanism was developed by Shockley and Read [52] and Hall [53]. It was further developed and expanded later [54, 55]. The theory can be explained with reference to Figure 3.4. For an energy level corresponding to the trap, four fundamental processes are possible: (1) An electron is captured by an unoccupied energy level; (2) an electron is emitted from an occupied level into the conduction band; (3) a hole is captured by an occupied energy level; (4) a hole is emitted into an unoccupied state in the valence band. The energy liberated during the recombination event is dissipated by lattice vibrations or phonons.

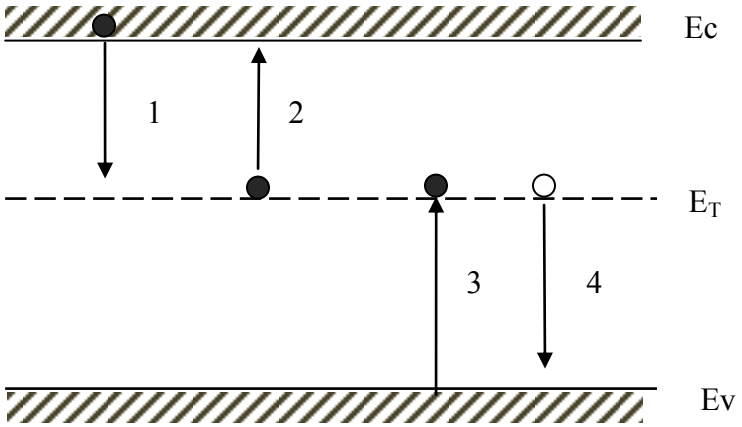

Figure 2.4 Recombination by defect levels.

The equation used to describe the Shockley-Read-Hall (SRH) recombination lifetime is as follows:

$$\tau_{SRH} = \frac{\tau_{po}(n_o + n_1 + \Delta n) + \tau_{no}(p_0 + p_1 + \Delta p)}{(n_0 + p_0 + \Delta n)} \tag{2.6}$$

where,

$$n_1 = n_i e^{(E_T - E_i)/kT}; p_1 = n_i e^{-(E_T - E_i)/kT} \tag{2.7}$$

$$\tau_{n0} = \frac{1}{\sigma_p v_{th} N_T}; \tau_{p0} = \frac{1}{\sigma_n v_{th} N_T} \tag{2.8}$$

and n_0 and p_0 are the equilibrium electron and hole concentration, n_i is the intrinsic carrier concentration Δn and Δp are the injected carrier concentrations, τ_{n0} and τ_{p0} are the carrier lifetimes if the trap resides at midgap, ν_{th} is the thermal velocity, σ_p and σ_n are the capture cross section for holes and electron, N_T is the trap concentration, E_i is the intrinsic Fermi level, and n_1 and p_1 are the number of electrons or holes in the conduction or valence band when the Fermi level coincides with the trap energy level, E_T [4, 56]. All the above

equations for SRH recombination have been written for one localized state group at some energy E_T in the energy gap. If gap state distribution is present, there must be corresponding states for the other gap states at other energies. Therefore, the total SRH recombination is the sum of all these contributions.

2.2.4.3 Radiative Band-to-Band Recombination. Electrons in the conduction band return to the valence band, with the release of light energy thus annihilating the same number of holes. Radiative recombination in silicon solar cells is often neglected because of its indirect bandgap structure. A photon assisted recombination event is often required for electrons in the conduction band, E_c, to recombine with the holes in valence band. Since it takes three quantum particles to consummate the recombination event, it is a slow process for indirect bandgap materials, such as silicon, which means indirect semiconductors should have longer charge carrier lifetime. Figure 2.5 demonstrates radiative recombination in a direct bandgap semiconductor.

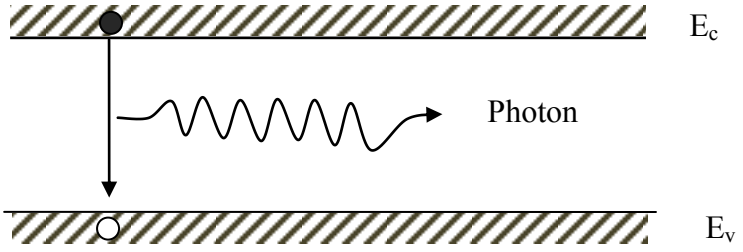

Figure 2.5 Radiative recombination in direct bandgap semiconductor.

The radiative lifetime, τ_R, is given by:

$$\tau_R = \frac{1}{B(n_0 + p_0 + \Delta n)} \tag{2.9}$$

where, band to band recombination coefficient B is $1x10^{-14}$ cm^3/s for crystalline silicon at 300 K [57]. The radiative lifetime in silicon is essentially constant below 10^{18} cm^{-3} injection level.

2.2.4.4 Auger Recombination. An electron in the conduction band will lose a large amount of energy while recombining with a defect center or a hole in the valence band if it can transmit this energy to another nearby electron in the conduction band. The second electron is thereby excited high into the band and can easily return to the bottom of the band by sequential phonon scattering. This process is called Auger recombination. It was originally proposed by Beattie and Landsberg [58]. Several types of Auger recombination are possible depending on either the recombination occuring in an ionized defect state or in the valence band. The energy set free during the Auger recombination can be used to accelerate a second electron or a hole. Smaller electron mass is the reason for a preference for the acceleration of a second electron. Figure 2.6 illustrates these two processes.

Auger recombination is dominant at high injection levels ($>10^{17}$ cm^{-3}) or in heavily doped regions. Auger lifetime is described by:

$$\tau_{Aug} = \frac{1}{c_n n^2 + c_p n \Delta n} \tag{2.10}$$

$$\tau_{Aug} = \frac{1}{c_p p^2 + c_n p \Delta n} \tag{2.11}$$

for n-type or p-type, respectively [50, 56].

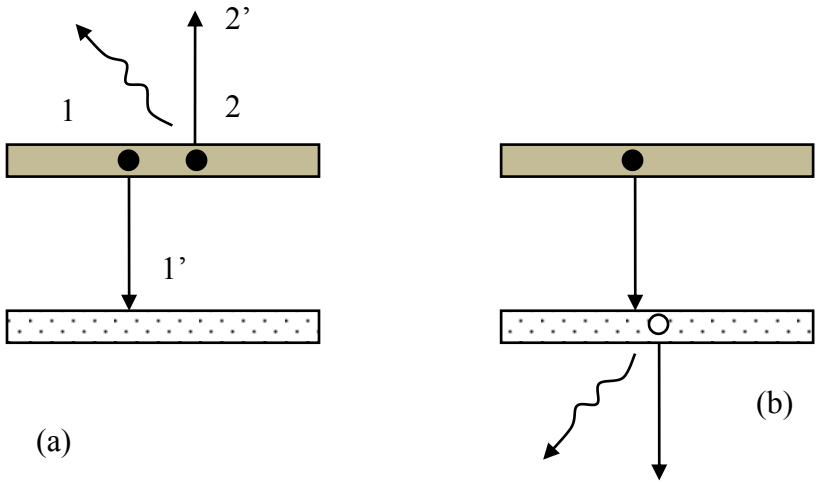

Figure 2.6 Auger recombination involving (a) a second electron (b) a second hole.

For terrestrially operated one sun solar cells, Auger lifetime is not important in the bulk or base of the device; however, it is dominant in the emitter and back surface field (BSF) regions.

2.2.4.5 Surface Recombination. In addition to the bulk recombination via the three mechanisms mentioned above, carriers also recombine at the surface. Any defects or impurities within or at the surface of the semiconductor promote recombination. The high recombination rate in the vicinity of a surface depletes this region of minority carriers. Therefore, surface recombination rate is limited by the rate at which minority carriers move toward the surface. At the surface of a semiconductor crystal, the bond structure is altered and the largest disturbance in the symmetry of the lattice is often observed. A large number of non-saturated (dangling) bonds exist and give rise to surface states that act as traps in the forbidden gap, as in SRH bulk defects discussed earlier. There are processing related surface defects due to dislocations or chemical residues and metallic depositions on the surface. Surface states are treated in the same manner as SRH traps but

are present only on a two-dimensional plane. Instead of a recombination lifetime for minority and majority carriers, a parameter called surface recombination velocity is used to specify the recombination at a surface. The equation governing the surface recombination velocity for a single trap (designated by n_1 or p_1) is given by:

$$S \cdot \Delta n_s \equiv U_s = \frac{S_{no} S_{po} (n_s p_s - n_i^2)}{S_{no}(n_s + n_1) + S_{po}(p_s + p_1)} \tag{2.12}$$

with $S_{no} = \sigma_n \nu_{th} N_{st}$ and $S_{po} = \sigma_p \nu_{th} N_{st,}$

S is the surface recombination velocity, Δn_s is the excess minority concentration at the surface, S_{no} and S_{po} are the surface recombination parameters for electrons and holes, n_s and p_s are the electron and hole concentrations at the surface, σ_n and σ_p the capture cross section for electron and holes, and N_{st} is the number of surface states per unit area. [50].

The effective lifetime given by the parallel contribution of four mechanisms for a given cell width (W) is described by:

$$\frac{1}{\tau} = \frac{1}{\tau_{SRH}} + \frac{1}{\tau_B} + \frac{1}{\tau_{Aug}} + \frac{2S}{W} \tag{2.13}$$

The solar cell's surface area, regardless of the surface finish, is a most critical area, for it is on or close to it where the photovoltaic effect takes place. The defective surface area will cause the cells to deteriorate quickly or fail after some time in the field. In order to properly characterize and analyze the surface parameters, the background information must be known because S is affected by the doping concentration, surface orientation (100) or (111), dopant type, diffusion, texturing, and chemical or dielectric passivation. Surface passivation is accomplished in two ways: (i) by reducing the number of surface states through deposition or growth of a passivating film (or submersion in a polar liquid) or (ii) by using field effect passivation that drastically reduces the number of

electrons or holes at the surface, thereby limiting recombination because both carriers need to be present. Two of the most successful passivating films for crystalline silicon are a deposited SiN_x film and a thermally grown SiO_2 layer. Lifetime spectroscopy has become a very powerful tool in characterizing the trap. Using Shockley-Read-Hall theory and measured effective lifetime data, a much better understanding of the trap has been achieved.

2.3 Solar Cells

Solar cell is a large area diode. Electrical charges created by the absorption of light in semiconductor diffuse at different rates within two types of layers in solar cells and are eventually collected and separated at the p-n junction. External contacts allow electrical currents to pass from solar cell to the load. Solar cells are fabricated by using various semiconductor materials but silicon is uniquely favorable as a photovoltaic material. Not only it is one of the most abundant elements in the earth's crust, but its indirect energy band gap, approximately 1.1 eV at room temperature, is a close match for the photons in the solar spectrum.

2.3.1 Solar Cell Fabrication

First of all, wafers are inspected visually and with optical equipment. Resistivity of the wafers is measured by using a four-point probe, and are sorted according to their resistivity. A sample of the wafers are also tested for metal and organic contaminations, which determine the quality of the finished solar cells. The wafers that pass all the initial inspections are cleaned and chemically etched to remove the damage and the oxide formed on the surface. Single crystalline wafers are treated for controlled chemical

etching which removes (4-10 microns) pyramid like structures from the wafer surface. Multi-crystalline wafers are etched with alkaline or acidic solution. The wafers are then rinsed, dried and stored in special containers for processing.

Dried wafers are placed in a diffusion furnace (900-950 °C). Reactive carrier gas, $POCl_3$, is used for n-layer diffusion on top of p-layer. This creates a p-n junction in lightly boron doped wafers. Diffusion process incorporates phosphorous in the wafers side edges, so it is necessary to remove the dopant with wet chemistry or plasma etch. Wafers are then etched in a bath of dilute HF solution to remove any oxides formed during the plasma etch step.

Antireflection (AR) coating (70-80 nm) is deposited via chemical vapor deposition (CVD), or by spraying the chemicals on the wafer and then baking. The purpose of AR coating is to reduce the amount of sunlight reflected from the finished cell surface. Several screen printing steps are used for the metallization on the front and back of the wafer. Silver paste is printed on top surface as fingers and busbars. When the paste dries, the back surface is also printed with aluminum paste.

The wafer metalized on both sides runs slowly through IR-heated furnace under controlled temperature condition. During this process, metal pastes on both sides of the wafer slowly diffuse into the substrate and makes contact with the p-n junction and the back surface. Solar cells are inspected and tested at several stages of the process sequence. Electrical tests are also performed and cells are sent for module preparation. Schematic of the cross section of a standard p-type silicon solar cell is shown in Figure 2.7.

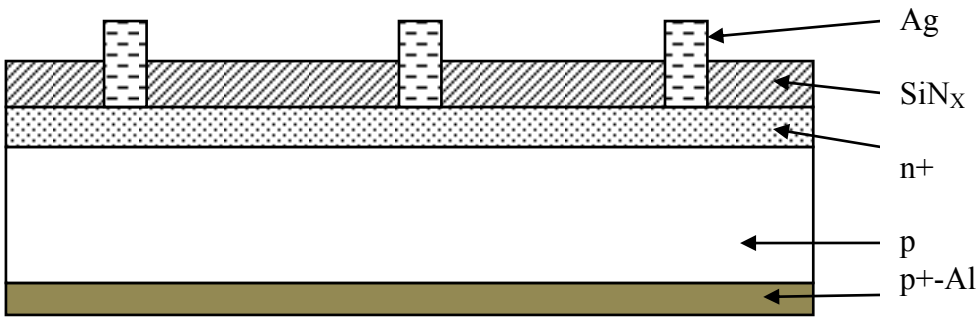

Figure 2.7 Schematic of a standard p-type silicon solar cell.

2.3.2 Current and Voltage

The semiconductor p-n junction forms the solar cell. The space charge region is formed as a result of diffusion of majority carriers across the metallurgical junction, and its width is fixed when the diffusion is counter balanced by the drift of the carriers in the opposite direction, thus setting up a compact but strong electric field as the "collecting junction" in the depletion region. In thermal equilibrium, drift and diffusion current through the depletion region oppose each other, resulting in zero net current flow.

Using light as an external stimulus allows the p-n junction to behave as follows: Part of the solar spectrum is absorbed in a semiconductor through the transfer of optical energy to electrons that are excited into the conduction band, E_c creating holes in the valence band, E_v. The electric field in the depletion region helps in separating these electron-hole pairs, resulting in a voltage or photovoltaic effect.

While discussing the current-voltage characteristics of a solar cell, it has to be started from the "equilibrium condition" (dark current) of the p-n junction. During this state, an equal number of electrons created by thermal excitation are destroyed when they recombine with holes. When a load is present, a potential difference develops between the terminals of the cell. This potential difference generates a current which acts in the

direction opposite to the photocurrent. This reverse current is usually called dark current, $I_{dark}(V)$ which flows across the device under a bias voltage. Figure 2.8 shows the equivalent circuit to analyze the ideal solar cell with short circuit flow of electrons and holes.

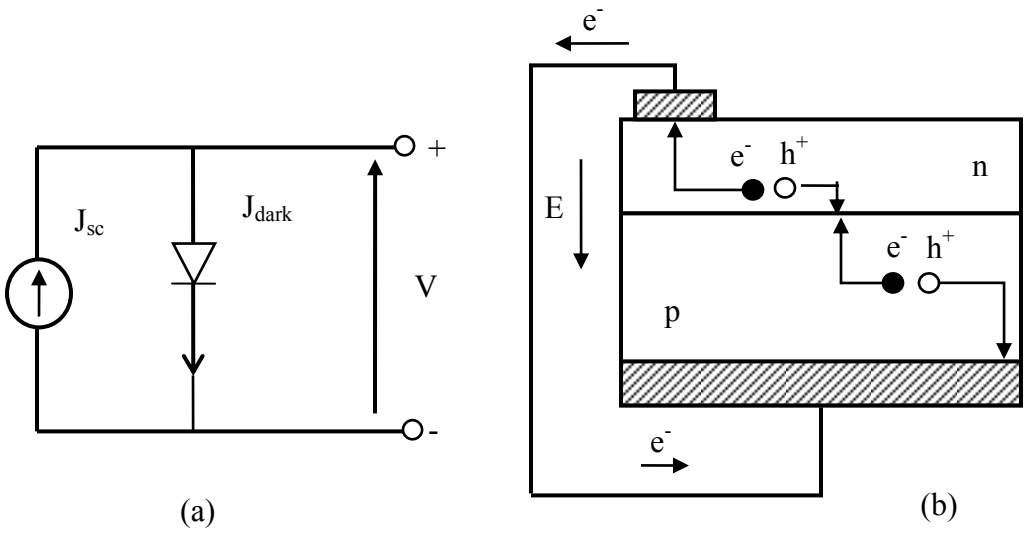

Figure 2.8 (a) Equivalent circuit of ideal solar cell (b) The ideal short circuit flow of electrons and holes at p-n junction.

It is constructive to start with simple diode equations that are used to describe the operation of a p-n junction. The dark current, I_{01}, is the "leakage" current that flows out a diode in the dark under reverse bias and is represented analytically by the following equation:

$$I_{01} = qn_i^2 A\left(\frac{D_n}{L_n N_A} + \frac{D_p}{L_p N_D}\right) \tag{2.14}$$

where, n_i is the intrinsic carrier concentration, A is the area of the diode, N_A and N_D are the ionized concentration of the acceptors and donors, L_n and L_p are the diffusion lengths of electrons and holes, q is the electron charge, and D_n and D_p are the diffusivity constant

for the minority carriers. I_{01} is primarily a drift current because reverse bias increases the barrier for diffusion current. On the other hand, forward bias lowers the barrier for diffusion and the current is largely dominated by diffusion, where,

$$I_L = I_{01}(e^{\frac{qV}{kT}}) \tag{2.15}$$

The total current of an ideal diode can be written as:

$$I_L = I_{01}(e^{qV/kT} - 1) \tag{2.16}$$

The overall current voltage response of the cell can be approximated as the sum of the short circuit photocurrent and dark current. Thus net current density in the cell is:

$$J_L(V) = J_{sc} - J_{dark}\,(V) \tag{2.17}$$

This becomes,

$$J_L = J_{sc} - J_0(e^{\frac{qV}{nkT}} - 1) \tag{2.18}$$

The term, n, in the denominator of the exponent is called diode quality factor (ideality) and, for a perfect diode, n is unity.

Figure 2.9 shows the light and dark current-voltage curves for a solar cell. I-V characteristic of an illuminated solar cell lies in the fourth quadrant. For the purpose of comparison, current voltage characteristic of an unilluminated and illuminated solar cell are plotted together. Voltages are same in both cases, whereas the current in the illuminated solar cell is negative, i.e., the solar current flows against the convectional direction of the forward biased diode.

Some important parameters of a solar cell are described below.

2.3.2.1 Short Circuit Current. This is the current obtained when the solar cell is short circuited i.e. there is no voltage at the cell. This current is denoted by I_{sc} (from short circuit current). Ideally, if V=0, then $I_L = I_{SC}$. The short circuit current is equal to the absolute light generated current. Therefore, short circuit current is the largest current which may be drawn from the solar cell. Short circuit current depends on various factors such as area of the cell, number of photons absorbed, spectrum of the incident light, optical properties of the cell etc.

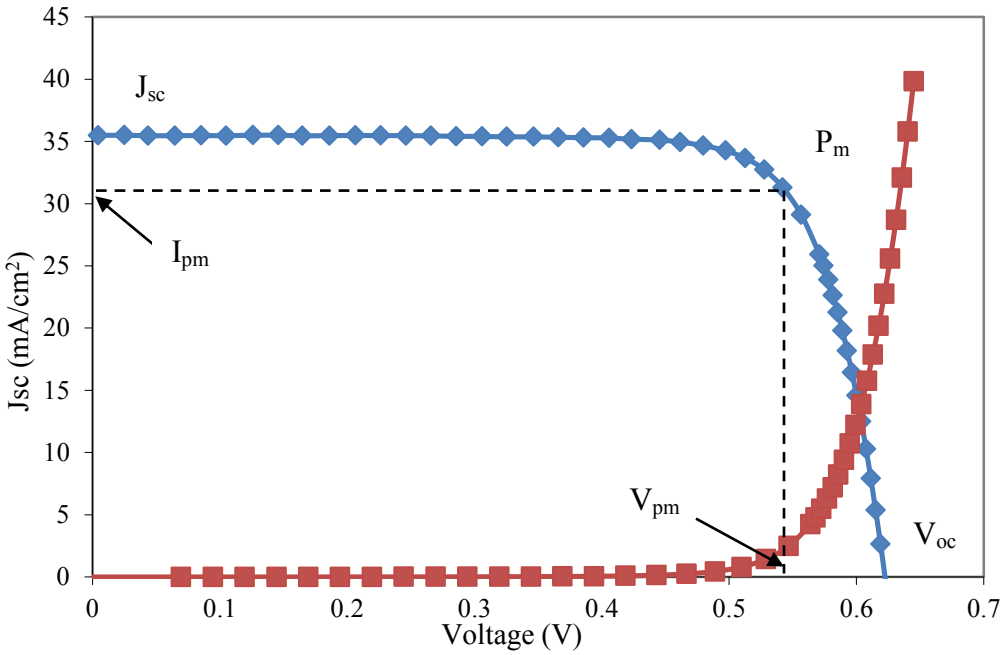

Figure 2.9 Current- Voltage characteristics of a solar cell.

2.3.2.2 Open Circuit Voltage. The open circuit voltage V_{oc} is obtained when no current is drawn from the circuit. Solving for open –circuit voltage (I=0), one obtains,

$$V_{oc} = \frac{nkT}{q} \ln\left(\frac{I_L}{I_0} + 1\right) \tag{2.19}$$

The open circuit voltage is proportional to the logarithmic of ratio of short circuit current to dark current; it is the maximum voltage available from the solar cell. To

maximize V_{oc}, the dark current I_0 must be minimized. To maximize J_{sc}, recombination in the cell must be minimized and light trapping must be maximized.

For each point on the I-V curve, the product of the current and voltage represents the power output for that operating condition. A solar cell can also be characterized by its maximum power point, when the product V_{mp} x I_{mp} is at maximum value.

2.3.2.3 Fill Factor and Cell Efficiency. Terrestrial solar cell efficiency is reported at the standard AM1.5 global conditions. The measuring temperature is 298 K, and the light intensity is 1000 W/m^2 given by zenith cycle of 48°. Cell efficiency is given mathematically by,

$$\eta = \frac{V_{oc} J_{sc} FF}{P_{in}} \tag{2.20}$$

P_{in} is the incident light intensity, and the fill factor FF, is the measure of the squareness of the illuminated curve, given by:

$$FF = \frac{V_{mp} I_{mp}}{V_{oc} J_{sc}} \tag{2.21}$$

The maximum power point of the cell is defined as (V_{mp}, I_{mp}); for maximum power output, the load curve should pass through the maximum power point or the voltage across the load should be the V_{mp} for optimum performance. The maximum power output of the cell is graphically given by the largest rectangle that can be fitted under the I-V curve (Figure 2.9). Photovoltaic panels are usually rated in terms of their peak Watts (W_p).

2.3.2.4 Effect of Parasitic Resistances. Solar cells generally have parasitic series and shunt resistance associated with them as shown in Figure 2.10. Both types of parasitic resistance act to reduce the fill-factor. The major contributors to the series resistance (R_s)

are the bulk resistance of the semiconductor material, particularly through the front surface to the metallic contacts and interconnections, carrier transport through the top diffused layer, and the base and emitter sheet resistance. Series resistance is a particular problem at high current densities.

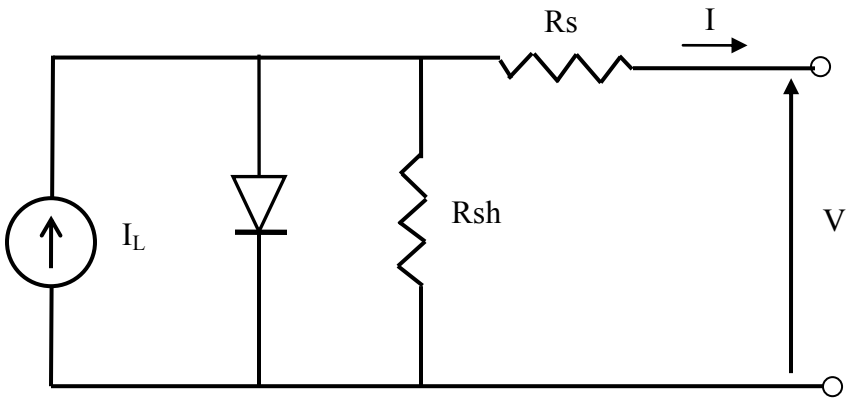

Figure 2.10 Parasitic series and shunt resistance of a solar cell circuit.

The shunt resistance (R_{sh}) arises from leakage of current through the cell, around the edge of the device and between contacts of different polarity, p-n junction non-idealities and impurities near the junction, which cause partial shorting of the junction. For an efficient cell, series resistance should be small and shunt resistance should be as large as possible.

In the presence of both series and shunt resistance, the diode equation become:

$$I = I_L - I_0\left[\exp\left(\frac{V + IR_s}{nkT/q}\right) - 1\right] - \frac{V + IR_s}{R_{sh}} \qquad (2.22)$$

2.3.2.5 Two Diode Model of a Solar Cell. In real solar cell p-n junction, the exponential relationship between voltage and current density, given by equation 2.16, is never observed at low voltage in the forward direction. In real solar cells, depletion region

recombination represents a substantial loss mechanism [59]. Traps located in the vicinity of the forbidden gap give a dominating contribution to the Shockley-Read-Hall recombination rate. It is further assumed that the recombination rate is constant across the space charge region. The resulting recombination rate can be expressed as a recombination current I_{DR} in the depletion region:

$$I_{DR} = I_{02}\left[\exp\left(\frac{qV}{2kT}\right)-1\right] \tag{2.23}$$

In general, the recombination current in the depletion region is a function of applied voltage and is not necessarily of single exponential form. Adding this space charge layer recombination current to equation 2.22 gives the two diode model expression [60]. Non-ideal diode behavior in a solar cell is typically a result of recombination in the depletion region, series resistance (R_s) and shunts resistance (R_{sh}) and can be described using the following equation:

$$I = I_{01}(e^{q(V-IR_s)/kT}-1) + I_{02}(e^{q(V-IR_s)/nkT}-1) + \frac{V-IR_s}{R_{sh}} \tag{2.24}$$

where, I_{02} and n = 2 are used to describe the recombination in the depletion region. When a light bias is applied to a solar cell, according to superposition, light and dark currents oppose each other, and the terminal current is given by:

$$I = I_{dark} - I_{light} \tag{2.25}$$

$$I = -I_L + \left[I_{01}(e^{q(V-IRs)/kT}-1) + I_{02}(e^{q(V-IRs)/2kT}-1) + \frac{V-IR_s}{R_{sh}} \right] \tag{2.26}$$

where, V is the terminal voltage, k is the Boltzmann's constant.

The non-ideal I-V characteristics can further be caused by an injection-level dependent surface recombination current. It was found that the origin of the non-ideal

diode behavior of a high efficiency silicon solar cell is a surface recombination velocity at the rear Si/SiO_2 interface that strongly depends on the minority carrier concentration [61]. Figure 2.11 shows the equivalent circuit of a real solar cell, consisting of two diodes with series and shunt resistance. The reverse saturation current, I_{01}, is composed of emitter saturation current, I_{0e}, and a base saturation current I_{0b} or correspondingly, the emitter and base saturation current densities J_{0e} and J_{0b} make up the reverse saturation current density J_{01}.

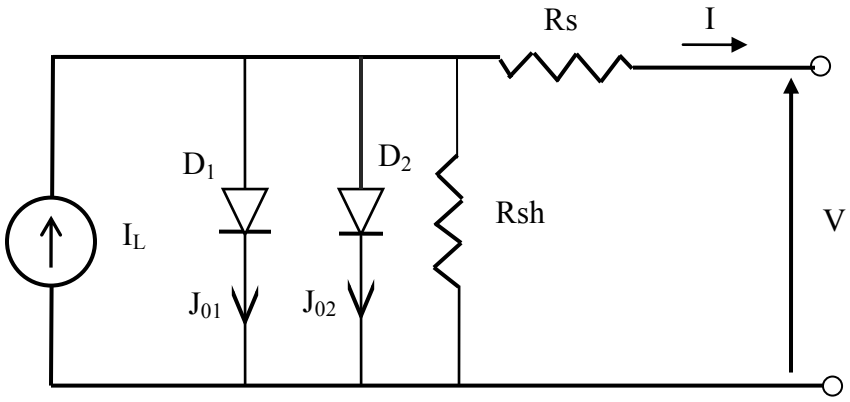

Figure 2.11 Equivalent circuit diagram for the two diode model of a real solar cell.

The solar cell equivalent circuit, in Figure 2.11, demonstrates the effects of high diode saturation current, high series resistance in the circuit, and low shunt resistance on the output power or the cell efficiency. High series resistance causes power loss because of the I^2R effect. A low shunt resistance (and/or high I_{02}) results in FF and voltage loss as a result of a shunt path through the collecting junction. A low surface recombination velocity and high bulk lifetime can greatly improve I_{01} and solar cell performance, as is discussed throughout this thesis. Bulk lifetime and surface recombination are important

for solar cells made from solar grade silicon substrates that suffer from LID and random grain orientation.

2.4 Cell Design for Loss Minimization

Under laboratory conditions, by using current technology, it is possible to produce single crystalline solar cell with efficiency in excess of 24% [62]. However, commercially mass produced cells are only 19-20% efficient. Efficiency is the major aim for laboratory research cells, irrespective of the cost and complexity of the processing steps. Laboratory methods of cell fabrication cannot directly be applied to the industrial production. To ensure a commercially viable product, industry requires simple techniques, large throughput, cheap raw materials, large contact area, and large area devices.

The efficiency of a solar cell in converting sunlight into electrical energy is the single most important factor defining the quality of a solar cell. The efficiencies of real solar cells have many limitations which, in principle, can be eliminated. These include losses due to reflection, contact shadowing, series resistance, incomplete collection of photogenerated carriers, absorption in inactive window layers, non radiative recombination etc. Even if these losses are completely eliminated, there remain two intrinsic losses which determine the efficiency of ideal solar cells. The first loss is because of the inability of a single energy gap solar cell to properly match the broad solar spectrum. Photons with energy less than the band gap (E_g) are not absorbed and photons with energy greater than band gap generate electron hole pairs which immediately lose the excess energy [63]. Second loss is due to radiative recombination. All the solar cells

absorb sunlight and radiate light. The radiative current subtracts from the current delivered to the load by the cell.

Light shining on a cell can behave in a numbers of ways as illustrated in Figure 2.12. Depending on the nature of the top surface, certain amount of light gets reflected by the metal grids and by the cell surface. Some are absorbed and be able to produce electron hole pairs. A fraction of the light gets reflected from the rear contact of the cells. The light reflected from back surface can also be absorbed to produce electron hole pairs. The remaining light that enters the cell can be absorbed by the rear contact. To maximize the power rating of a solar cell, it must be designed so as to maximize the desired absorption (3) and absorption after reflection (5) as shown in Figure 2.12. Optical and recombination losses reduce the cell output from the ideal values. Light reflected from the top surfaces and rear contact of the cell is the optical loss that needs to be decreased to improve the cell efficiency. Researchers have tried a number of ways to reduce these losses.

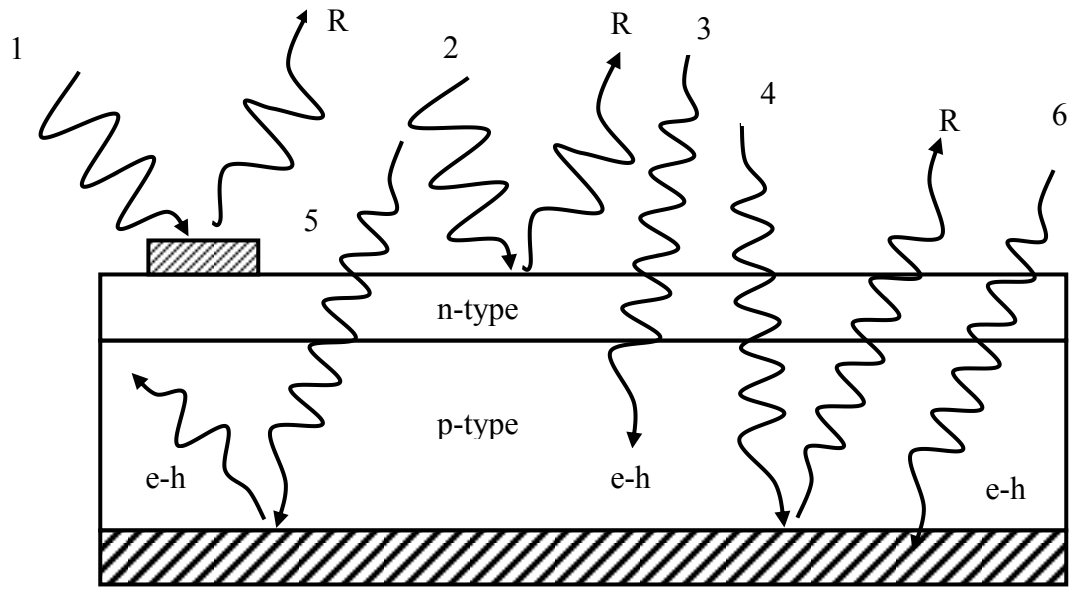

Figure 2.12 Behavior of light falling on a solar cell. (1) Reflection and absorption at top contact. (2) Reflection at cell surface. (3) Desired absorption. (4) Reflection from rear out of cell-weakly absorbed light only (5) Absorption after reflection. (6) Absorption in rear contact.

The busbars and the fingers are the sources of various losses such as shading losses, resistive losses and contact resistance losses. Top contact coverage of the cell surface can be minimized for less shading effect and low contact resistance. By heavily doping the top surface of the cell (n^+ region), sheet resistance decreases which ultimately improves the contact resistance losses.

Reflection of light from the surface of the cell can be decreased by using suitable antireflection coatings on the top surface of the cell. A quarter wavelength antireflection coating, that is, transparent coating of thickness d_1 and refractive index n_1, such that

$$d_1 = \frac{\lambda_0}{4n_1} \tag{2.27}$$

will ideally cancel the light reflected from the top surface by interference effects from the light reflected at the coating-semiconductor interface, which will be 180° out of phase.

Reflection is further minimized if the refractive index of the antireflection coating (n_1) is the geometric mean of that of the materials on either side, i.e., glass or air (n_0) and the semiconductor (n_2), i.e, if:

$$n_1 = \sqrt{n_o n_2} \tag{2.28}$$

surface reflection can be reduced, in this case, to zero.

Surface texturing can also be used to minimize reflection. Rough surface reduces the reflection by increasing the chances of reflected light bouncing back onto the surface, rather than out to the surrounding air. The surface of crystalline silicon can be textured uniformly by etching along the faces of the crystal planes. An additional benefit of textured surfaces is that light is obliquely coupled into silicon in accordance with Snell's law given by:

$$n_1 \sin\theta_1 = n_2 \sin\theta_2 \tag{2.29}$$

where, θ_1 and θ_2 are the angles for the light incident on the interface relative to normal plane of the interface within the medium with refractive indices n_1 and n_2 respectively.

High reflection from the rear cell surface reduces absorption in the rear cell contacts, allowing the light to bounce back into the cell for possible absorption. If the back surface reflector can randomize the direction of the reflected light, it can be trapped in the cell by total internal reflection. The possibility of light absorption can be dramatically increased in this way, since the path length of the incident light can be enhanced by a factor up to $4n^2$ by such light trapping [64].

The efficiency of utilizing light of higher wavelengths –the red response, can be improved by adding a back surface field (BSF) to the cell, as a means of reducing back surface recombination velocity. This is typically achieved by including a heavily doped

region, such as a screen printed layer of aluminum, at the back of the cell. The interface between this layer and the relatively light doped bulk region of the cell acts as a low recombination velocity surface.

CHAPTER 3

CHARACTERIZATION TECHNIQUES

Solar cells that are commercially available in the market are used for the initial experimental study of LID effect in mono and multi crystalline silicon solar cells. The mono crystalline cells were <100> oriented, p-type silicon grown on 200 μm thick Cz wafers. Resistivity of the wafer was 1-2 Ωcm. The area of the device was 238.65 cm^2. Electrical characterization such as current-voltage (I-V) curve under illumination, forward biased dark I-V plots and quantum efficiency are used to test the stability of cells for varying durations and conditions, e.g. before light soaking, after light soaking or after annealing etc. Characteristic quantities V_{oc}, J_{sc}, FF, and efficiency were measured as a function of light soaking time. The experimental procedures and techniques used in this study together with a description of the instrumentation are described in the following section.

3.1 XT-10 DC Testing System

Light and dark I-V measurements of the solar cells were performed on an AM1.5 calibrated XT-10 solar simulator as shown in Figure 3.1. This system provides quick and reliable solar cell efficiency measurements.

The light source is a height adjustable xenon ultra-high pressure lamp, which gives an almost white spectrum. The high intensities which still occur in some spectral ranges are reduced by special filters to the extent that a good approximation of the AM1.5 spectrum is achieved. The lamp intensity is set manually by adjusting the current output

of the lamp's power supply. Ideally, a specially calibrated silicon reference cell has to be used to set the lamp intensity.

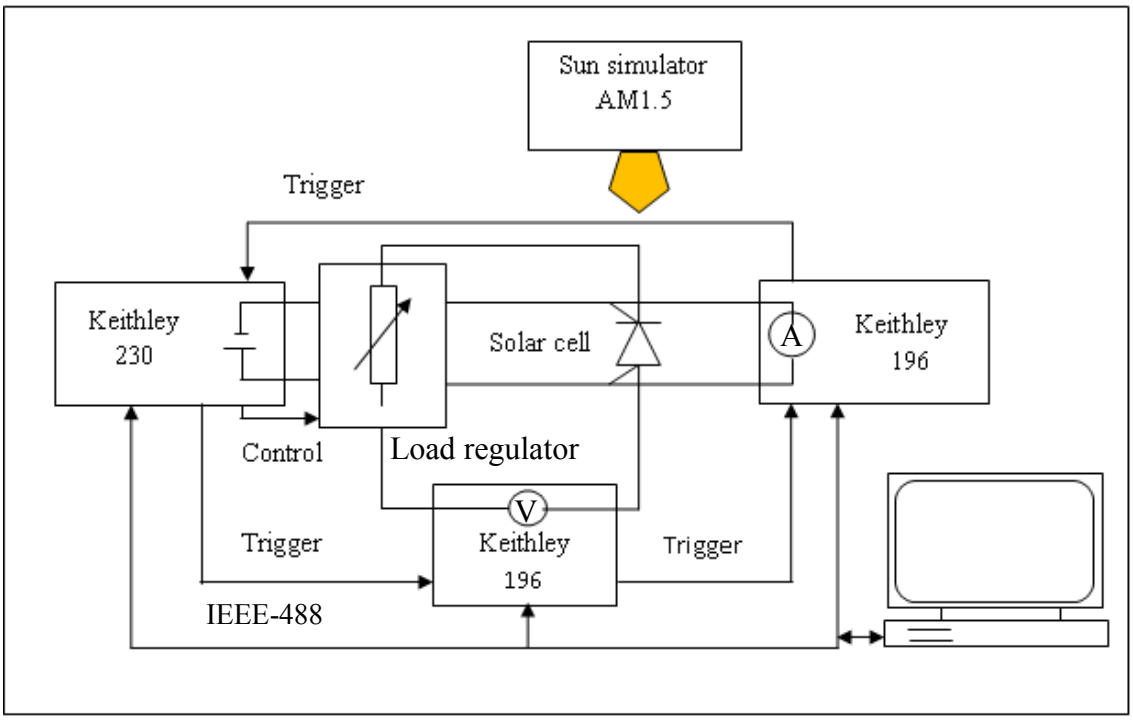

Figure 3.1 Block diagram of XT-10 solar simulator.

The instrumentation consists of a Keithley 238 Source Measure Unit, a Keithley 619 Electrometer/Multimeter and a computer. The source measure unit can simultaneously source a voltage and measure a current or source a current and measure a voltage. This obviates the need for independent meters and power supply. Essentially, there are four probes at the device under test. Two of the probes (one high and one low) provide both source and measurement connections. The additional two probes (one high and one low) are the sensor probes.

The current voltage characteristic are measured by monitoring the current from the solar cell point by point from zero to the short circuit current using an electrical load

regulator. A computer is used to acquire and store the I-V data, as well as to calculate standard device parameters such as V_{oc}, J_{sc}, fill factor (FF) and efficiency (η). It also calculates the current I_m and voltage V_m at the maximum power point. All cell parameters are thus available, which are required for an assessment of the quality of the cell. The software has been written in LabVIEW^{TM}. The software offers significant flexibility in specifying the measurement range for the I-V curves. A negative number in voltage always refers to reverse bias while a positive number refers to forward bias.

The cell is placed on water cooled, vacuum stage made from oxygen free copper coated with nickel. A close-loop temperature controller system assisted by Peltier devices (resistance temperature detectors) placed inside the stage maintains the temperature of the stage and cell at ~25 °C. Carefully designed series of current and voltage probes, loaded with springs, are placed on top of the cell along busbars so that probes create minimum shadow over the cell. The number of current collecting probes increases with increase in area of the cell. A voltage probe is also placed underneath the cell and the entire back surface of the cell acts as a current collection probe. Both current and voltage channels are separated to lower the series resistance losses.

The dark current characteristics, which determine the current voltage characteristics for the solar cell as a normal diode, can be acquired using the measuring system described above. For the dark current measurements, a higher voltage (V_a) is required than the open circuit voltage (V_{oc}) to obtain a current which has the same value as the short circuit current, because the additional voltage drop at the series resistance must be overcome.

3.2. Concentrator Cell Flash Tester

This equipment is used for the measurement of light and dark I-V characteristics of the solar cells. This technique is fast in the sense that once it is calibrated, it can be used all the time unless major changes are made in the set up of the equipment. It uses flash light to illuminate the cell, which offers one sun or multiple sun (if needed) illumination intensity over the sample in a short time without significant sample heating.

The flash tester used during this research for IV characteristics study is Sinton Instrument's multi-flash system. The equipment consists of a large capacitor (~ 1F), which is directly connected across the cell and a power amplifier. During the flash, the capacitor operates as a passive load and maintains a nearly constant voltage across the cell. The capacitor being large, the charging from the cell current is minimal. Between flashes, the amplifier changes the bias voltage on the cell and the capacitor. It uses many flashes to build up the I-V curve, taking only a single I-V point with each flash [65]. A stationary reference cell (light detector) is used to correct for flash to flash variations. When using the multi-flash method for characterizing the cell, one flash is required for the open circuit voltage (V_{oc}). Figure 3.2 shows the block diagram of the components of flash tester system.

The main advantage of flash tester over continuous illumination tester is that it can provide high light intensity with good uniformity over large areas. Multi flash simulator makes use of a flash lamp which produces each 80 ms (adjustable) a light flash with duration of about 2 ms (adjustable). As the resulting cycle is very small (1:80), the module under test does not heat up during the data sampling period. Each flash pulse runs through an array of flash intensities from peak to a minimum determined by the length of

the data acquisition. During each single light pulse, an electric load sends a current to the cell under test, and the corresponding voltage is sampled together. The value of the imposed current is decreased at the next flash until a full set of I-V pairs is obtained.

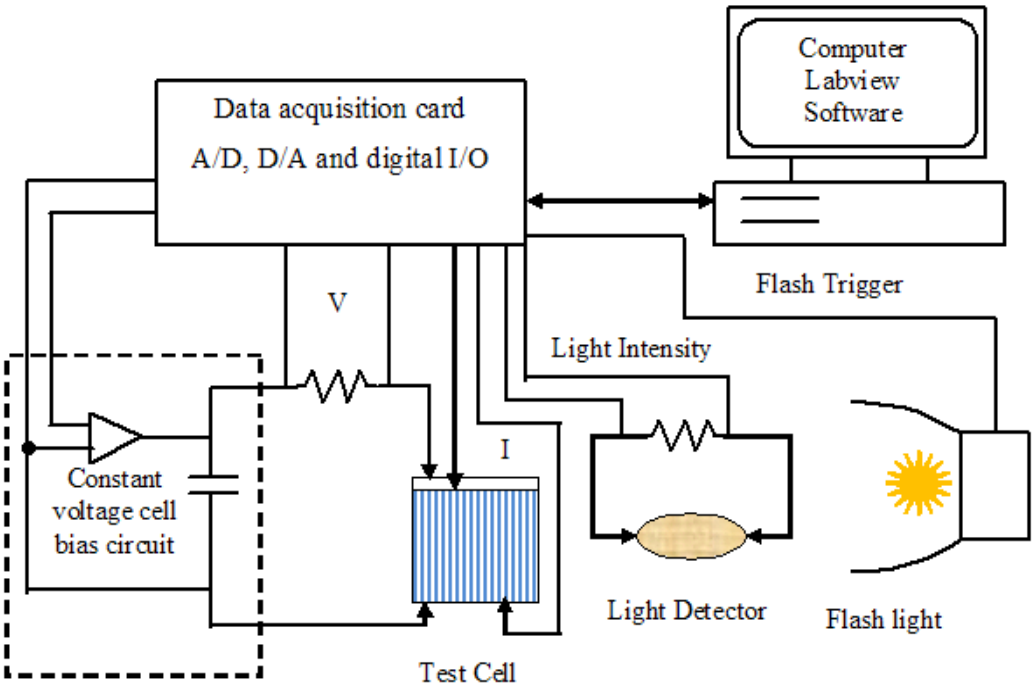

Figure 3.2 Block diagram of concentrator cell flash tester.

The instance where the I-V pair is sampled is determined by an adjustable delay relative to the rising edge of the irradiance of a single light pulse. Usually, the delay should be adjusted to allow sampling near the peak intensity of light and is triggered after the irradiance has reached a certain minimum level. When the sampling occurs, the solar cell under test is stabilized at the current as imposed by the load and at the voltage of its I-V characteristics at that level. After the flash decays, the electronic load returns to the ideal state.

3.3. Quantum Efficiency

Quantum efficiency of a photo sensitive device is defined as the percentage of photons that are incident on the photo reactive surface that will produce an electron hole pair. The longest wavelength for which this is finite is limited by the bandgap of the material. Maximum use can only be made of incoming sunlight if the bandgap is in the range of 1.0-1.6 eV. Thus quantum efficiency is measured over a range of wavelengths to characterize the device efficiency at various photon energies. Quantum efficiency of a solar cell is a very important measurement, as it gives information on the current that a given cell will produce when illuminated by a particular wavelength photon. When quantum efficiency is integrated over the entire solar spectrum, it gives the current that a cell will produce when exposed to the solar spectrum [66].

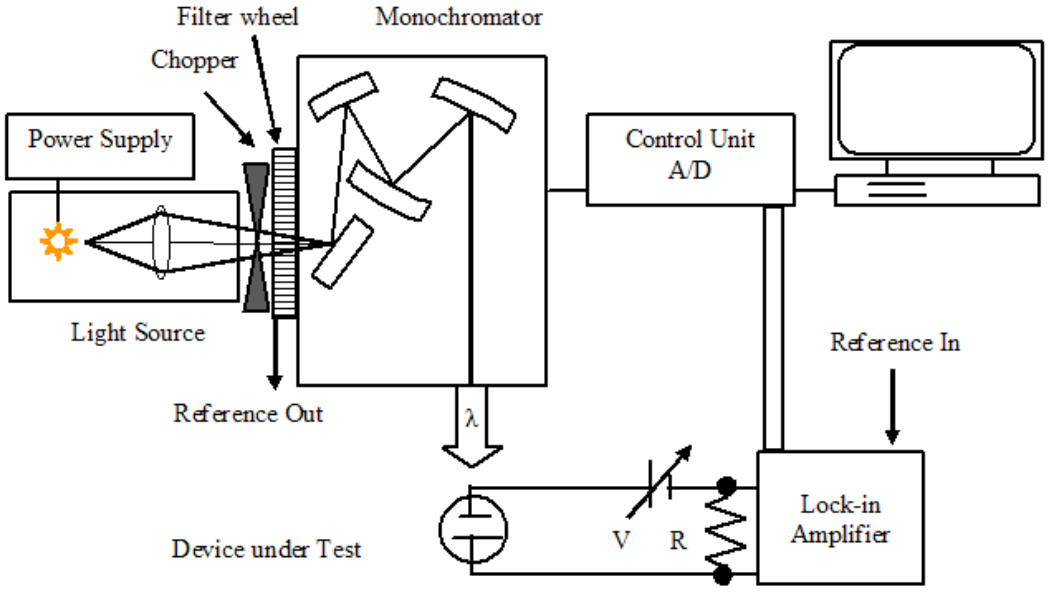

Figure 3.3 Block diagram for the determination of quantum efficiency of a solar cell.

In order to determine this value, the solar cell is illuminated with light from different spectral regions. The layout of this measuring instrument is shown in the block diagram in Figure 3.3.

NREL has a QE measurement set up which is based on filter-monochromator system. The system originally used stepping solenoids that were controlled by digital logic. An operational amplifier rated at +40 V, 8 A is used as a current to voltage converter with a computer controlled gain of 50 to 10,000. Insertion of a power supply in series with the PV device allows bias voltage up to +40 V. When an AC amplifier with a gain of 1, 10, or 100 is used, the ac signal is typically in the 0.3 to 3 V range, allowing the ac signal to be measured with an ac voltmeter instead of the traditional lockin amplifier. The monochromatic beam power is measured with a Laser Probe model 5710 radiometer with an RKP 575 pyroelectric head and a calibrated Si detector. The monochromatic power density can be increased by focusing the beam to a smaller spot.

The grating system used is capable of measuring QE of photovoltaic cells from 400 to 2800 nm. The system uses a Laser Probe 5900 electrically calibrated pyroelectric radiometer (RSP-590/RSV head). Silicon detectors calibrated by the National Institute of Standards and Technology are also used for calibration of the system. Semiconductor-based calibrations allow the test and reference signals to be filtered independently to maximize the signal to noise ratio. The region where the monochromatic light strikes the sample does not need light bias for the linear QE device. For the nonlinear device, quantum efficiency is typically measured with bias light simulating reference conditions. The spectral correction factor for efficiency measurements is calculated based on QE measurements near 0 V and is assumed to be the same as at the maximum power point.

This assumption is valid for most of the PV systems and results in negligible error for amorphous silicon, which has the voltage dependent quantum efficiency.

Also of interest is the spectral responsivity of a solar cell, given by amperes generated per watt of incident light. Ideally, this increases with wavelength. However, at short wavelength, cells cannot use all the energy of the photons, whereas, at long wavelength, the weak absorption of light means that most photons are absorbed a long way from the collecting junction and the finite diffusion length in the cell material limits the cell's response [67]. Spectral responsivity can be calculated as follows:

$$SR = \frac{I_{sc}}{P_{in}(\lambda)} = \frac{qn_e}{\frac{hc}{\lambda} n_{ph}} = \frac{q\lambda}{hc} QE \tag{3.1}$$

where, n_e is the flux of electrons, per unit time, flowing in an external circuit at short circuit conditions and I_{sc} is the short circuit current, n_{ph} is the flux of photons of wavelength λ incident on the cell per unit time, P_{in} is the incident light power and QE is external quantum efficiency. Spectral response approaches zero as λ approaches zero, since there are fewer photons in each watt of incident light. This strong wavelength dependence of responsivity makes cell performance in turn strongly dependent on the spectral content of sunlight.

3.4. Photo-Conductance Decay (PCD) Lifetime Measurement Device

Injection level dependent life time spectroscopy (IDLS) is one of the techniques that has been used to measure minority carrier lifetime. This technique uses Photo Conductance Decay (PCD) measurements. This method is fast and thus has a high potential for process monitoring.

For lifetime measurements, charge carriers are created in the silicon wafer using a flash lamp with a decay time constant of several ms and illumination area of several cm^2. Due to a slow decay time, the sample is under quasi-steady state condition during measurement as the light intensity varies from its maximum to zero. Steady state condition is maintained as long as flash lamp time constant is longer than the effective carrier lifetime. As the lamp flashes, the conductivity of the silicon wafer is thus greatly increased, the time varying photoconductance is detected by the inductive coupling. The resulting detuning of the resonant circuit causes the bridge current. After the light source is switched off, the conductivity of the silicon wafer returns to its original state and the bridge current decays. The decay of this current is measured. The photoconductivity is measured during the flash and the actual generation rate within the sample is measured by using an additional monitor cell. The coil coupled to the conductivity of the wafer and a signal proportional to this conductivity is observed on a digital oscilloscope and transferred to the computer for analysis. Figure 3.4 shows the block diagram of QSSPCD lifetime measurement system.

Generally, the wafer does not have passivation layers on the front and the back side. Such wafer is placed in a thin plastic bag with iodine-ethanol or quinhydron solution to passivate the surface of the wafer. The plastic bag rests on the stage and excess carriers are generated within the sample using a conventional xenon photo flash. In the stage underneath the wafer, are an inductively coupled coil and a capacitor included in an oscillating circuit. The coil is sensitive to any change in the charge developed in the wafer when it is illuminated. The frequency used is 10 MHz.

The associated computer program calculates the carrier mobility, based on the doping density, and excess carrier density. The reference cell measures the instantaneous generation rate, and then average lifetime is computed and displayed. The display shows lifetime versus injection level as the intensity of the flash decays.

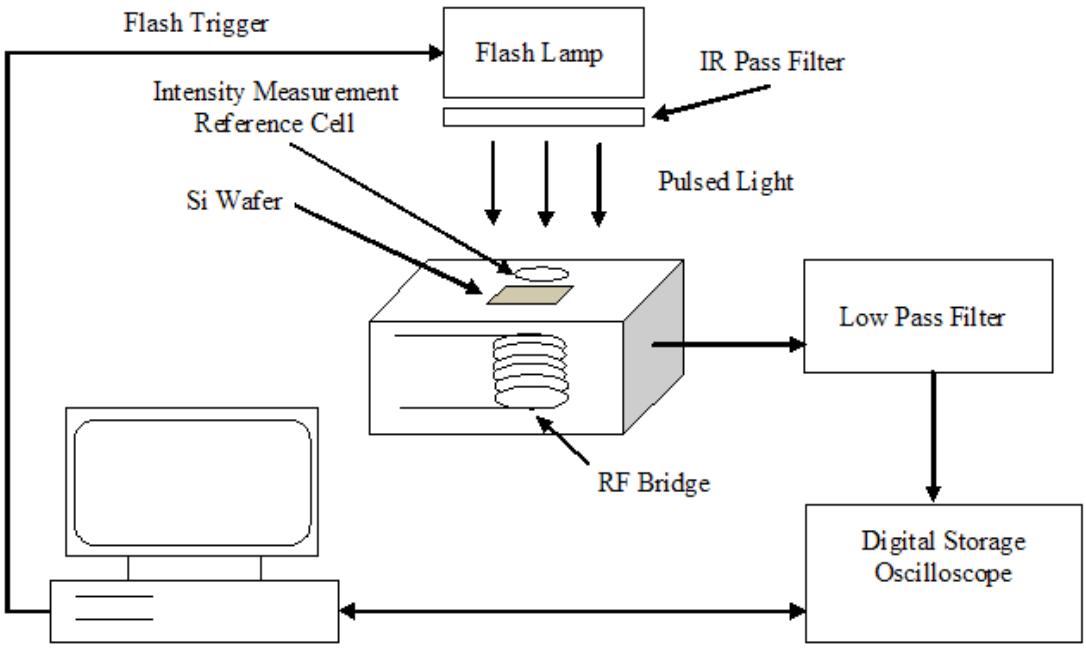

Figure 3.4 Block diagram of QSSPCD lifetime measurement system.

Lifetime of minority carriers is measured by using contact less photoconductance device from Sinton Instruments. It is used in quasi-steady state mode. It has a capability of measuring lifetime in the nanosecond to millisecond range in broad range of injections. This measurement technique is neither affected by excess carriers accumulated in space charge region nor by trapping [68, 69]. This instrument consists of three main

components; a stage with a flash light, an oscilloscope, and a computer. A detail of the working principle is explained elsewhere [70].

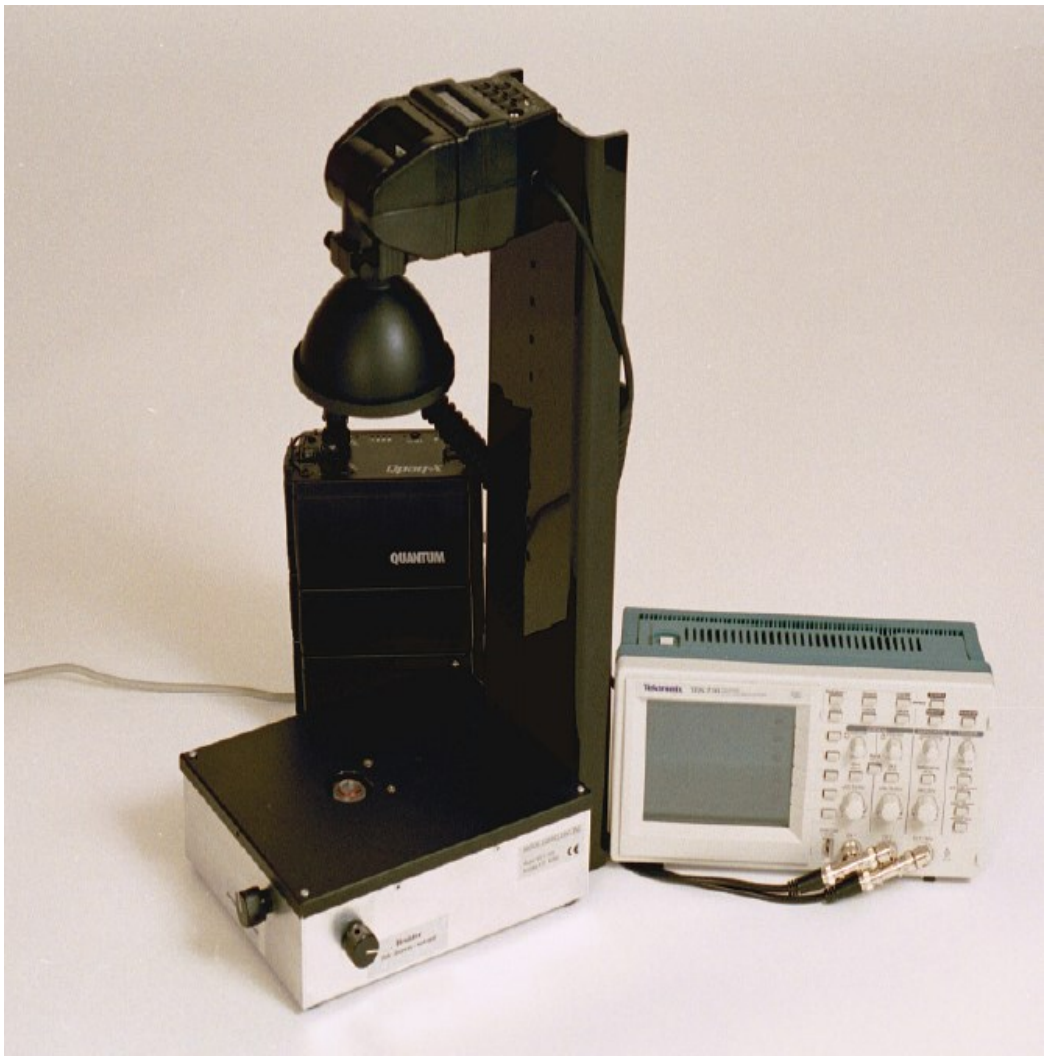

Figure 3.5 Photo of Sinton Consultancy lifetime tester with oscilloscope.

3.5. PVSCAN for LBIC Measurements

The PVSCAN instrument was developed at the National Renewable Energy Laboratory by Dr. Sopori [71]. It is an optical scanning system that has many applications in PV industry, including high speed mapping of large area crystalline silicon wafer and solar

cells. This device is used to measure defect distribution, reflectance, and light beam induced current (LBIC) of photovoltaic materials and devices. The schematic diagram of PVSCAN is shown in Figure 3.6. The following is a brief description of the working of the PVSCAN to determine dislocation and LBIC maps of a solar cell.

PVSCAN consists of two lasers of different wavelengths (630 nm and 980 nm). The illuminated surface of the solar cell has a diameter of approximately 0.2 mm. It has x-y stage for the movement of the device. The x-y table has minimum step size of 0.011 inch per second (~ 0.3 mm per second) and permits tracing accuracy up to 25 μm practical sampling interval by using a computer program developed at NREL. The entire system is computer controlled and housed inside an enclosure.

PVSCAN can be operated under three different modes, defect mode, reflectance mode and LBIC mode. Information is collected by a number of photo detectors placed at various points. It uses the optical scattering from a defect etched sample to count the density of defects statistically. It shines a laser beam on the surface of the device and measures the intensity of the reflected (scattered) light. The total integrated reflected light is proportional to the number of scattering centers. The system provides a signal that is proportional to the local dislocation density. By scanning over the sample, the instrument can map the defect distribution. Grain boundaries and dislocations have different characteristic scattering patterns, and PVSCAN uses these patterns to distinguish between different kinds of defects.

By attaching a probe to one of the front side busbars and using the platform as backside contacts, the current can be measured when an incident light beam from one of the lasers is shown on the cell. PVSCAN provides a quantitative means of measuring the

LBIC response of solar cell at two different wavelengths, 630 nm and 980 nm of light excitation. This enables the instrument to separate the surface and bulk recombination characteristics of cell. The current response for each excitation can be measured and saved in the online computer. PVSCAN also has the capability of measuring reflectance. By combining the LBIC reading with reflection losses, the instrument calculates the cell performance as a function of the light that is actually absorbed into the cell to get an internal photo-response.

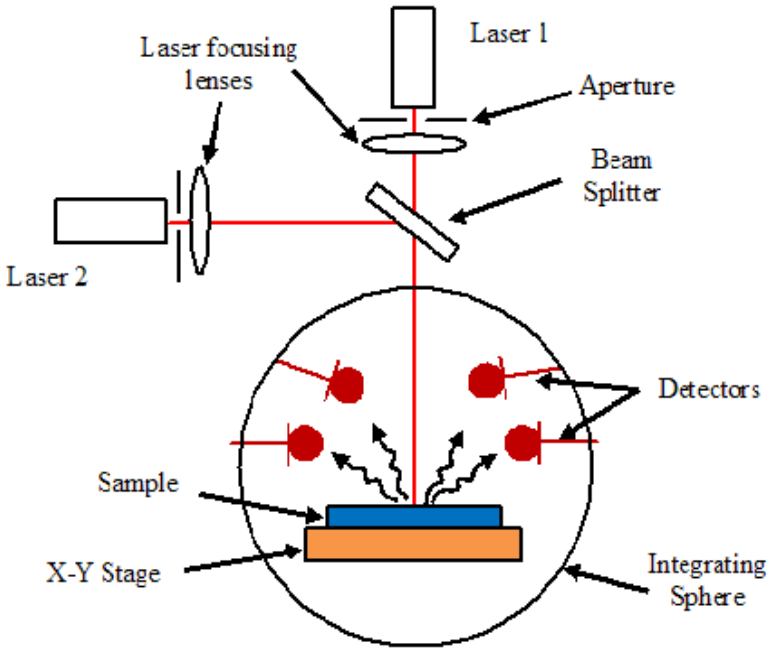

Figure 3.6 Schematic diagram of optical system of PVSCAN.

The short circuit current of the test cell is measured for each point illuminated. The level of current is then stored and converted for display on a screen. From the assignment of colors to currents, the effective and less effective regions of the solar cell are clearly seen.

3.6 Four-Point Probe

As a measure of purity of the material, one usually measures the resistivity. The higher the resistivity, the better is the quality. The resistivity of a semiconductor is proportional to the reciprocal of the density of carriers:

$$\rho = \frac{1}{e(\mu_n n + \mu_p p)} \tag{3.2}$$

which in turn is a function of uncompensated donors or acceptors.

Four-point probe technique is the most common method for measuring the resistivity of a semiconductor. As the name implies, it has four probes, two of them carry current and the rest two probes sense the voltage. Schematic of a four point probe is shown in Figure 3.7.

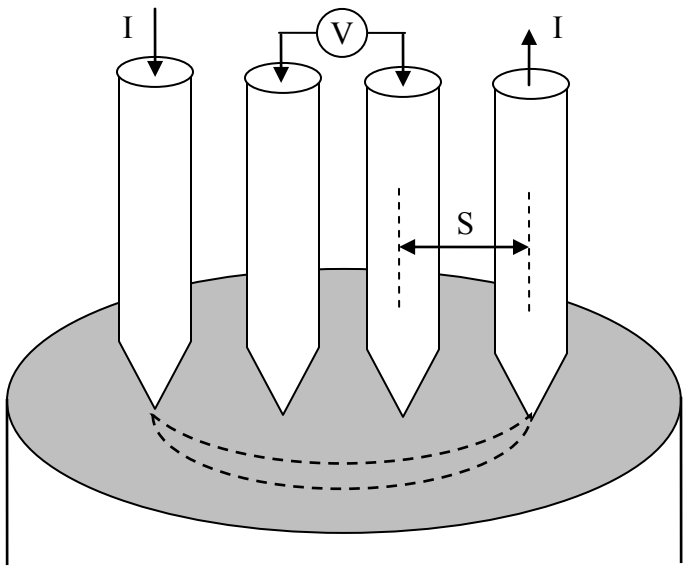

Figure 3.7 Use of four-point probe to measure resistivity of a wafer.

The four-point probe contains four thin collinear tungsten wires which are made to contact the sample under test. Current I is made to flow between the outer probes and

voltage V is measured between the two inner probes, ideally without drawing any current. If the sample has a semi-infinite volume and spacing between the probes is "s", the resistivity is given by:

$$\rho = 2\pi s \frac{V}{I} \tag{3.3}$$

With some correction for the sample whose thickness is $t \leq 5s$ and non-semi-infinite, the bulk resistance is given as [72]:

$$\rho = \frac{\pi}{\ln 2} t \frac{V}{I} \tag{3.4}$$

Sheet resistance ρ_s for uniformly doped sample is expressed as:

$$\rho_s = \frac{\rho}{t} = 4.532 \frac{V}{I} \tag{3.5}$$

Unit of sheet resistance is taken as Ohm per square.

CHAPTER 4

LIGHT INDUCED DEGRADATION

4.1 Review of Light Induced Degradation in Silicon Solar Cells

The first observation of LID in solar cells fabricated on boron-doped Cz-Si wafer was made by Fischer and Pschunder in 1973 [8]. They found that the performance of solar cell made on low resistivity (~1 Ω-cm) Cz Si degraded during the first few hours of illumination. No degradation was found in high resistivity (10 Ω-cm) B-doped Cz Si. This degradation occurred only in the long wavelength response of the cells, suggesting that the degradation is the result of the bulk carrier lifetime. The degradation was found to be reversible when the cell was annealed in the dark at 200 °C. At that time, details of the defect formation was not given. In the following years, several attempts were made to develop a defect model which explains the observed lifetime instabilities in boron doped Cz-Si solar cells. Corbett, Jaworowski et al. reported that lifetime degradation in CZ silicon is not due to direct creation of defects by photons but a dissociation of donor-acceptor defect caused by excess carriers generated by light irradiation [56]. In 1995, a similar degradation was reported by Knobloch, Glunz et al. that lifetime degradation occurred not only under illumination, but also in dark when forward bias voltage was applied to solar cells [73]. Weizer, Brandhorst, et al. proposed a model which explained LID effect being associated with complex of a lattice defect and a silver atom or cluster of silver atoms [4]. Graff and Pieper proposed a vacancy-gold (heavy metal impurities) complex as the lifetime-limiting recombination center in the material [50]. But none of

these models were capable of explaining the complete degradation-recovery cycle observed in boron doped Cz-Si solar cells. .

Reiss, King et al. investigated solar cells fabricated on boron doped Cz silicon wafers with comparatively high iron contamination levels [23]. They observed a pronounced degradation in cell performance under the following conditions: (i) during illumination, (ii) during application of forward bias voltage in dark, and (iii) during thermal treatment above 250° C. The observed degradation cycle was different from the one observed by Fisher and Pschunder. Cell parameters recovered fully when the cell was left overnight in dark at room temperature. But Reiss et al. could not explain the LID observed in highest purity electronic grade boron-doped Cz-Si with virtually no metal contamination.

In 1997 Schmidt, Aberle et al. proposed a defect reaction model which did not involve metallic impurities [9]. The important feature of this model was the formation of a defect pair composed of one interstitial boron and one interstitial oxygen atom (B_iO_i) during illumination of Cz Silicon. This model was successful in explaining lifetime degradation under illumination or lifetime degradation under minority carrier injection in dark as well as lifetime recovery during annealing at temperatures above 200 °C. In their work, it was shown that the degradation occurred only in Cz Si that was doped with B; no degradation was observed when either Ga or P was used as a dopant.

Kimerling, Asom et al. determined, by DLTS, the energy level of B_iO_i to be at $E_c - 0.26$ eV [7], which is much shallower than the level of the light-induced boron-oxygen center. Ohshita, Khanh Vu et al. later showed, by theoretical calculations, that B_iO_i pair could only exist in stable configuration if a substitutional silicon atom resides

between the boron and the oxygen atom [25]. Thus the interstitial boron-interstitial oxygen (B_iO_i) pair which had been detected by deep level transient spectroscopy (DLTS) was excluded as a possible candidate of recombination center resulting in decreasing the minority carrier lifetime in Cz silicon.

Glunz et al. measured lifetime on a very large number of boron doped Cz- silicon samples [74]. They found an approximately linear increase in the lifetime degradation with boron doping concentration and approximately to the power of five of the concentration of the interstitial oxygen. This result gave rise to the assumption that the Cz recombination center is probably associated with defect complex other than B_iO_i pair. These considerations were further supported by measurements of Schmidt and Cuevas using injection level dependent lifetime spectroscopy [3]. They showed that the energy level of the light induced recombination center is very different from that of B_iO_i pair and proposed a new core structure consisting of one substitutional boron atom and several interstitial oxygen atoms.

In 2000, Bourgoin et al. proposed a possible atomic configuration of the boron-oxygen complex in which the B_s atom is surrounded by three O_i atoms [11]. The model assumes that illumination or injected carriers induce the degradation. This model tried to explain the difference in degradation behavior between B and Ga doped materials. In 2001, Rein, Rehrl et al. investigated the defect generation as a function of the doping concentration and found that it shows a quadratic increase with doping level and was weakly dependent on the injection level [75].The defect annihilation process was shown to be thermally activated.

Based on measured normalized defect concentration as functions of boron concentration [B_s] and oxygen concentration [O_i], Schmidt and Bothe, in 2002, proposed a defect model involving interstitial oxygen dimers (O_{2i}) [13]. In this model, fast diffusing oxygen dimers are captured by substitutional boron to form a B_s-O_{2i} complex, which acts as a highly effective recombination center.

In 2003, Rein and Glunz applied temperature dependent lifetime spectroscopy and injection level dependent lifetime spectroscopy to obtain more information about the electronic configuration of the LID defects [76]. They established that the electron capture cross section of the LID defect is an inverse quadratic function of the temperature which suggested that the LID defect is an attractive Coulombic type center. They proposed that the defect lies at E_c-0.41 eV.

Herguth, Hahn et al. in 2006, put forward a hypothetical three state model for the explanation of the formation and annihilation of the complexes responsible for degradation of solar cells [77]. In this model, they reported that prolonged carrier injection (either by illumination or electrical bias) at an elevated temperature (100-160 °C) could recover the degraded cell performance. They attributed this recovery process to transformation of the degraded state to a new state called “regenerated state” which is relatively inactive in terms of recombination. This regenerated state was found to be stable under a normal solar cell operating condition, but was found to be unstable when the sample was heated to more than 200 °C in dark. They proposed that annealing above 200 °C converted the regenerated state back to non-degraded state which then can be transformed into the degraded state by carrier injection. Finally, they found the activation energy of the regeneration process to be 0.62 eV.

Recent studies on compensated p-type CZ silicon (boron and phosphorous doped) showed results that could not be explained with the traditional B_sO_{2i} model. Voronkov and Falster, in 2010, proposed a new defect model, in which the defect is composed of one interstitial boron atom B_i and an interstitial oxygen dimer O_{2i} [78]. According to this model, the defect B_iO_{2i} is formed during ingot cooling, which results in fixed concentration of B_iO_{2i} at room temperature. Initially, the defect is not recombination active, but under illumination or injection of excess carriers by forward bias, the defect is recharged and subsequently reconstructed into its recombination active form. The proposed recharging and subsequent reconstruction of the defect is in excellent agreement with the experimental findings of Schmidt and Bothe [12, 26] that the defect generation rate is proportional to the intensity of illumination at low intensity level (below 1 mW/cm^2) but independent of the illumination intensity at higher intensities. According to this model, recovery time is proportional to the hole concentration.

The experimental data on fast recombination center, so far, has been obtained on boron doped silicon. With regard to the new theory, the nature of slow recombination center, provided by the experiments on compensated n-Si, seems to raise questions on the nature of the fast recombination process. Due to short time scale in the fast degradation in boron doped silicon, a conclusive investigation in compensated material has faced major difficulty.

4.2 Lifetime Analysis of the Metastable Defect

Light induced degradation of B-doped Cz silicon results in strong reduction of carrier lifetime [3, 8, 9, 20]. Both illumination and application of a forward bias in the dark result in exponential lifetime degradation [4, 20] until approaching a constant saturation level. These results lead to the conclusion that the transformation of the defect in its active state is carrier induced, and not photon induced. Many researchers attempted to correlate lifetime degradation with the metastable defect formed by B-O complex. Various silicon samples such as gallium doped CZ grown with high oxygen content, and magnetic CZ grown silicon with low oxygen content, intentionally oxygen doped FZ material, standard boron doped CZ-silicon materials etc. were used for the study.

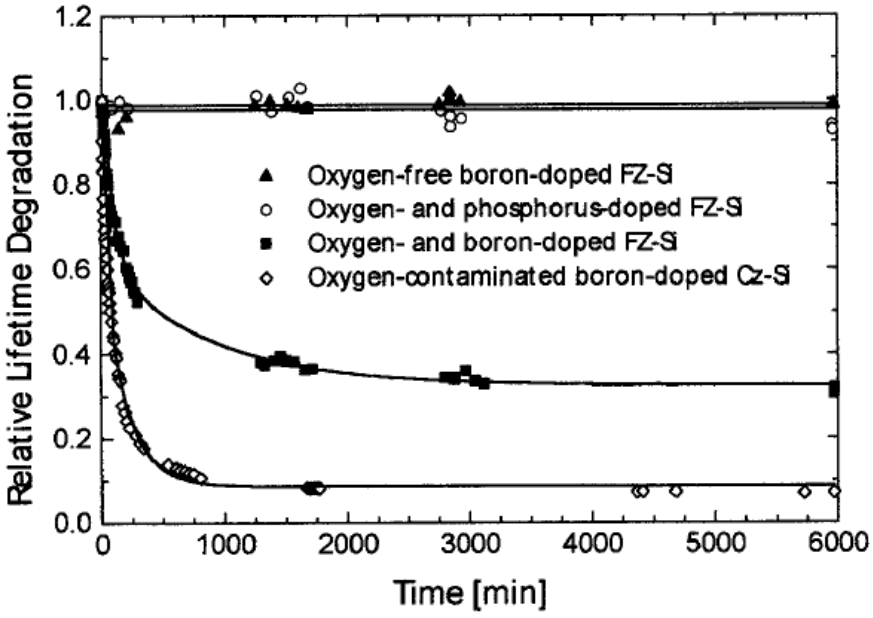

Figure 4.1 Lifetime degradation by light intensity of 50 mW/cm^2 on oxygen free or oxygen contaminated boron-doped FZ, phosphorus-doped FZ and boron doped CZ (from [22]).

Figure 4.1 shows one of the examples for the light-induced lifetime degradation of various FZ and CZ silicon samples exposed to illumination for long periods of time.

Figure 4.2 shows lifetime of a 1.9 Ωcm n-type CZ-Si plotted as a function of light soaking time which is perfectly stable under illumination at room temperature. The carrier lifetime in a boron and phosphorous doped sample significantly decreases and has not saturated with 10 hours of illumination [79]. These two results confirm that the only samples to suffer degradation in lifetime are those which contain both boron and oxygen.

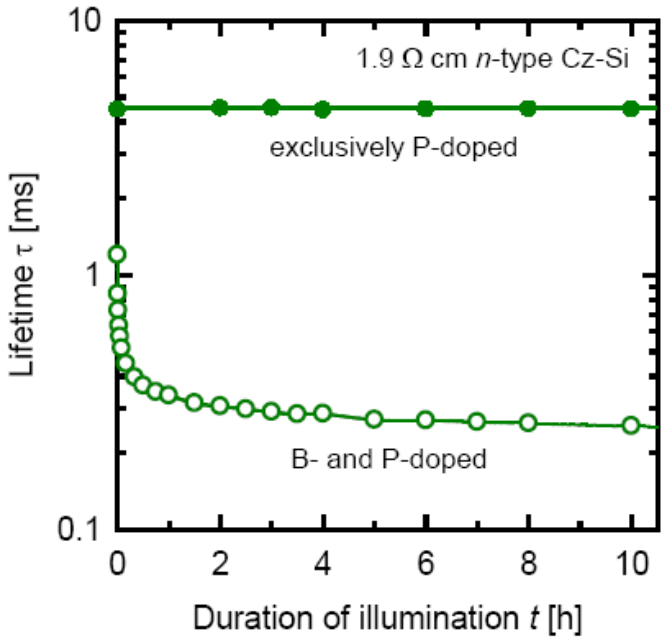

Figure 4.2 Carrier lifetime in phosphorous doped CZ-Si compared with compensated n-type CZ-Si (from [79]).

The lifetime degradation can be completely reversed by a short annealing step around 200 °C. The degradation-annealing cycle transform between active to passive state of the defect. Significant progress has been made in physical understanding of the metastable defect, but the structural composition and electrical properties are still unknown.

Deep Level Transient Spectroscopy (DLTS) is a powerful tool to study trap characteristics, but the trap location and concentration in CZ silicon could not be detected

by DLTS technique till now. Other methods such as temperature dependent and injection level dependent lifetime spectroscopy are being used for the characterization of the traps. Most attempts to detect the defect center by other techniques, such as photoluminescence, capacitance spectroscopy, or electron paramagnetic resonance, failed.

Multiple studies have been done to investigate the relationship between boron-oxygen trap and degradation of lifetime. All these observations are summarized in Table 4.1.

Table 4.1 Studies of Different Material Systems Showing Light Induced Degradation of Lifetime.

Material	Reference	Dopant	Interstitial Oxygen	Lifetime degradation
Boron doped FZ	[8,22,26,80,81]	Boron (10^{18} cm^{-3})	No	No
Phosphorous and oxygen doped FZ	[22,79]	Phosphorous	Yes	No
Phosphorous doped CZ	[9,79,80]	Phosphorous	Yes	No
Boron doped MCZ	[22]	Boron	Very low ($5x10^{15}$ cm^{-3})	No
Gallium doped CZ	[9,22,26]	Gallium	Yes ($5x10^{17}$ cm^{-3})	No
Boron and Oxygen doped FZ	[22,26]	Boron	Yes ($8x10^{17}$ cm^{-3})	Yes
Boron doped CZ	[8,9, 22,73,76]	Boron (10^{18} cm^{-3})	Yes ($6\text{-}7x10^{17}$ cm^{-3})	Yes
Phosphorous and Boron doped CZ	[79,82]	Boron and Phosphorus	Yes	Yes

As mentioned earlier in Section 4.1, the recombination-active boron oxygen related defect is composed of one substitutional boron atom B_s and an interstitial oxygen dimer O_{2i}. This model was based on the numerous experimental results obtained on B doped p-type CZ silicon. Similarly, B_iO_{2i} model provides a detailed explanation of the basic features of the degradation, and subsequent recovery by annealing in dark. It is

obvious that in low resistivity samples, i.e., samples with higher boron concentration, a recombination center exists in the forbidden gap which shows a strongly decreased recombination activity than in the high resistivity samples when annealed.

4.2.1 Normalized Defect Concentration of Wafer

Lifetime spectroscopic measurements can be used to investigate metastable defect concentration quantitatively. The initial lifetime of recovered state (after annealing) is τ_0 and stable lifetime of degraded state after illumination under one sun (AM1.5) is τ_d. The metastable defect concentration is then assumed to be proportional to the difference between the inverse of the degraded-state lifetime and the inverse of the recovered-state lifetime. Assuming that the metastable defect is completely deactivated after annealing step and completely activated after the light soaking step and other recombination channels not related to degradation effect, such as surface recombination and Auger recombination, are completely eliminated, then the normalized defect concentration in an arbitrary illumination state is $N_t^*(t)$:

$$N_t^*(t) = \frac{1}{\tau(t)} - \frac{1}{\tau_0} = \left(\frac{1}{\tau_{Cz}(t)} + \frac{1}{\tau_{res}}\right) - \frac{1}{\tau_{res}} \tag{4.1}$$

$$= N_t(t) \text{ x } f(\sigma_n, \sigma_p, E_t\ ;\ \Delta n, T)$$

$$= (\nu_{th}\sigma_n N_t + \nu_{th}\sigma_{res} N_{res}) - \nu_{th}\sigma_{res} N_{res}$$

where, $N_t(t)$ is the concentration of the CZ-specific defect activated in current illuminated state, N_{res} the concentration of residual defects state, $\tau_{Cz}(t)$ being the lifetime corresponding to the recombination center under investigation, τ_{res} corresponds to lifetime due to all residual recombination channels, ν_{th} is the thermal velocity, σ_n and σ_{res}

are the electron capture cross section, respectively. The maximum defect concentration is obtained when $\tau(t) = \tau_d$.

For an accurate determination of defect concentration, the complete elimination of other recombination channels is essential, which is done by measuring effective lifetime in both states at the same injection level and at same temperature [26]. According to the SRH statistics, the bulk lifetime in CZ silicon strongly depends on both the injection density Δn and doping concentration N_A. Figure 4.3 shows the measured dependencies of defect concentration on injection density for various resistivity samples [10].

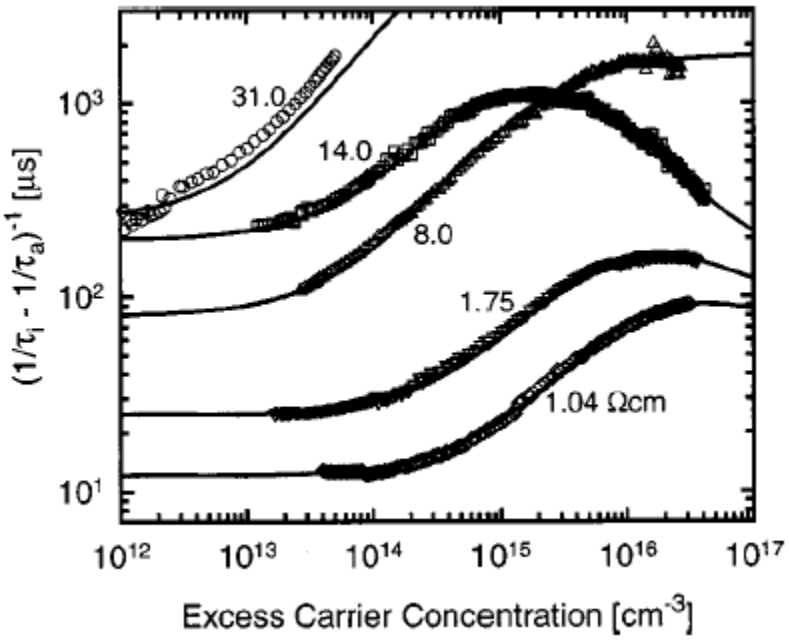

Figure 4.3 Measured injection level dependent defect concentration as a function of excess carrier concentration (Δn) for various resistivity CZ-silicon samples (from [10]).

Normalized defect concentration can also be expressed as a function of the substitutional boron concentration [B_s] and interstitial oxygen concentration [O_i]. There

exists a linear relationship between defect and boron concentration ($N_t^* \propto [B_s]^{1.1}$) and nearly quadratic increase ($N_t^* \propto [O_i]^{1.9}$) with increasing oxygen concentration [22, 26].

Temperature dependence of trap generation and annihilation, along with illumination wavelength and intensity, has also been frequently used to analyze trap behavior. Defect annihilation seems to be thermally activated. In a simplest case, the defect annihilation process follows a single exponential function given by:

$$N_t(T,t) = N_t(T,0)e^{-R_{ann}(T)xt} \tag{4.2}$$

Assuming the annihilation rate increases exponentially with temperature:

$$R_{ann}(T) = R_{ann}(T \to \infty)e^{\frac{-E_{ann}}{kT}} \tag{4.3}$$

Thus, kinetic defect annihilation is controlled by activation energy E_{ann}. Experimentally, the activation energy for an annihilation process was found to be in the range of 1.3-1.4 eV [26] or 0.98-1.0 eV [77].

Similarly, the trap generation rate is also expressed as a function of temperature and density of defect in active and passive state should then follow the exponential law,

$$N(t,T) = N(t \to \infty)[1 - \exp(\frac{-t}{\tau_{gen}})] \tag{4.4}$$

where, τ_{gen} is the generation time constant describing the activation process. Activation energy of generation can be calculated by fitting Arrhenius plot:

$$\frac{1}{\tau_{gen}} = R_{gen}(T) = R_{gen}(t \to \infty)\exp(\frac{-E_g}{kT}) \tag{4.5}$$

where, T is temperature, N(t,T) is the normalized defect concentration as a function time and temperature, R_{gen} is the generation rate of the defect, E_g is generation energy. Activation energy for degradation process is found to be 0.4-0.5 eV [26]. By using decay

constant from temperature dependent V_{oc} of solar cell and Arrhenius equation, Herguth et. al calculated the activation energy of regeneration to be 0.62±0.02 eV [77].

4.2.2 Normalized Defect Concentration of Solar Cells

Normalized metastable defect concentration generated in a cell due to illumination is measured by using V_{oc} value as a function of t, the time elapsed since the start of illumination. It is given by the expression:

$$N^{*}_{Voc}(t) = \frac{1}{\exp(qV_{oc}(t)/nkT)} - \frac{1}{\exp(qV_{oc}(t=0)/nkT)} \qquad (4.6)$$

For solar cells having doping concentration of the order of 10^{16} atoms/cm^3, ideality factor n is very close to unity and does not change significantly for the boron-oxygen related recombination centers.

4.3 Electronic Structure of B-O Defect

Concerning the multitude of experimental findings and the different models proposed for the metastable defect over the past years, progress has been made in physical understanding of the defect responsible for LID. But the exact configuration of the boron-oxygen complex and its electrical properties which is given by the energy level E_T and the ratio of capture cross section of electron and hole has not yet been convincingly clarified. All the known properties of the CZ defect have been determined by means of lifetime spectroscopy. By using injection-level dependent carrier lifetime measurement, Schmidt and Cuevas found that the recombination center responsible for the lifetime degradation has an energy level located close to the middle of the silicon band gap [10]. Their experiments indicate that allowed energy of trap E_T lies in between E_V+0.35 and

E_C-0.45 eV which is close to the earlier published defect energy level between E_V+0.30 eV and E_C-0.27 eV measured by transient capacitance spectroscopy [6].

Rein and Glunz, with detailed Shockley-Read-Hall analysis of the entire TDLS curve, revealed that the CZ defect acts as an attractive Coulomb center which is localized in the upper half of the band gap at E_C-E_T= 0.41 eV and the ratio of electron capture cross section to that of hole is 9.3 [76]. The unambiguous localization of the recombination-active defect state below 0.41 eV below the conduction band allows to judge one of the metastable model proposed earlier. Schmidt, Aberle et al. suggested boron-oxygen complex (B_iO_i) to explain the degradation and regeneration of the lifetime [9]. Since the energy level associated with B_iO_i pair is known to lie at E_C-E_t = 0.26 eV, as determined by DLTS measurement, after Rein and Glunz's findings, B_iO_i is definitely excluded as a possible candidate for degradation of CZ silicon solar cells.

Bothe and Schmidt, in 2006, determined the energy level of the fast forming defect center to lie between 0.35 and 0.85 eV below the conduction band edge E_C. On the other hand, the ratio of the capture cross section for electron and hole was determined to be 100±10 which is 10 times larger than that for slowly forming B-O defect [26].

4.4 Role of Oxygen

Oxygen is a dominant impurity present in CZ grown silicon crystals with concentration from 5 to15x10^{17} cm^{-3}. Oxygen is an unintended dopant which enters the molten silicon continuously by dissolving the silica (quartz) crucible. The silica crucible is an infinite source for oxygen. Oxygen dissolved interstitially in crucible grown silicon crystal will usually precipitate as SiO_2 in thermal processing at temperature lower than the silicon

melting point. The presence of oxygen in silicon always leads to an expansion of the material and to built-in stresses. In the case of large precipitates, these stresses can be relieved by the growth of dislocations.

Individual oxygen atoms occupy interstitial bond-center positions. Such oxygen atoms (O_i) diffuse by hopping between neighboring bond center-sites with activation energy of 2.5 eV in a wide range of temperatures 300-1200 °C [16]. Clustering of oxygen occurring under heat treatments during manufacturing processes is a natural consequence due to the supersaturation of oxygen. From the initial state where oxygen is dispersed in silicon, it is possible to reach into another state after annealing where the whole oxygen content is precipitated. The process is reversible and oxygen can be dispersed again by dissolution of the precipitates at very high temperature (~1350 °C) and quenching to room temperature.

Oxygen, in its usual interstitial configuration, in silicon is electrically inactive. Upon heat treatment in the temperature range of 300-350 °C, electrically active centers are formed in oxygen rich silicon ($[O_i] \sim 10^{18}$ cm^{-3}). The first stage of O_i precipitation is considered to be the formation of dimer. It appears that a pair of nearest neighbor bonded interstitial oxygen atom is more stable than involving in the formation of an oxygen molecule [83]. The oxygen dimer consists of di-oxygen interstitial defect bonded to the silicon lattice.

When boron doped CZ silicon is illuminated or forward biased under dark, B-O complex is formed. Interstitial boron is a highly reactive defect and can combine with other common impurities such as oxygen and hydrogen. In heavily doped CZ silicon, interstitial boron forms defects with interstitial oxygen having donor energy level at E_C-

0.23 eV [84]. The binding energy E_B of oxygen with B_i was found to be 0.6 eV. Donor energy level of B_iO_i is much shallower than the level of the light-induced boron-oxygen center. Thus the interstitial boron-interstitial oxygen (B_iO_i) pair was excluded as a possible candidate of recombination center.

Another defect model was proposed involving interstitial oxygen dimers (O_{2i}). In this model, fast diffusing oxygen dimers are captured by substitutional boron to form a B_s-O_{2i} complex, which acts as a highly effective recombination center.

CHAPTER 5

EXPERIMENTAL DETAILS

5.1 Light Soaking and I-V Measurements

For the study of light induced degradation on mono-crystalline silicon solar cell, a large number of single crystalline, boron doped CZ-grown silicon solar cells were tested. The cells used in the course of this study are commercially available and of size 156 mm x 156 mm mono-crystalline solar cells. The cells were fabricated on high-quality (minority-carrier lifetime between 300 and 350 μs) wafers, which have very low Fe content ($<10^{12}$ atoms/cm^3), to minimize Fe-B effects. Boron doping concentration is around 10^{16} atoms/cm^3, whereas the oxygen content is high ($\sim10^{17}$ atoms/cm^3, ASTM F121-83 Standard). Hence, the main effect of light is expected to be related to B-O. The resistivity of the p-type mono-crystalline, [100] oriented wafers was 1 to 2 Ω-cm. The solar cells under investigation were about 250 μm thick, metal-insulator-semiconductor contacted p-n^+ structure and also passivated emitter and, on the rear, locally diffused p-n^+ solar cells. Surface passivation was performed by SiN deposited by PECVD. All the cells were processed by a screen printing method according to the typical industrial solar cell process.

Initially, the cell was annealed at 200 °C for half an hour in dark. Dark and light current-voltage characteristics were measured either by XT-10 solar simulator or by pulse tester. The illuminated current versus voltage (I-V) characteristics of a solar cell is typically measured with respect to standard reference conditions defined by the spectrum, intensity, temperature and area of the cell. Calibrated standard cells were used to adjust

the intensity of the light. Once the solar simulator intensity has been set to match the standard intensity and spectrum using a reference cell for the particular device being evaluated, the I-V characteristics can be measured.

The solar cells were light soaked under open circuit condition using the Oriel Solar simulator under an illumination of one sun. The temperature of the stage was maintained at 25 °C. Illuminated I-V measurements were done in two modes: in one case, the I-V measurements were done during the light soaking itself using a DC testing system (XT-10); in the other case, cells were light soaked by using AM1.5 Oriel Solar simulator, were removed from the light-soaking station and tested under a (Sinton) pulse tester. The temperature of the solar cells was monitored by using a thermoelectric module during light soaking and I-V measurements, to verify that the device temperature remains at 25 °C. I-V measurements were done at different stages of light soaking, at an interval of 5 minutes to a span of up to 20 hours. After total about 72 hours of light soaking, the cells were annealed, and in some cases, they were cycled through light soaking and annealing. Annealing was done at 200°C for 30 minutes following the procedure described in ref. [85]. All the measurements were done to promote reliable determination of the small changes in the cell parameters that occur as a result of LID.

5.2 Quantum Efficiency

The internal quantum efficiency of the cell is measured at 25 °C by using spectral responsivity equipment at NREL. All QE measurements were performed without one sun light bias. First of all, the calibrated cell, CZ-Si cell of [100] orientation, is placed on vacuum stage. Visible range of light at 550 nm is used to adjust the beam size such that

light is focused in between two consecutive fingers. Electrical back contact is made through back surface of the cell and front contact is made with magnetic probe. Front contact probe is placed on a busbar close to the beam spot. The useful solar spectrum lies in between wavelength of 300-1200 nm for silicon solar cell. So the quantum efficiency measurement is done in the range of 300-1200 nm range.

Once the system is calibrated, the test device is used to measure its quantum efficiency in the same range as that of the calibration cell. The software corrects the quantum efficiency of the device comparing with the quantum efficiency of the cell used for the system calibration.

In this study, quantum efficiency of the cell was measured after different light soaking time to see the effect of boron oxygen defect generated because of the extra charge carriers through the cell.

5.3 Lifetime Measurement of Silicon Wafer

Lifetime measurements were performed at room temperature using the quasi-steady state photoconductance (QSSPC) technique in "generalized mode". The set-up of the equipment involves a zeroing procedure that accounts for the dark conductivity of the wafer under measurement. User has to enter the estimated carrier concentration.

In order to start from the defined state, all the samples were annealed at 200 °C in dark for 30 minutes. As was expected, all the boron-oxygen complexes were completely dissociated before lifetime monitoring was started. Before measuring the lifetime, the wafers were subjected to a polishing etch containing HNO_3, HF, and CH_3COOH

(removal of about 6 μm from both sides of the wafer) and a subsequent surface clean by piranha solution followed by HF dip.

Generally, the wafer does not have passivation layers on the front and the back side. Thus the wafer is placed in a thin plastic bag with iodine-ethanol or quinhydron solution to passivate the surface of the wafer. After performing lifetime measurement, the wafers were light soaked for various durations under one sun illumination and lifetime was measured to study the change in bulk lifetime due to B-O complex formation in p-type wafer. The wafers were prepared by a procedure described in Ref. [86].

To remove the effect of the residue (if any) of the chemical used for surface passivation during lifetime measurement, the wafers were chemically etched before each measurement. Some of the wafers were annealed and lifetime was measured to see whether original lifetime is restored or not.

5.4 Bulk Resistivity of the Wafer

Bulk resistivity of the wafer was measured by using four point probe technique. It is a simple method of measuring sheet resistivity. The thickness of the wafer is measured by using dial gauze at different points and average thickness is calculated.

Since the bulk resistivity is given by, $\rho = 4.532t\frac{V}{I}$, the current through the probes are adjusted so as it reads 4.532 mA, then the corresponding voltage multiplied by the thickness in proper unit gives the resistivity of the wafer.

CHAPTER 6

RESULTS AND DISCUSSION

This chapter discusses variation in the electrical properties of the mono-crystalline silicon solar cell as a function of illumination time. Formation of B-O complex and its effect on carrier lifetime of silicon wafer due to excess charge carriers is discussed. Based on the observed changes in cell parameters, a new component of light induced degradation is proposed. Interface between metal-insulator-semiconductor is considered as one contributor to the LID of silicon solar cells.

6.1 Changes in Cell Parameters as a Function of Light Soaking Time

Figure 6.1(a) shows the time dependent degradation behavior of the open-circuit voltage (V_{oc}) and short circuit current density (J_{sc}) of one of the typical singe crystalline silicon solar cells. Figure 6.1(b) shows the corresponding changes in the fill factor (FF) and efficiency of the same cell. From Figure 6.1, it is clear that the degradation of the cell parameter does not follow exponential decay as claimed by other researchers earlier [20,73,77,87] for the B-O complexes formed by excess carriers developed because of the illumination of light. Before V_{oc} or J_{sc} approach a stable final value, both try to stay at their previous states if I-V measurements are done at an interval of 1-2 hours. Decrease in V_{oc} and J_{sc} value is seen between two consecutive measurements that are long enough in duration. Almost all cells tested showed similar behavior. FF is more sensitive to resistance of the cell; so fluctuation in the value of FF, seen in Figure 6.1 (b), is linked with the contact resistance of the series of current and voltage probes loaded with the

spring. This effect appears in the measurement of the efficiency as well. Figures 6.1(a) and (b) also confirm that there appears to be an initial fast decay followed by a slower decay of cell parameters, as observed by Bothe and Schmidt [26].

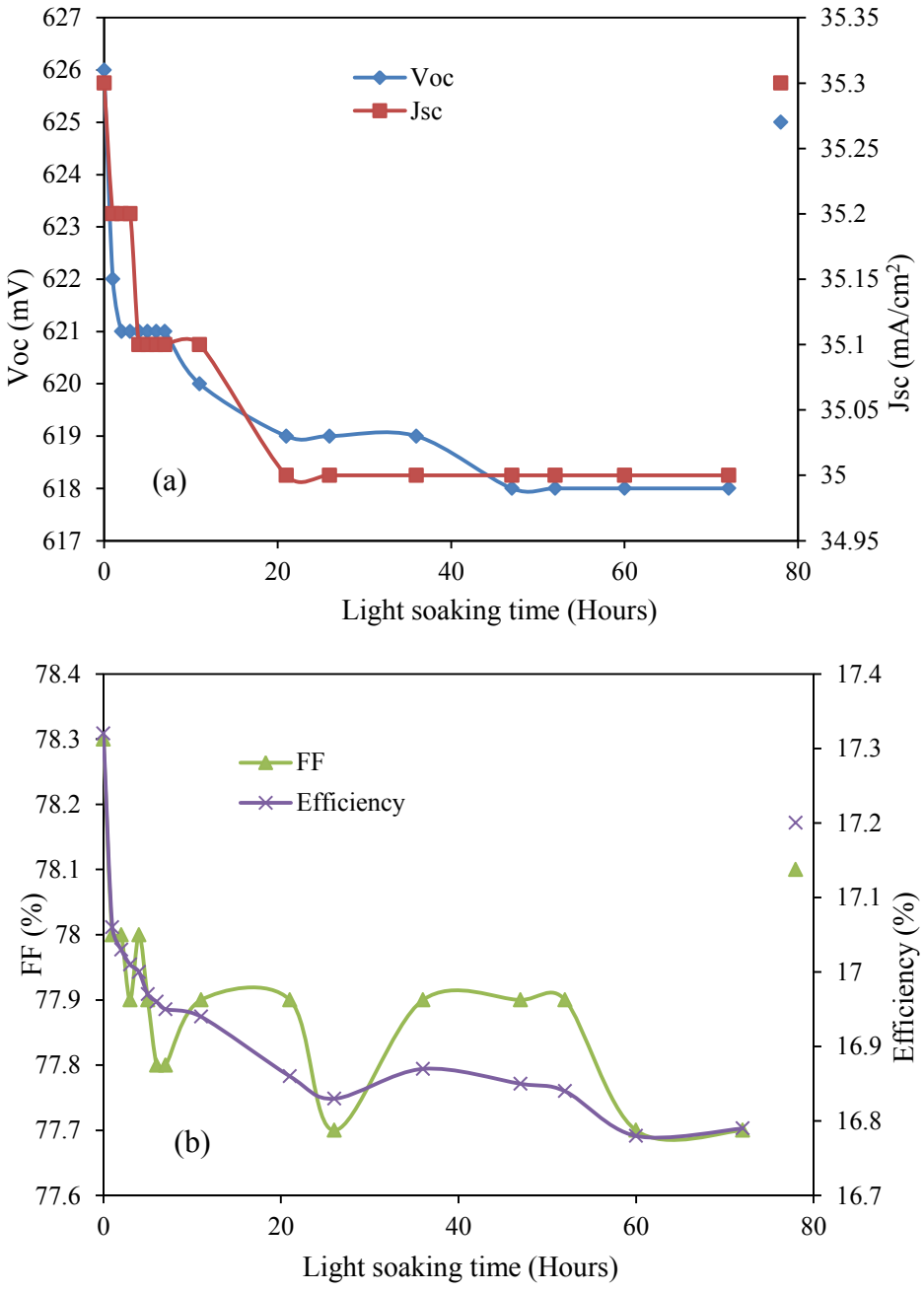

Figure 6.1 (a) Variation of V_{oc} and J_{sc} (b) FF and efficiency of one of the single crystalline silicon cell plotted as a function of light soaking time.

For the first hour, the cell was taken out every 5 minutes and the I-V data measured with a pulse tester. Figure 6.2 shows the changes in the cell V_{oc} and J_{sc} during the first 60 minutes. Following the first hour of soaking, the cell was exposed for one hour at a time and taken out for measurements. Figure 6.2 suggests that there is a sort of recovery of the V_{oc} for the first one hour of light soaking of the cell. This type of recovery was not observed for J_{sc} values during the same time. Results from other cells (of this batch and others) also show similar effects of partial recovery in the initial phase of light soaking. It is important to point out that this happens only if the cell is withdrawn from the light-soaking source. I-V measurements for cells that were soaked continuously do not show any partial recovery in electrical properties.

It is felt that this is a manifestation of interface activity and that defects are either generated at the interface and/or there is charge redistribution during light soaking [88,89]. The result is a higher effective surface recombination. This conclusion is also attested by the change in spectral response of the cell that will be discussed in later section.

Interface from one semiconductor to a metal determines one of the important properties of the electronic structure, i.e., connection of bands. It is caused by a number of factors such as (i) the difference between work function of the involved semiconductors or metals, (ii) the valence band offset, (iii) the lattice misfit at the interface, (iv) the interface defect levels, (v) the induced interface dipole, etc. Depending on the conductivity and other material parameters, compensating charges are distributed over the interface.

In case of silicon solar cells, a thin layer of insulating film (SiN:H) stays in between metal (silver fingers, or busbar) and semiconductor. This thin layer consists of additional dipole layer that equalizes Fermi-level across the entire interface in equilibrium. During illumination, the dipole layer at interface is modified that produces change in bonding or charge redistribution at the interface states. The effect of thin insulating layer that tend to restore the barrier height between metal-semiconductor interfaces block the effect of illumination [90].

Figures 6.1(a) and 6.1(b) also confirm that there appears to be an initial fast decay followed by a slower decay of cell parameters, as observed by Bothe and Schmidt [26].

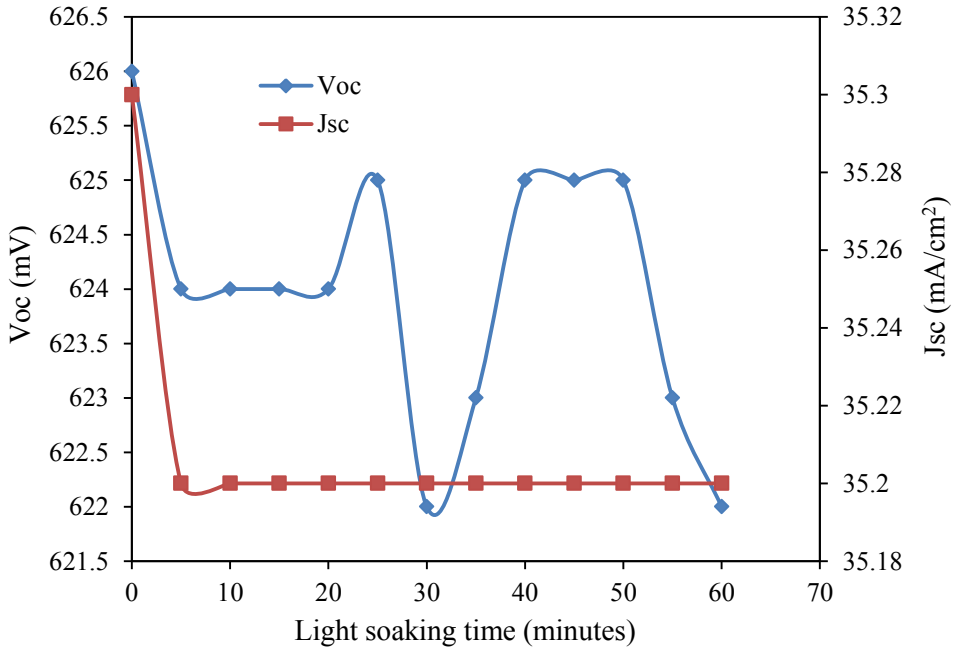

Figure 6.2 Decrease of V_{oc} and J_{sc} of a cell for the first hour of light soaking.

The reduction in efficiency of p-n^+ solar cell is by the decrease in the lifetime τ of the minority carrier electron in p-silicon active layer of the solar cell and that change in τ depends on the concentration of the defect. Defect concentration generated by light soaking is also a function of time dependent V_{oc} [5,91].

Figure 6.3(a) shows illuminated I-V plots of a typical cell for three different conditions; before light soaking, after light soaking for 72 hours, and after annealing of the cell. Figure 6.3 (b) shows the corresponding semi log plot of dark I-V characteristics of the cell before and after light soaking and after annealing.

The semilog plot of dark I-V of a cell reveals much more information about the cell. The cell performance in the low voltage region is dominated by shunt resistance. Two exponential regions can be seen starting at 0.2 V, with slopes of qV/2kT and qV/kT respectively. The decreasing slope of the current at higher voltage region is a result of series resistance of the device. Almost all large area silicon solar cells show some shunt resistance effect. Table 6.1 shows the cell parameters before light soaking, after light soaking, and after annealing.

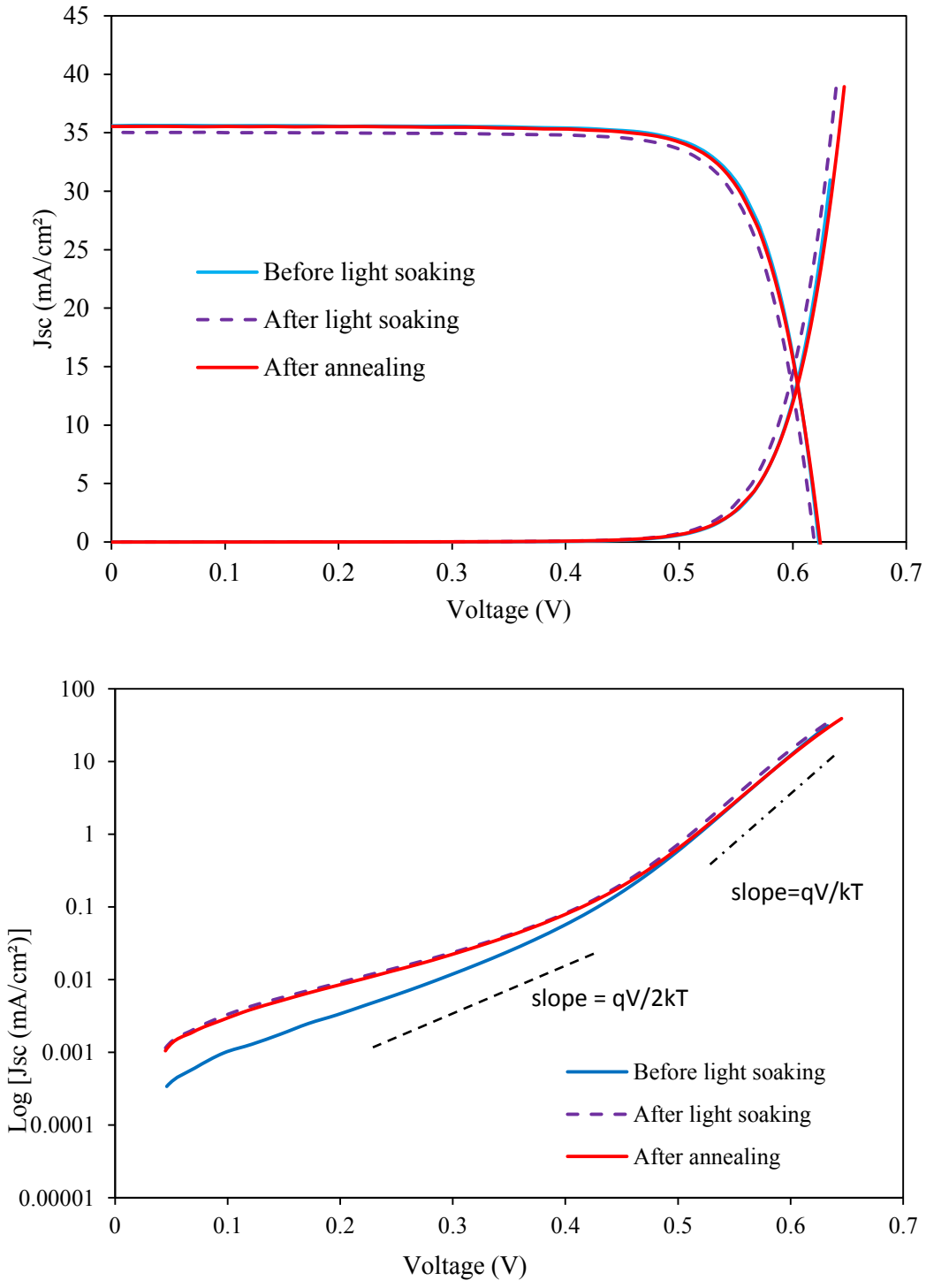

Figure 6.3 (a) Light and dark I-V characteristics of a cell under different conditions plotted together (b) Semi log plot of dark I-V of the same cell under different conditions.

It is seen that all cell parameters (V_{oc}, J_{sc}, and FF) degrade with light soaking and then recover: in this case, the J_{sc} recovered fully, whereas V_{oc} and FF recovered only partially. Values of V_{oc}, J_{sc}, FF, and efficiency are shown in Figure 6.1 (a) and (b) after annealing the cell.

Working with many cells, it is found that there are some cases in which V_{oc} recovers fully after annealing but J_{sc} and FF recovers partially. To our knowledge, the partial irreversible degradation of crystalline silicon solar cells has not yet been reported. Moreover such partial recovery cannot be explained by the conventional way alone; so a different physical origin must exist. Either of the result indicates that the degradation produced by B-O complexes (bulk effect) can be regenerated upon annealing but the degradation due to interface effect does not recover.

Table 6.1 Parameters of a Cell under Three Different States

Parameters	Before light soaking	After light soaking	After annealing
V_{oc} (mV)	626	618	625
J_{sc} (mA/cm^2)	35.3	35	35.3
FF (%)	78.3	77.7	78.1
Efficiency (%)	17.32	16.79	17.20

6.2 Recovery of Cell Parameters upon Annealing

As discussed in Section 6.1, Figure 6.1 (a) and (b) show the recovery of the V_{oc}, J_{sc}, FF and efficiency after annealing the cell. In this case, J_{sc} is recovered fully but V_{oc} and FF are recovered partially.

The dark I-V data were fitted by using the software developed at NREL. From the dark I-V data, the parameters, the diffusion current density (J_{01}), recombination current density (J_{02}), series resistance (R_s) and shunt resistance (R_{sh}) are derived according to the double diode model. The first diode represents the solar cell itself while the second diode

represents the leakage or recombination in the depletion region of the p-n junction. The R_{sh} of all cells is sufficiently high to exclude shunting losses, which would result in a low FF.

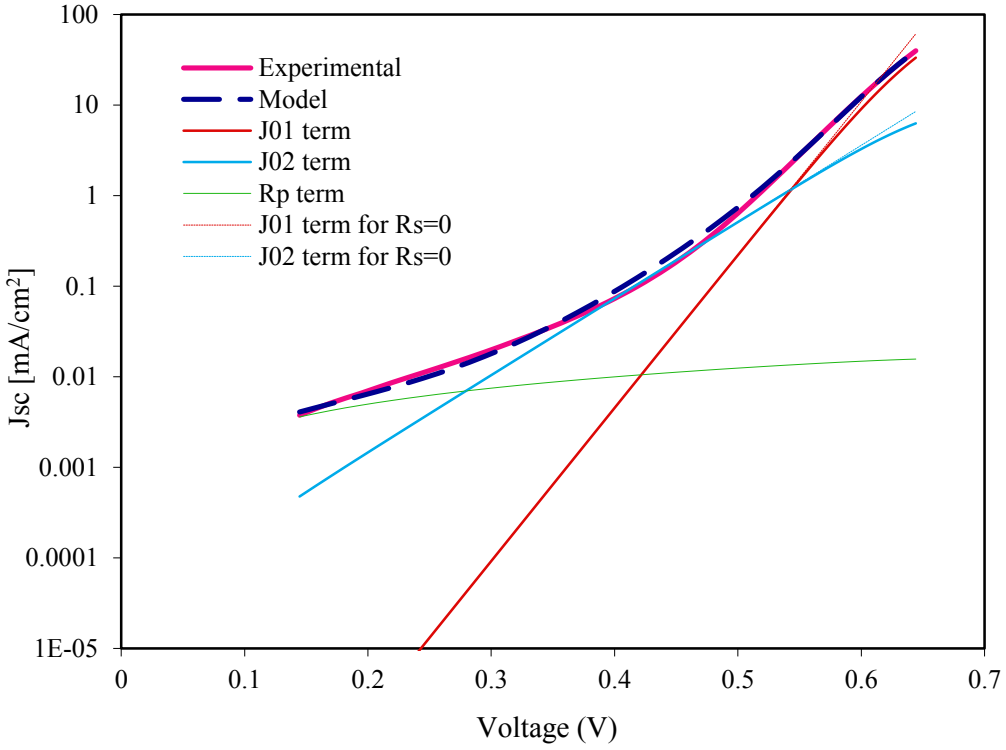

Figure 6.4 Fitting of dark I-V characteristics by using double diode model.

J_{02} is traditionally considered to be a measure of recombination in the space charge region and can be related to the density of recombination centers in solar cells. A more effective gettering should reduce the SRH recombination (by removing traps), yielding a low J_{02}. The lowest J_{02} values of 1.77×10^{-5} mA/cm^2 are observed in one single crystalline silicon solar cell with series resistance 2.0 mΩ and shunt resistance 43.5 kΩ.

It is seen that both J_{01} and J_{02} increases after light soaking. An interesting feature is that, upon annealing, J_{01} decreases back to its original value, but J_{02} does not recover**.** This is a clear indication of surface instability and is believed to be related to the

SiN:H/Si interface effects. It is pointed out that degradation of J_{01} with light soaking and its full recovery upon annealing has been observed and reported by Herguth et al. [92]. The values of J_{01}, J_{02}, R_s, and R_{sh} are also shown in Table 6.2.

Table 6.2 Parameters of the I-V Data Fit by Double Diode Model of a Single Crystalline Silicon Solar Cell

Parameters	Before light soaking	After light soaking (72 h, 1-sun, 25 °C)	After annealing (200 °C, 30 min)
J_{01} (mA/cm^2)	7.88x 10^{-10}	9.36x 10^{-10}	7.05x 10^{-10}
J_{02} (mA/cm^2)	2.49x 10^{-5}	3.62x 10^{-5}	3.3x 10^{-5}
R_s (mΩ)	1.45	1.65	1.65
R_{sh} (kΩ)	135	32	35

The degradation at the SiN:H/Si interface and within SiN:H has been reported previously and is thought to be due to an increase in D_{it} and the defect density within SiN:H film [93,94]. It has been shown that exposure to light will cause an increase in the interface state density D_{it} in both p- and n-type Si. This effect is also expected to cause the observed changes in J_{02}.

6.3 Minority Carrier Lifetime Degradation

6.3.1 Minority Carrier Lifetime Degradation in Wafer

It is instructive to examine if the LID in the cells is fully controlled by the degradation in carrier lifetime τ. To accomplish this, the changes in the minority-carrier lifetime with light soaking of similar wafers (prepared by the same crystal/wafer technology) corresponding to various cells was measured. Figure 6.5 shows the bulk lifetime decreasing phenomena of p-type CZ silicon wafer as a function of illumination time for AM1.5 solar simulator.

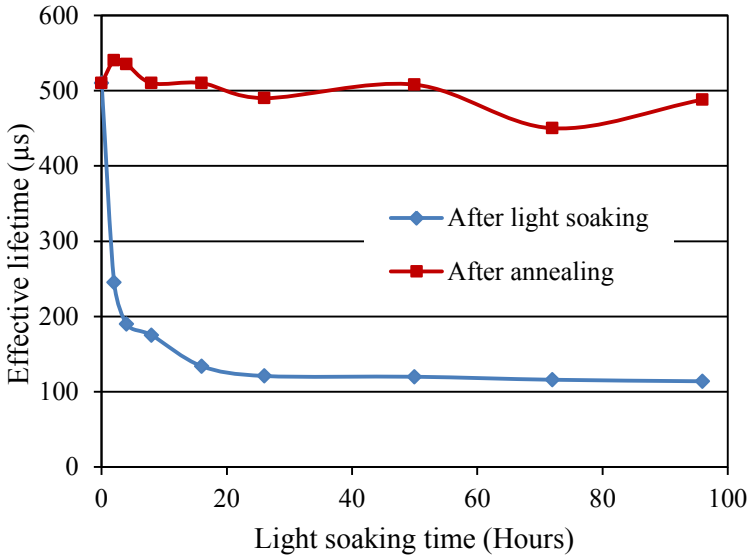

Figure 6.5 Measured changes in the minority-carrier lifetime as a function of light soaking and annealing on a sc-Si wafer.

The injection level density dependence of carrier lifetime in the annealed state and degraded state was measured by using quasi steady state photoconductive decay (QSSPCD) technique. Maximum effective lifetime for wafers light soaked for different length of time is plotted as a function of light soaking time. One can see that the behavior of the time dependence of lifetime degradation is about the same as degradation of V_{oc} and J_{sc} for the cell as shown in Figure 6.1(a). The lifetime decays rapidly in the first hour of light soaking and slowly reaches the minimum saturation value. The defects are deactivated by an annealing step of 30 minutes at 200 °C. According to SRH statistics, the bulk lifetime in CZ silicon strongly depends on both the injection density and the doping concentration [95,96].

Maximum value of injection dependent carrier lifetime of each wafer after annealing is shown in Figure 6.5. It is seen that annealing recovers the bulk lifetime to the level of the wafer before illumination assuming an accuracy of 10% for the underlying lifetime measurements. In this work, it is confirmed, by means of direct measurement of

recombination lifetimes, that high and stable lifetimes can be achieved in B-doped CZ-silicon wafers by subsequently annealing and illuminating them.

Based on the comprehensive lifetime study, the cell performance of the boron doped CZ silicon solar cell can be explained. Degradation of the cell parameters due to bulk effect is fully recovered by annealing at 200 °C. To reconcile the fact that cells exhibit a full recovery of bulk effect, even if there is incomplete recovery of the bulk lifetime, one needs to consider the following argument. Because the cell efficiency is about 17.5%, this can be satisfied by a bulk lifetime of about 150 μs. Clearly, a 30 minutes annealing is sufficient to raise the lifetime above this level.

6.3.2 Bulk Minority-Carrier Lifetimes in the Finished Solar Cells

The bulk lifetime in the dielectric and BSF back passivated cells were measured with the help of the adjacent cells that were subjected to the same processes. The lifetime was measured by stripping off all the fingers, busbars, and passivation down to the silicon substrate and then performing lifetime measurement with surface passivation by using iodine-ethanol solution. Initial lifetime of the wafer was 500 μs. The lifetime value of 500 μs is sufficiently higher than the lifetime of the cell which has 17.5% conversion efficiency. Concentrations of metal impurities would be much lower because of the gettering of the wafer due to different high temperature processing steps during cell fabrication.

The lifetime of the wafer decreases on light soaking. Interestingly, the lifetime was not recovered fully after annealing. Our experimental data have shown that, even after two hours of annealing at 200 °C, the lifetime is not recovered fully. We have also observed that the wafers with high lifetime are sensitive even to the light in the wafer

preparation hoods. These results seem to indicate that perhaps multiple defects are associated with B-O interactions and some of the defects are stable at 200 °C.

6.4 Quantum Efficiency

Figure 6.6 shows the quantum efficiency of one of the single crystalline silicon solar cell before and after light soaking. The UV light is absorbed near the surface while illumination and infrared light is absorbed deep in the wafer. In case of silicon solar cells, the UV light favors surface recombination whereas IR light emphasizes bulk recombination.

It is seen that, although the response in most of the wavelength range is reduced, the reduction in response at the shortest wavelength is relatively large. Magnified short wavelength region is shown in the inset. Wavelength, in the range of 500- 1000 nm, of the QE curve holds information about the bulk lifetime and some surface effects. As expected, the QE data in the mid to long wavelength range indicates that the bulk lifetime of the cell has shown some change due to degradation. However, the QE data in the short wavelength range reveals that the front surface interface changes after light soaking. But the long wavelength response was virtually the same before and after light soaking. The loss of external quantum efficiency in the visible region of the spectrum is 1.6% which is the same as the degradation of the J_{sc} value of the cell. This allows to explain the lowering of the short-circuit current shown in Figure 6.1 (a) in terms of reduction in external quantum efficiency.

The above results clearly suggest that light soaking also has a surface effect, which we believe is a result of increase in D_{it} at the SiN:H/Si interface. Because

multicrystalline Si solar cells also use SiN:H as an antireflection coating, a similar behavior of mc-Si solar cells under light soaking is expected.

Study of the UV light below 350 nm was limited by the capability of the equipment. Since this equipment uses tungsten halogen lamp, basically there is no signal at that region but detector picks some signal which has very rare chances of repetability.

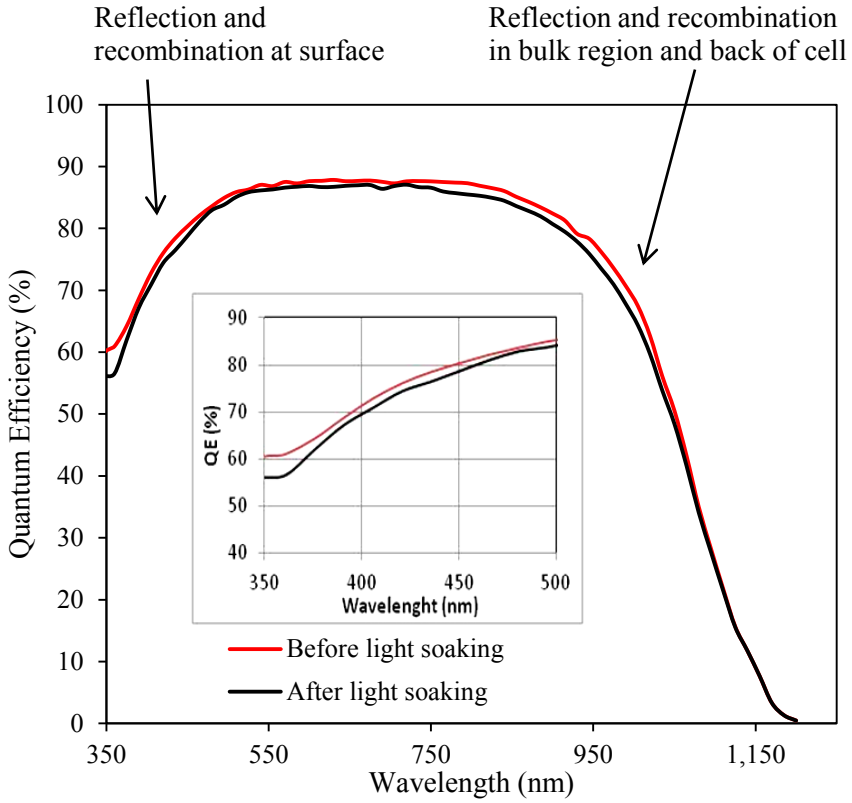

Figure 6.6 Quantum efficiency of a cell before and after light soaking. The inset shows magnified short wavelength region.

6.5 LBIC

To gain a better understanding of the effect of LID on solar cells, LBIC maps using short wavelength (630 nm) laser were obtained on some of the cells. The 630 nm is absorbed deep in the bulk and is therefore indicative of the surface recombination and the bulk

lifetime. Since the lifetime of the cells used in this study are fairly high (>350 μs) and uniform, variation in LBIC response primarily reflects the variation in the bulk lifetime as well as surface recombination.

It is very hard to see any difference by observing the LBIC maps of a cell before and after light soaking but we can see difference in the value of induced current. It is found that the laser beam induced current decreases with light soaking and recovers partially upon annealing. LBIC response is in very good agreement with the V_{oc} and J_{sc} data.

6.6 Correlation between Light and Current Induced Degradation

Single crystalline silicon solar cells were also tested for the degradation produced by applying forward bias under dark condition. Initially the cell was annealed at 200 °C for half an hour in dark. Dark and light current-voltage characteristics were measured by pulse tester. The solar cells were degraded by applying 700 mV (DC) forward bias under dark. The temperature of the stage was maintained at 25 °C. I-V measurements were done after various durations of applying current. After a total of about 72 hours of forward bias, the cells were annealed, and I-V characteristics were measured. Figure 6.7 shows the degradation of V_{oc} and J_{sc} upon application of a forward bias voltage of 700 mV, the cell being stored in dark.

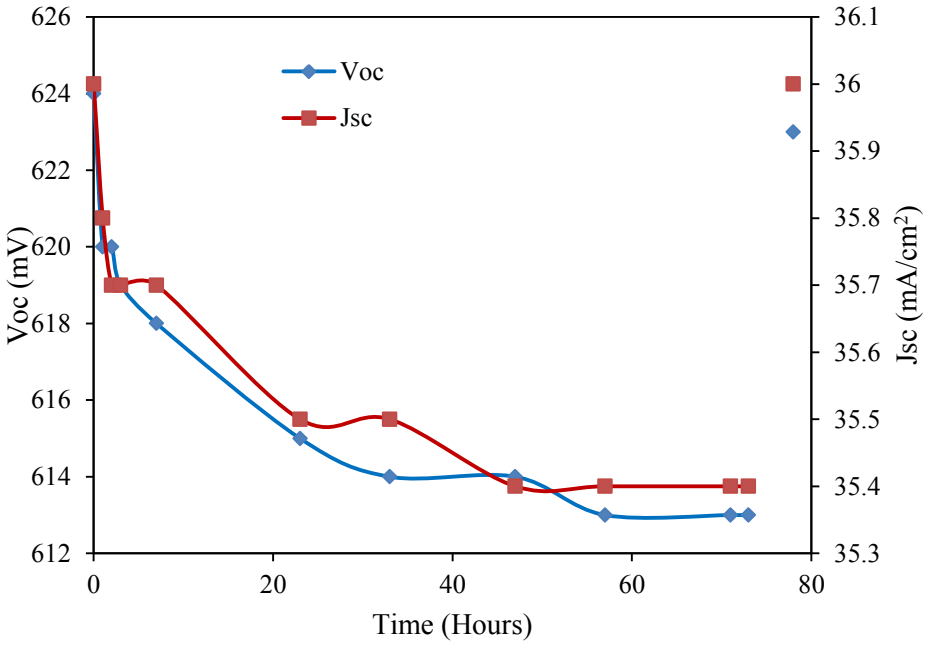

Figure 6.7 Degradation of V_{oc} and J_{sc} of a single crystalline silicon solar cell under application of a forward bias in dark.

As in the case of a cell degraded under illumination, the degradation of the cell parameter does not follow exponential decay as claimed by other researchers earlier [20,81]. Before V_{oc} or J_{sc} approach a stable final value, both try to stay at their previous states. Excess carrier produced by the application of forward bias also shows that the cell has partial recovery of its cell parameters. In Figure 6.7, J_{sc} recovers fully and V_{oc} and FF (not shown here) recover partially.

6.7 Resistivity Measurements

Resistivity of silicon wafer is a function of doping concentration and mobility of charge carriers. Since the doping concentration of the wafers used during the course of this study was not changed on purpose, it is tried to see whether mobility of the charge carriers changes due to generation of B-O complex because of illumination. Resistivity was determined at various positions of the wafer by using four point probe technique. In this

observation, resistivity of wafer does not change with light soaking time. Even if there is a small change, it does not follow the pattern of illumination time. That change was considered to be within the instrumental error of four point probe technique. It is concluded that the change in mobility of charge carrier, due to formation of B-O complex, could not alter the bulk resistivity of the wafer at least to be detectable by four point probe.

6.8 Multi-crystalline Silicon Solar Cell Degradation

In the previous sections, the impact of LID on single crystalline silicon materials was investigated. This section deals with the investigation of LID in low cost PV grade Si materials, especially on multi-crystalline silicon solar cells. To check the characteristics of degradation and recovery cycle resulting from illumination, similar procedure was followed as the case of single crystalline silicon solar cell (discussed in section 5.1). Although standard multi-crystalline silicon contains less oxygen than Czochralski grown silicon, initial lifetime of such wafer are in the range of 30- 80 μs. High dislocation density region are responsible for an increase in dark forward current and a decrease in efficiency and cell parameters [97].

Due to high segregation coefficient, oxygen is preferentially incorporated in the crystal and is therefore primarily present in high concentration in the lower part of the ingot while the boron concentration increases towards the top. In fact degradation can be a serious issue if oxygen concentration exceeds a certain value. Because oxygen and defect concentration could vary significantly over a given multi-crystalline silicon wafer, this could result in spatial variation in LID.

Multicrystalline silicon has a low concentration of oxygen (typically ~10^{17} atoms/cm^3) and is not expected to display significant B-O defect formation. Hence, solar cells made from cast material are not expected to have LID. Yet, some researchers have reported degradation in the cell performance upon exposure to light [39,40,98,99].

Many mc-Si solar cells have been tested (>20) to investigate if the mechanism of the observed LID is also related to the surface effect that was observed earlier in CZ cells. Figures 6.8 (a) and (b) show the measured variations in cell parameters with light soaking under 1-sun at 25°C. The cell parameters before and after light soaking are given in Table 6.3. It can be seen that there is a very small change in the cell parameters. However, it is interesting to note that Figure 6.8 (a) and (b) have recovery features similar to that of Figure 6.1 and 6.2.

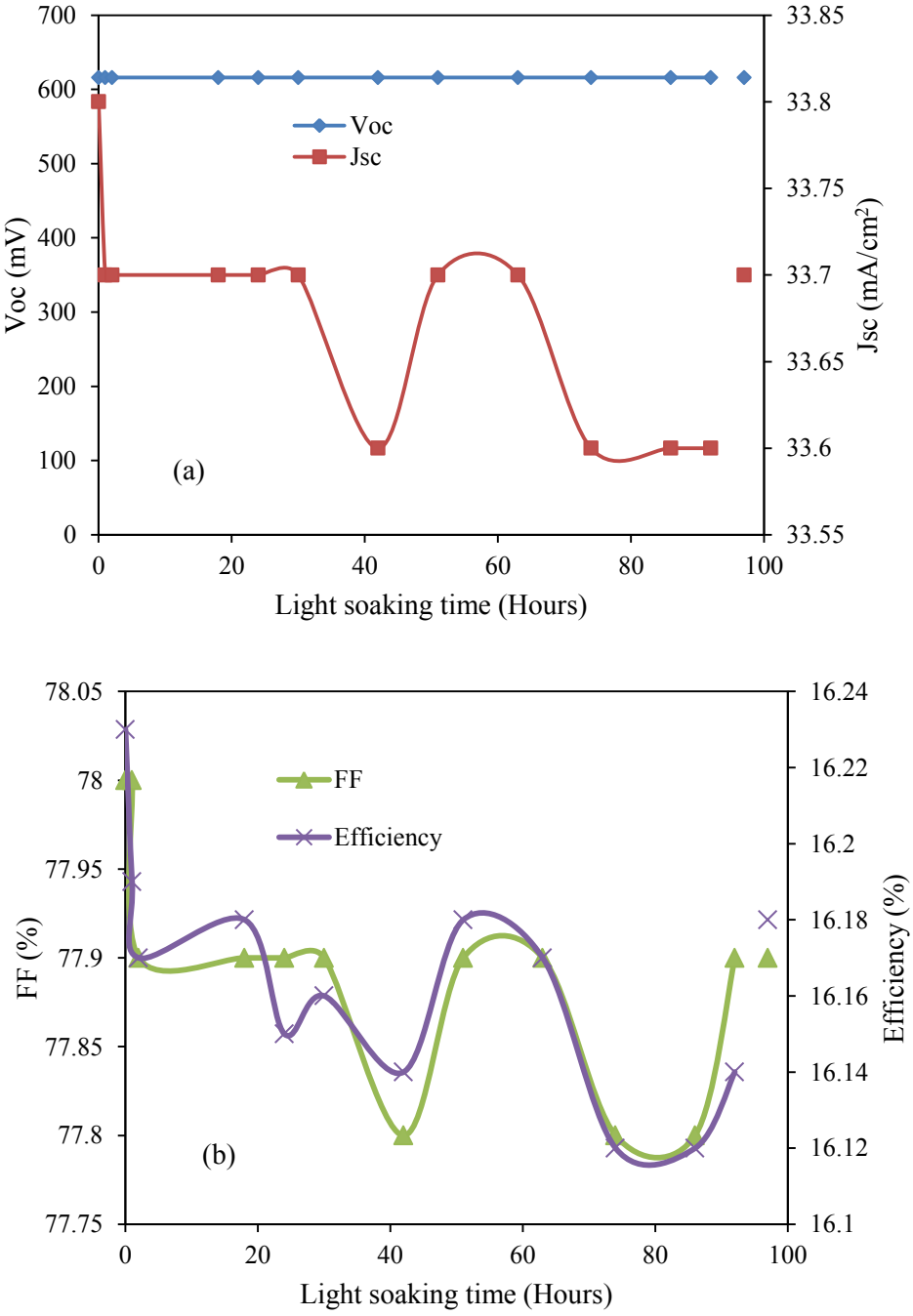

Figure 6.8 Measured variation in the (a) V_{oc} and J_{sc} (b) FF and cell efficiency as a function of light soaking time.

Figures 6.9 (a) and (b) show the illuminated and dark I-V plots before and after light soaking, and after annealing.

Table 6.3 Cell Parameter of One mc-silicon Solar Cell before Degradation, after Degradation and after Annealing

Parameters	Before light soaking	After light soaking (86 hours, 1-sun, 25°C)	After annealing (200°C, 30 min)
V_{oc} (mV)	616	616	616
J_{sc} (mA/cm^2)	33.8	33.6	33.7
FF (%)	78	77.9	77.9
Efficiency (%)	16.23	16.14	16.18
J_{01} (mA/cm^2)	12.0×10^{-10}	10.5×10^{-10}	9.8×10^{-10}
J_{02} (mA/cm^2)	1.61×10^{-5}	2.88×10^{-5}	3.41×10^{-5}
R_s (mΩ)	2.3771	2.2335	2.0179
R_{sh} (kΩ)	50	35	55

The degradation in efficiency is only 0.1%. Since the degradation of efficiency is small, LID is not viewed as a serious problem in mc-silicon solar cells. Even this small change in J_{sc} and efficiency did not recover after annealing which is different from what was observed before [100]. Again, it is seen that the J_{02} component of the dark current does not recover upon annealing. Table 6.3 also includes J_{01}, J_{02}, R_s, and R_{sh} values. These results clearly suggest that degradation produced in mc-silicon solar cell due to light soaking is not from bulk effect but also has a surface effect. These mc- cells were also passivated by using same techniques as in the case of single crystalline silicon solar cells.

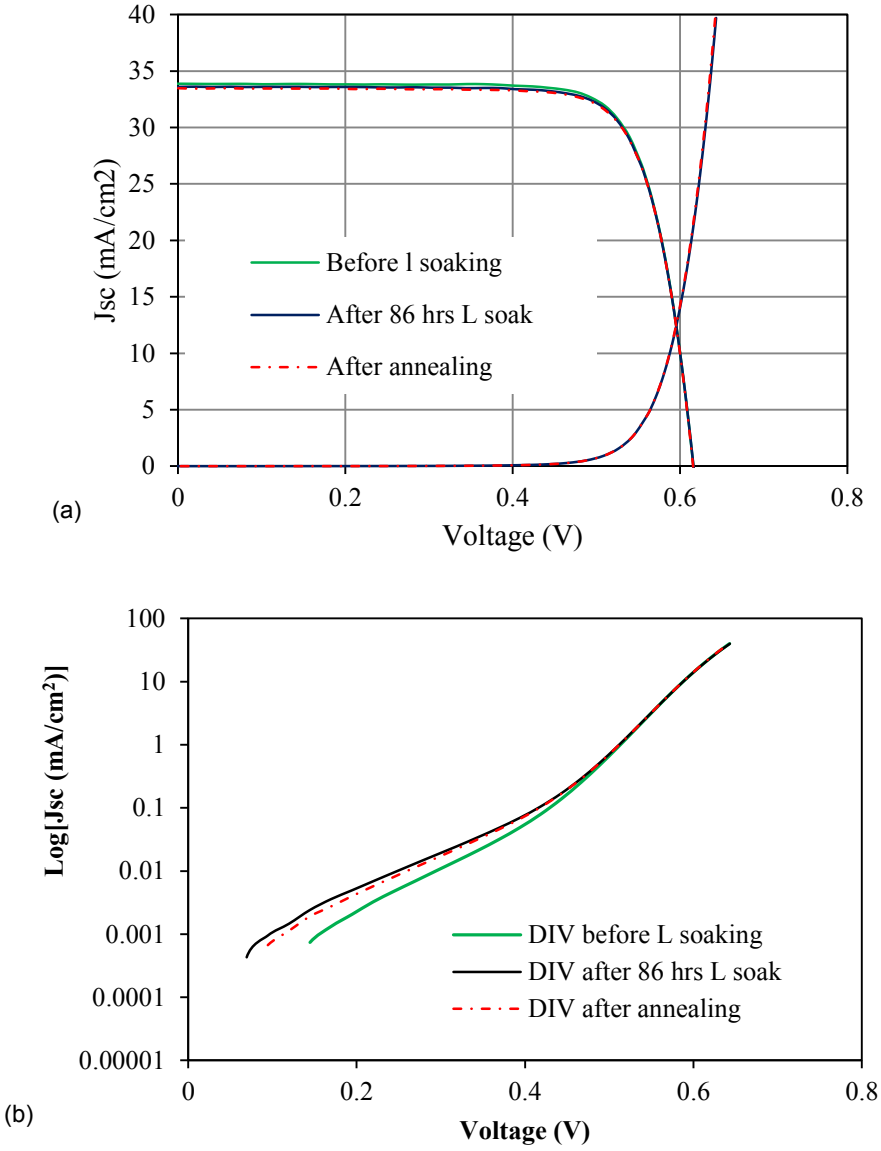

Figure 6.9 (a) Illuminated and dark I-V plots before and after light soaking, and after annealing. (b) Change in the log plot of the dark I-V characteristics of the same mc-Si solar cell as a function of light soaking.

Thus it is claimed that, for low oxygen and low boron content, mc-silicon solar cells degrade as a result of increase in D_{it} at the SiN:H/Si interface. Because multicrystalline Si solar cells also use SiN:H as an antireflection coating, a similar behavior of mc-Si solar cells under light soaking is expected.

CHAPTER 7

CONCLUSIONS AND FUTURE WORK

7.1 Conclusions

A detailed experimental study of light induced degradation of industrial crystalline silicon solar cell was investigated. Initial degradation of cell parameters due to excess charge carriers generated either by illumination or by carrier injection shows partial recovery. Boron oxygen complex formed acts as trap and activation of the trap results in the well known lifetime degradation by up to 80% of its initial value. This results in decrease in conversion efficiency of the solar cell. Degradation and recovery of LID traps are affected differently by heat and illumination. We described some results of analyses of LID of c-Si and mc-Si solar cells to further understand the bulk and surface components. Results have shown that degradation mechanisms are bulk and surface related.

Significant LID was detected on cast multi-crystalline silicon solar cell by degrading efficiency of 0.1-0.2 % absolute value. It is said that oxygen content in mc-silicon varies with the position of the wafer in the ingot. The cell tested just showed minimum amount of degradation and did not correlate with the position of the wafer in the ingot because of no prior information about them. Since the amount of oxygen possessed by mc-silicon is low, it cannot play a role in the bulk degradation but the degradation of such cells is associated with the interface effect between SiN:H-Si surfaces.

A comprehensive study on carrier lifetime in p-type CZ silicon revealed that degraded bulk lifetime can be recovered by annealing at 200 °C for 30 minutes. Bulk effect as observed on cell was compared with observed effect in the lifetime of the wafer. In some cases, the wafer consisted of the stripped cell. The bulk effect is primarily B-O related. The degradation behavior of cell parameters and the lifetime (in wafer) are similar—they exhibit a sharp decay followed by a gentler slope. However, the annealing results in the cells and wafers appear to be quite different. The bulk lifetime recovers almost fully after 200 °C, 30 minute annealing but the cell exhibits only partial recovery after 200 °C, 30 minutes annealing. This partial recovery is due to surface effect that appears to be related to SiN:H/Si interface. Although their manifestation is very little in the illuminated cell characteristics, it can be easily seen in the J_{01} component of the dark plot. This loss in efficiency was also verified by using similarly passivated low oxygen content mc- silicon solar cell. Likewise, it appears as a slightly lower short-wavelength response in the spectral response after light soaking.

The other salient characteristics of LID that have been seen are the following:

1. As is already known, there is an initial rapid decay of all cell parameters (within a few minutes), followed by a slower degradation. In general, all cell parameters experience a reduction.
2. Under 1-sun at 25°C, it takes about 72 hours for complete light-induced degradation.
3. The total effect of LID is about 0.5% absolute (< 0.5% degradation).
4. In the initial course of light soaking, there is evidence of partial recovery of cell parameters if the cell is taken out of illumination for I-V measurements.

7.2 Future Work

The experimental studies and discussion of results allow the following recommendations that would help to develop a better understanding of LID and carry out important steps to lower its effect on solar cell performance:

1. All the results presented here for claiming interface effect of LID are based on indirect observations. Measurements were performed to directly determine changes in the density of interface states (D_{it}) and fixed charges (Q_f) at the SiN:H/Si surface of the cell as a result of light soaking and annealing. As Q_f and D_{it} are properties of the interface structure between the materials, SiN_x:H/Si cause local field effect which can be determined by using capacitance-voltage (CV) MIS analysis. These results, along with LBIC studies (which can detect smaller spatial changes), will be presented in forthcoming publications.

2. In crystalline silicon solar cells, the amount and pattern of LID depend on the structure and manufacturing process. Depending on the research groups working in production and studies of the solar cells, degradation model and rate varies. Therefore silicon solar cell community should work for establishing a universal degradation model.

3. Complete degradation of a solar cell takes about 3 days and working with various cells is time consuming. Thus it is also necessary to establish a fast and accurate degradation test method which can estimate long-term field degradation and lifetime.

4. As the lifetime degradation leads to significant loss of solar cell efficiency, the reduction or elimination of the metastable defect has a high potential for improving CZ silicon solar cells. The degradation can be lowered either by reducing one of the two major components (boron or oxygen) of the metastable defect. This study clearly shows

that effort should be made to grow low oxygen contained CZ, or MCZ to eliminate LID in crucible grown CZ.

5. Another alternative is to modify the cell design so that efficiency of the cell is less sensitive to the bulk lifetime. The cell with high lifetime and sufficiently thin can improve the degradation produced by the effect of light. If the lifetime of the wafer is 500 μs, then the corresponding diffusion length will be around 1200 μm which is almost four times the thickness of the solar cell (~300 μm).

6. The spatial non uniformity of multi-crystalline silicon needs to be further investigated. If the trap responsible for LID is dependent on spatial distribution of oxygen in wafer position in ingots, a model for the distribution of oxygen as a function of ingot dimensions would be very helpful. Further investigations of light induced degradation may provide alternative methods to mitigate or reduce the boron-oxygen complex in finished solar cells. Effect of grain boundary region on light induced degradation should be further studied.

7. So far, the determination of activation energy of association and dissociation of boron-oxygen trap are based either on injection level dependent lifetime spectroscopy or temperature dependent lifetime spectroscopy. If some changes in the DLTS techniques will be able to detect energy of metastable trap, it would be a great accomplishment to cross verify the results so far obtained or to open new ways for studying LID effect of solar cells.

8. For the reduction in interface effect in LID, excellent and reproducible quality SiNx:H should be deposited as antireflection and passivating layer, so that it remains stable during illumination and Q_f and D_{it} will be as minimum as possible.

9. This study confirms that LID is responsible for the efficiency degradation. It is important to note that about 1% absolute loss in efficiency of a 16% efficient solar cell amounts to a 6% reduction in the production capacity. In terms of monetary units, this translates to $25 million/year loss for a 100 MW production plant, assuming a module cost of $4/$W_p$. Even for lower loss of efficiency to 0.5% absolute by improving the cell structure, it will lower the cost by $ 0.12/W_p which will be a big step towards DOE's Sunshot goal.

REFERENCES

[1] Martin A. Green, Solar Cells, Operating principles, technology, and system applications, Prentice-Hall, Inc., Englewood Cliffs, NJ (1982).

[2] D.L. King, M.A. Quintana, J.A. Kratochvil, D.E. Ellibee, and B.R. Hansen, "Photovoltaic module performance and durability following long term field exposure", *Prog. Photovolt. Res. Appl.*, vol. 8, pp. 241 (2000).

[3] P. Drevinsky, C. Caefer, S. Tobin, J. Mikkelsen, L. Kimerling, "Influence of oxygen and boron on defect production in irradiated silicon", *Mat. Res. Soc. Symp. Proc*., vol. 104, pp. 167 (1988).

[4] V.G. Weizer, H.W. Brandhorst, J.D. Broder, R.E. Hart, and J.H. Lamneck; *J. Appl. Phys.* vol. 50, no. 6, pp. 4443 (1979).

[5] K. Bothe, R. Hezel, J. Schmidt, "Recombination enhanced formation of the metastable boron-oxygen complex in crystalline silicon", *Appl. Phys. Lett.* vol. 83, no. 6 pp. 1125 (2003).

[6] P.M. Mooney, L.J. Cheng, M. Suli, J.D. Gerson, and J.W. Corbett, "defect energy levels in boron doped silicon irradiated with 1-MeV electrons" *Phys. Rev. B*, vol. 15, no. 8, pp. 3836 (1977).

[7] L.C. Kimerling, M.T. Asom, J.L. Benton, P.J. Drevinsky, and C.E. Caefer, "Interstitial defect reactions in silicon" *Mater. Sci. Forum*, Vols. 38-41, pp. 141 (1989).

[8] H. Fischer, and W. Pschunder; "Investigation of photon and thermal induced changes in silicon solar cells", *Proc. 10th IEEE Photovoltaic Specialists Conf.*, Palo Alto, CA, pp. 404 (1973).

[9] J. Schmidt, A.G. Aberle, and R. Hezel, "Investigation of carrier lifetime instabilities in CZ-grown silicon", *Proc. 26th IEEE Photovoltaic Specialists Conf.*, Anaheim, CA, pp. 13 (1997).

[10] J. Schmidt, and A. Cuevas, "Electronic properties of light induced recombination centres in boron doped Czochralski silicon", *J. Appl. Phys.*, vol. 86, no. 6, pp. 3175 (1999).

[11] J.C. Bourgoin, N. de Angelis, and G. Strobl, "Light induced degradation of Si cells, model of metastable defect", *Proc. 16th European Photovoltaic Solar Energy*, pp. 1356 (2000).

[12] J. Schmidt, and K. Bothe, "Structure and transformation of the metastable boron and oxygen related defect center in crystalline silicon" *Phys. Rev. B,* vol. 69, no. 2, pp. 024107 (2004).

[13] J. Schmidt, K. Bothe, and R. Hezel, " Formation and annihilation of the metastable defect in boron-doped Czochralski silicon", *Proc. 29th IEEE Photovoltaic Specialists Conf*., New York, NY, pp. 178 (2002).

[14] P. Deak, L. C. Snyder, J, Corbett, "Theoretical studies on the core structure of the 450 °C oxygen thermal donors in silicon", *Phys. Rev. B*., vol. 45, no. 20, pp.11612 (1992).

[15] J. Coutinho, R. Jones, P.R. Briddon, and S. Öberg, "Oxygen and dioxygen centers in Si and Ge: density functional calculations", *Phys. Rev. B.*, vol. 62, no. 16, pp. 10824 (2000).

[16] Y.J. Lee, J. Boehm, M. Pesola, R.M. Nieminen, "First-principles study of migration, restructuring, and dissociation energies of oxygen complexes in silicon", *Phys. Rev. B*, vol. 65, no. 8, pp. 085205 (2002).

[17] J. Adey, R. Jones, D.W. Palmer, "Degradation of boron doped Czochralski grown silicon solar cells", *Phys. Rev. Lett*., vol. 93, no. 5, pp. 055504 (2004).

[18] M.H. Du, H.M. Branz, R.S. Crandall, S.B. Zhang, "Bistability-mediated carrier recombination at light induced boron-oxygen complexes in silicon", *Phys. Rev. Lett*., vol. 97, no. 25, pp. 256602 (2006).

[19] P. Chen, X. Yu, X. Liu, X. Chen, Y. Wu, D. Yang, " Experimental evidence of staggered oxygen dimmers as a component of boron-oxygen complexes in silicon", *Appl. Phys. Lett.*, vol. 102, no. 8, pp. 082107 (2013).

[20] J. Knobloch, S.W. Glunz, D. Biro, W. Warta, E. Schaffer, W. Wettling, " Solar cells with efficiencies above 21% processed from Czochralski grown silicon", *Proc. 25th IEEE Photovoltaic Specialists Conf*. Washington, DC, pp. 405 (1996).

[21] J. Schmidt, A. Cuevas, "Progress in understanding and reducing the light degradation of Cz silicon solar cells", *Proc. 16th European Photovoltaic Solar Energy*, Glasgow, UK, pp. 1193 (2000).

[22] T. Saitoh, H. Hasigami, S. Rein, S. Glunz, "Overview of light degradation research on crystalline silicon solar cells", *Prog. Photovolt: Res. Appl*., vol. 8, pp. 537 (2000).

[23] J.H. Reiss, R.R. King, and K.W. Mitchell; "Characterization of diffusion length degradation in Czochralski silicon solar cells",*Appl. Phys. Lett*., vol. 68, no. 23, pp. 3302 (1996).

[24] M. Sanati, S.K. Estreicher, "Boron-oxygen complexes in Si", *Physica B*, vol. 376-377, pp. 133 (2006).

[25] Y. Ohshita, T. K. Vu, M. Yamaguchi, "Interstitial boron and oxygen related defects as the origin of the deep energy level in Czochralski-grown silicon", *J. of Appl. Phys*., vol. 91, no. 6, pp. 3741 (2002).

[26] K. Bothe, J. Schmidt, "Electronically activated boron-oxygen related recombination centers in crystalline silicon", *J. Appl. Phys*., vol. 99, no. 1, pp. 013701 (2006).

[27] H. Nagel, A. Merkle, A. Metz, R. Hezel, "Permanent reduction of excess carrier induced recombination centers in solar grade Czochralski silicon by a short yet effective anneal", *Proc. 16th European Photovoltaic Solar Energy*, Glasgow, UK, pp. 1193 (2000).

[28] K. Graff, H. Piper, "The properties of iron in silicon", *J. Electrochem. Soc*., vol. 128, no. 3, pp. 669 (1981).

[29] L.C. Kimerling, J.L. Benton, "Electronically controlled reactions of interstitial iron in silicon", *Physica B*, vol. 116, pp. 297 (1983).

[30] B. Sopori, "Dielectric films for Si solar cell application", *J. Electron. Mater*., vol. 34, no. 5, pp. 564 (2005).

[31] M.W. Lamers, K.T. Butler, J.H. Harding, A. Weeber, "Interface properties of a-SiN_x:H/Si to improve surface passivation", *Sol. Energy Mater. Sol. Cells*, vol. 106, pp. 17 (2012).

[32] Annual Energy Outlook 2012, U.S. Energy Information Administration, Washington, DC.

[33] Solar Annual, 2013, Photon Consulting, Boston, MA.

[34] U.S. Solar Market Insight, 2012 Year in Review, Green Tech Media Inc. and Solar Energy Industries Association, 2013.

[35] W. Shockley, H.J. Queisser, "Detailed balance limit of efficiency of p-n junction solar cells", *J. Appl. Phys*., vol. 32, no. 3, pp. 510 (1961).

[36] T. Tiedje, E. Yablonovitch, G. Cody, B. Brooks, "Limiting efficiency of silicon solar cells", *IEEE Transactions on electron devices*, vol. 31, no. 5, pp. 711 (1984).

[37] M. Green, K. Emery, Y. Hishikawa, W. Warta, E.D. Dunlop, "Solar cell efficiency tables (version 40)", *Prog. Photovolt: Res. Appl*., Vol. 20, pp. 606 (2012).

[38] T. Razykov, C. Ferekides, D. Morel, E. Stefanakos, H. Ullal, H. Upadhyaya, "Solar photovoltaic electricity: current status and future prospects", *Sol. Energ*., vol. 85, pp. 1580 (2011).

[39] S. Wolf, P. Choulat, J. Szlufcik, I. Perichaud, S. Martinuzzi, C. Habler, W. Krumbe, "Light induced degradation of very low resistivity multi-crystalline silicon solar cells", *Proc. 28th IEEE Photovoltaic Specialists Conf*., Anchorage, Alaska, pp. 53 (2000).

[40] B. Damiani, K. Nakayashiki, D. Kim, V. Yelundur, S. Ostapenko, I. Tarasov, A. Rohatgi, "Light induced degradation in promising multi-crystalline silicon materials for solar cell fabrication", *Proc. 3rd World Conf. Photovoltaic Energ. Conversion*, Osaka, Japan, pp. 927 (2003).

[41] K. Peter, P. Preis, P.E. Diaz-Perez, J. Theobald et al, "Light induced degradation in multicrystalline solar grade silicon solar cells evaluated using accelerated LID''; *Proc. 26th European Photovoltaic Sol. Energ. Conf. Exhib*. , Valencia, Spain, (2010)

[42] Geological Survey, US, (1975), Denver, CO.

[43] B. Fickett, G. Mihalik, "Multiple batch recharging for industrial CZ silicon growth", *J. Cryst. Growth*, vol. 225, no. 2-4, pp. 580 (2001).

[44] T. Kamins, Polycrystalline Silicon for integrated Circuit applications, Kluwer Academic Publishers, Boston, MA, 1988, pp 92-96, 178-179.

[45] T. Ciszek, "Some applications of cold crucible technology for silicon photovoltaic material preparation", J. Electrochem. Soc., vol. 132, no. 4, pp. 963 (1985).

[46] A. Bidiville, K. Wasmer, J. Michler, P. Nasch, M. Van der Meer, C. Ballif, "Mechanisms of wafer sawing and impact on wafer properties", *Prog. Photovolt: Res. Appl.,* vol. 18, no. 8, pp. 563 (2010).

[47] J. Nelson, "The physics of solar cells", Imperial College Press, 57 Shelton Street, Covent Garden, London WC2H 9HE. UK, 1st Ed. (2009).

[48] J.D.J. Ingle, S.R. Crouch, "Spectrochemical Analysis, 1st Ed.", Prentice Hall,One Lake St. Upper Saddle River, New Jersey (1988).

[49] E. Rosencher, "Optoelectronics", Cambridge University Press, The Edinburg Building, Cambridge, CB2 2RU, UK (2002).

[50] K. Graff, H. Pieper, "Degradation of carrier lifetime in silicon crystals at room temperature", *Phys. Stat. Sol. (a)*, vol. 49, pp. 137 (1978).

[51] K. W. Boer, "Survey of semiconductor physics, 2nd Ed. vol. 1" John Wiley and Sons, Inc. 605 Third Av., New York, NY (2002).

[52] W. Shockley, W. Read, "Statistics of the recombination of holes and electrons", *Phys. Rev*. vol. 87, no. 5, pp. 835(1952).

[53] R.N. Hall, "Electron hole recombination in Germanium", *Phys. Rev*., vol. 87, no. 3, pp. 387 (1952).

[54] W. Roosbroeck, W. Shockley, "Photon-radiative recombination of electrons and holes in germanium", *Phys. Rev*., vol. 94, no. 6, pp. 1558 (1954).

[55] R.N. Hall, "Recombination process in semiconductors", *Proc. IEE*, vol. 106B, pp. 924 (1960).

[56] J. W. Corbett, A. Jaworowski, R.L. Kleinhenz, C.B. Pierce, N.D. Wilsey, "Photodegradation in silicon", *Sol. Cells*, vol. 2, pp. 11 (1980).

[57] K. Rajkanan, R. Singh, J. Shewchun, "Absorption coefficient of silicon for solar cell calculation", *Sol. Stat. Elect*., vol. 22, pp. 793 (1979).

[58] P.T. Landsberg, "The band-band Auger effect in semiconductors", *Sol. Stat. Elect*., vol. 30, no. 11, pp. 1107 (1987).

[59] C.T. Sah, R.N. Noyce, W. Shockley, "Carrier generation and recombination in p-n junction and p-n characteristics", *Proc. IRE*., vol. 45, pp. 1228 (1957).

[60] M. Wolf, H. Rauschenbach, "Series resistance effects on solar cell measurements", *Advanced Energy Conversion*, vol. 3, pp. 455 (1961).

[61] A. Aberle, S. Robinson, A. Wang, J. Zhao, S. Wenham, M. Green, "High efficiency silicon solar cells: fill factor limitations and non-ideal diode behavior due to voltage dependent rear surface recombination velocity", *Prog. Photovolt.: Res. Appl*., vol. 1, no. 2 , pp. 113 (1993).

[62] L. Kazmerski, "Best research cell efficiencies", Data compiled by National Renewable Energy Laboratory, Golden, CO, 03/07/2013.

[63] C.H. Henry, "Limiting efficiencies of ideal single and multiple energy gap terrestrial solar cells", *J. Appl. Phys*., vol. 51, no. 8, pp. 4494 (1980).

[64] E. Yablonovich, G. Cody, "Intensity enhancement in textured optical sheets for solar cells", *IEEE Transactions on Electron Devices*, vol. ED 29, no. 2, pp.300 (1982).

[65] W. Keogh, A. Blakers, A. Cuevas, "Constant voltage I-V curve flash tester for solar cells", *Sol. Energy Mat. Sol. Cells*, vol. 81, pp. 183 (2004).

[66] J. Schumacher, S. Sterk, B. Wagner, W. Warta, "Quantum efficiency analysis of high efficiency solar cells with textured surfaces", *Proc. 13th European Photovolt. Sol. Energy Conf.*, Nice, France, pp. 96(1995).

[67] E. Zalewski, J. Geist, "Solar cell spectral response characterization", *Appl. Optics*, vol. 18, no. 23, pp. 3942 (1979).

[68] T. Trupke, R. Bardos, "Photoluminescence: a surprisingly sensitive lifetime technique", *Proc. 31st IEEE Photovoltaic Specialists Conf.,* Orlando, FL, pp. 903 (2005).

[69] R. Bardos, T. Trupke, M. Schubert, T. Roth, "Trapping artifacts in quasi-steady-state photoluminescence and photoconductance lifetime measurement on silicon wafer", *Appl. Phys. Lett*., vol. 88, no. 5, pp. 53504 (2006).

[70] R. Sinton, A. Cuevas, M. Stuckings, "Quasi-steady-state photoconductance, a new method for solar cell material and device characterization", *Proc. 25th IEEE Photovoltaic Specialists Conf.,* Washington, DC, pp. 457 (1996).

[71] B. L. Sopori, "System for characterizing semiconductor materials and photovoltaic devices", U.S. Patent No. 5581346.

[72] D.K. Schroder, "Semiconductor material and device characterization, 3rd Ed., John Wiley & Sons Inc., 605 Third Av., New York, NY (2007).

[73] J. Knobloch, S. Glunz, V. Henninger, W. Warta, W. Wettling, "21% efficient solar cells processed from Czochralski grown silicon", *Proc. 13th European Photovoltaic Sol. Energ. Conf.,* Nice, France, pp. 9 (1995).

[74] S. W. Glunz, S. Rein, W. Warta, J. Knobloch, W. Wettling, "Degradation of carrier lifetime in CZ silicon solar cells", *Sol. Energy Mater. Sol. Cells,* vol. 65, pp. 219 (2001).

[75] S. Rein, T. Rehrl, W. Warta, S. Glunz, and G. Willeke, "Electrical and thermal properties of the metastable defect in boron doped Czochralski silicon (CZ-Si)", *Proc. 17th European Photovoltaic Sol. Energy Conf.*, Munich, Germany, pp. 1555 (2001).

[76] S. Rein and S. Glunz, " Electronic properties of the metastable defect in boron doped Czochralski silicon: Unambigious determination by advanced lifetime spectroscopy",*Appl. Phys. Lett*., vol. 82, no. 7, pp. 1054 (2003).

[77] A. Herguth, G. Schubert, M. Kaes, G. Hahn, "A new approach to prevent the negative impact of the metastable defect in boron doped Cz silicon solar cells", *Proc. IEEE 4th World Conf. Photovoltaic Energy Conversion*, Hawaii, pp. 940 (2006).

[78] V. Voronkov, R. Falster, "Latent complexes of interstitial boron and oxygen dimers as a reaction for degradation of silicon based solar cells", *J. Appl. Phys*., vol. 107, no. 5, pp. 053509 (2010).

[79] B. Lim, K. Bothe, V. Voronkov, R. Falster, J. Schmidt, "Light induced degradation of the carrier lifetime in n-type Czochralski grown silicon doped with boron and phosphorous", *Proc. 26th European Photovoltaic Sol. Energy Conf. Exhibition*, Hamburg, Germany, pp. 944 (2011).

[80] T. Yoshida, Y. Kitagawara, "Bulk lifetime decreasing phenomena induced by light illumination in high purity p-type CZ-Si crystals", *Electrochem. Soc. Proc*., vol. 96-13, pp. 450 (1996).

[81] S. Glunz, S. Rein, W. Warta, J. Knobloch, W. Wettling, "On the degradation of CZ silicon solar cells", *Proc. 2nd Conf. Exhibit. Photovoltaic Sol. Energy Conversion,* Vienna, Austria, pp. 1343 (1998).

[82] K. Bothe, J. Schmidt, R. Hezel, "Effective reduction of the metastable defect concentration in boron doped Czochralski silicon for solar cell", *Proc. 29th IEEE Photovoltaic Specialists Conf.,* New Orleans, LA, pp. 194 (2002).

[83] P.J. Kelly, "Equilibrium geometries and electronic structure of oxygen related defects in silicon", *Mater. Sci. Forum*, vol. 38-41, pp. 269 (1989).

[84] J. Adey, R. Jones, P. Briddon, "Formation of B_iO_i, B_iC_s, and $B_iB_SH_i$ defects in e-irradiated or ion-implanted silicon containing boron", *Appl. Phys. Lett*., vol. 83, no. 4, pp. 665 (2003).

[85] B. Lim, F. Rougieux, D. Macdonald, K. Bothe, J. Schmidt, "Generation and annihilation of boron-oxygen related recombination centers in compensated p and n-type silicon", *J. Appl. Phys*., vol. 108, no. 10, pp. 103722 (2010).

[86] B. Sopori, P. Rupnowski, J. Appel, V. Mehta, C. Li, S. Johnston, "Wafer preparation and iodine-ethanol passivation procedure for reproducible minority-carrier lifetime measurement", *Proc. 33rd IEEE Photovoltaic Specialists Conf*., San Diego, California, pp. 1 (2008).

[87] A. Herguth, G. Hahn, "Kinetics of the boron-oxygen related defect in theory and experiment", *J. Appl. Phys*., vol. 108, no. 11, pp. 114509 (2010).

[88] B. Sopori, P. Basnyat, S. Devayajanam, S. Shet, V. Mehta, J. Binns, J. Appel, "Understanding light-induced degradation of c-Si solar cells", *Proc.38th IEEE Photovoltaic Specialists Conf*., Austin, Texas, pp. 1115 (2012).

[89] B. Sopori, P. Basnyat, S. Devayajanam, S. Shet, V. Mehta, J. Binns, J. Appel, "Experimental study of light induced degradation in c-Si solar cells: separating the bulk and the surface contributions", *Proc. 22nd Workshop Crystalline Silicon Sol. Cells Modules: Mater. Processes*, Vail, Colorado, pp. 135 (2012).

[90] L. Brillson, "Interface chemical reaction and diffusion of thin metal films on semiconductors", *Thin solid films*, vol. 89, no. 4, pp. 461 (1982).

[91] D. Palmer, K. Bothe, J. Schmidt, "Kinetics of the electronically stimulated formation of a boron-oxygen complex in crystalline silicon", *Phys. Rev. B*, vol. 76, no. 3, pp. 035210 (2007).

[92] A. Herguth, G. Schubert, M. Kaes, G. Hahn, "Investigation on the long time behavior of the metastable boron-oxygen complex in crystalline silicon", *Prog. Photovolt: Res. Appl.*, vol. 16, pp. 135 (2008).

[93] M. Tucci, L. Serenelli, S. De Iuliis, M. Izzi, "Characterization of SiN_xa-Si:H crystalline silicon surface passivation under UV light exposure", *Thin Solid Films*, vol. 515, no. , pp. 7625 (2007).

[94] D.T. Krick, P.M. Lenahan, J. Kanicki, "Electrically active point defects in amorphous silicon nitride: An illumination and charge injection study", *J. Appl. Phys*., vol. 64, no. 7, pp. 3558 (1988).

[95] F. Rougieux, B. Lim, J. Schmidt, M. Forster, D. Macdonald, A. Cuevas, "Influence of net doping, excess carrier density and annealing on boron oxygen related defect density in compensated n-type silicon", *J. Appl. Phys*., vol. 110, no. 6, pp. 063708 (2011).

[96] J. Schmidt, K. Bothe, D. Macdonald, J. Adey, R. Jones, D. Palmer, "Electronically stimulated degradation of silicon solar cells", *J. Mater. Res*., vol. 21, no. 1, pp. 5 (2006).

[97] B. Sopori, "Silicon solar cell material research: current progress and future needs", *Sol. Cells*, vol. 30, pp. 373 (1991).

[98] G. Colletti, C. Mulder, G. Galbiati, L. Geerlings, "Reduced effect of B-O degradation on multicrystalline silicon wafers", *Proc. 21st European Photovoltaic Sol. Energy Conf. Exhibition*, Dresden, Germany, pp. 94 (2006).

[99] S. Dubois, N. Enjalbert, J. Garandet, "Slowdown of the light induced degradation in compensated solar grade multicrystalline silicon" *Appl. Phys. Lett*., vol 93, no. 10, pp. 103510 (2008).

[100] M. Sheoran, A. Upadhyaya, A. Rohatgi, "A comparision of bulk lifetime, efficiency, and light induced degradation in boron and gallium doped cast mc- Si solar cells", *IEEE Transaction on Electron Devices,* vol. 53, no. 11, pp. 2764 (2006).